AIR POLLUTION MODELLING FOR THE GREATER CAPE TOWN REGION

D. A. DRACOULIDES

A dissertation submitted to the Faculty of Engineering at the University of Cape Town for the fulfilment of the degree of Master of Science in Engineering.

Energy Research Institute, University of Cape Town

Cape Town, 1994

Declaration

This dissertation is submitted to the Faculty of Engineering, University of Cape Town, for the degree of Master of Science in Engineering. This is to declare that this dissertation is my original work and has not been previously submitted for any degree to any other University.

.....

D. A. Dracoulides

University of Cape Town, __/__/__

Acknowledgments

The invaluable guidance and expert advice during the duration of this study of my supervisor Professor R. K. Dutkiewicz is gratefully acknowledged.

The emission information in the inventory data base was collected with the collaboration of the Cape Town City Council's Air Pollution Control and of the Air Pollution Group of the Western Cape Regional Services Council. The assistance of both groups is kindly acknowledged.

Synopsis

The two main factors which control the ground-level concentrations of air pollutants are the state of the surrounding atmosphere and the location and emitted amount of the pollutants. Dispersion models combine these two factors for the prediction of the ground-level concentrations, using existing sources and those planned for the future. In this manner several air-pollution control strategies can be tested. Thus, the strategy which best improves air-quality and is most cost-effective can be chosen. Before the application of such a dispersion model, its accuracy and applicability to a particular area should be tested.

Limited research on dispersion modelling for the Cape Town metropolitan area has been undertaken. This thesis deals with air-pollution aspects in relation to dispersion modelling, as well as with the input requirements and application of a dispersion model in the Greater Cape Town region. An EPA approved Gaussian plume model, the Industrial Source Complex Short Term 2 (ISCST2), was chosen for the pollution simulation. The model requires one point meteorological measurements and can accommodate multiple point, line and area sources.

Meteorological data used in the study were collected from D. F. Malan airport for the years 1991 and 1992. However, required parameters, such as the mixing height and the atmospheric stability class, are not readily available and thus needed to be calculated. Three methods for determining the mixing heights and three methods for determining atmospheric stability class were used in the model and the accuracy for each combination was assessed.

Appropriate emission information for use with dispersion modelling is not available for the Greater Cape Town area. Therefore, the compilation of an emission inventory formed a considerable part of this study. Emission data from the large industries was collected with the collaboration of the Cape Town City Council's Air Pollution Control and of the Air Pollution Group of the Western Cape Regional Services Council. The rest of the sources (i.e. residential, vehicular and industrial), were grouped into areas, and their emissions were based on their fuel consumption.

The emission and meteorological data were incorporated into the ISCST2 model to yield the ground-level concentrations. The performance of the ISCST2 model was evaluated with the use of 53 days of hourly SO_2 concentrations, at three monitoring stations. The locations of these monitoring sites were at Bellville, Cape Town's CBD and Goodwood. Several statistical measures, as proposed in the Woods Hole EPA/AMS Workshop and other studies, were employed in order to quantify the model performance. The evaluation analysis consisted of the 1h, 24h and maximum concentration comparisons, as well as examination of the model's accuracy under different meteorological conditions. These meteorological groups were categorised

according to the atmospheric state (i.e. stable, neutral and unstable), as well as according to wind velocity (i.e. light, medium and strong winds).

Only at Bellville monitoring site did the model predict the 1h and 24h averaged SO_2 concentrations, within the desired accuracy limits. At Goodwood and Cape Town's CBD, the model under-predicted the observed values by a factor of 2 and 4 respectively.

When the hourly maximum concentrations, independent of the time of occurance, were examined, the predictions at Bellville and Goodwood were within a factor of two from the observations, with a tendency towards over-prediction. Examination of the same concentrations at the CBD site revealed a bias towards under-prediction, although, on average, the performance was also within a factor of two.

Emissions from point sources account for most of the observed concentrations during the unstable hours of the day (i.e. 8h00 to 18h00). Area sources, due to their low release height, account for most of the ground-level concentrations at night-time. Therefore, an accurate emission inventory should not only focus on the correct amounts of the pollutants emitted, but also on the proper characterization of the sources.

In conclusion, the evaluation of the ISCST2 model indicated that it could be employed for predictions of pollutant maximum concentrations at locations away from Table Mountain and the coast lines, such as Goodwood and Bellville.

Lastly, the importance of further air-pollution simulation studies is stressed. The collection and regular update of the emissions input to such models should form one of the first priorities, before the implementation of computer simulated air-pollution control strategies.

Table of Contents

Chapter THREE

Chapter FOUR

Chapter FIVE

APPENDIXES

List of Figures

Chapter THREE

Chapter FOUR

Chapter FIVE

APPENDIXES

List of Tables

Table | Page

Chapter FOUR

APPENDIXES

Nomenclature

C : Concentration of a pollutant ($\mu g/m^3$)
C_p : Specific heat at constant pressure (J kg^{-1} K^{-1})
$\overline{d}$: Mean difference = $\overline{P}$ - $\overline{d}$
D : Index of agreement
D_c : Decay term (see Equation (1.9))
f : Coriolis parameter
FB : Fractional bias
g : Gravitational acceleration (m s^{-2})
h_e : Effective stack height (i.e. stack height plus plume rise) (m)
k : von Karman constant $\simeq$ 0.4
K_x : Eddy diffusivity along the X axis (m^2 s^{-1})
K_y : Eddy diffusivity along the Y axis (m^2 s^{-1})
K_z : Eddy diffusivity along the Z axis (m^2 s^{-1})
L : Monin-Obukhov length
MSE : Mean square error
MSE_s : Systematic mean square error
MSE_u : Unsystematic mean square error
$NMSE$: Normalised mean square error
O : Observed Concentration ($\mu g/m^{-3}$)
$\overline{O}$: Mean Observed concentration
p : Atmospheric Pressure (kPa)
p_0 : Atmospheric pressure at ground level (kPa)
$P_{60...68}$: Prediction data sets
P : Predicted Concentration ($\mu g/m^{-3}$)
$\overline{P}$: Mean predicted concentration
Q : Emission rate of a gaseous pollutant (g s^{-1})
r_0' : Effective radius = $x_0 / \sqrt{\pi}$ (m)
R : Universal constant = 8.3143 J K^{-1} · mole
R_i : Richardson number
R_{iB} : Bulk Richardson number
$RMSE$: Root mean square error
$RMSE_s$: Systematic root mean square error
$RMSE_u$: Unsystematic root mean square error
s_d^2 : Variance of the difference
t : Time (s)
$T_{1/2}$: Half life of a pollutant (s)
u : Wind velocity along the X axis (m s^{-1})
u_* : Friction velocity
u_s : Wind speed at stack height (m s^{-1})
v : Wind velocity along the Y axis (m s^{-1})
w : Wind velocity along the Z axis (m s^{-1})

x : Horizontal distance downwind from a source (m)
x_0 : Length of the side of an area source (m)
y : Horizontal distance crosswind from a source (m)
z : Vertical distance above the ground (m)
z_i : Mixing height (m)
z_o : Roughness length (m)
z_p : Height of the planetary boundary layer (m)
z_r : Receptor height (m)

γ : Ratio of the specific heat at constant pressure over that at constant volume
Γ : Adiabatic lapse rate = 9.8×10^{-3} (K m^{-1})
θ : Potential temperature
μ' : Modified Kazanski-Monin parameter (see Equarion (A1.4))
σ_θ : Standard deviation of the vertical wind component
σ_ϕ : Standard deviation of the lateral wind component
σ_v : Standard deviation of the lateral wind fluctuation
σ_w : Standard deviation of the vertical wind fluctuation
σ_y : Standard deviation of the concentration distribution in the Y direction (m)
σ_z : Standard deviation of the concentration distribution in the Z direction (m)
ψ : Decay coefficient = $0.693/T_{1/2}$ (s^{-1})

List of Abbreviations

ASCII	: American Standard Code for Information Interchange
CBD	: Central Business District
DH	: Department of Health
EI	: Emission Inventory
EPA	: Environmental Protection Agency
ISCST2	: Industrial Source Complex Short Term 2
NACA	: National Association for Clean Air

Chapter ONE

INTRODUCTION

1 INTRODUCTION

The last decade has been characterised by a growing interest in air pollution transport phenomena. Air quality of modern cities continues to deteriorate due to the continuous increase in urbanisation. This results in an accumulation of vehicles and industrial activities in areas with already existing pollution problems. Public awareness and concern about the degradation of air quality in South Africa's major cities has increased over the past few years.

The Atmospheric Pollution Prevention Act No. 45 of 1965 assisted in setting the basis for air quality control policies in South Africa. In Cape Town, the initiation of an air pollution control programme in 1968 resulted in great improvement in the measured concentrations (Popkiss, 1992). One of the main and least expensive tools for the development of air pollution control policies are computer simulation dispersion models. They provide the capability of assessing the pollution impact from possible additional sources or worst scenario situations. To date, there is no dispersion model which could be employed for every region, due to the complexity of the physical processes which govern the transport of pollutants into the atmosphere.

In order to determine if a model is applicable to a particular area and its atmospheric conditions, the model's reliability and prediction accuracy have to be evaluated. Model evaluation is the quantification of the model's performance, using real emission data and atmospheric scenarios. The aim of this study is to evaluate the applicability and performance of the Industrial Source Complex Short Term 2 (ISCST2) model for the Greater Cape Town region.

1.1 Air Pollution Related Aspects in the Greater Cape Town

Cape Town is situated on the southwestern tip of South Africa. It is one of the five largest cities with major industrial activities and a population of 1.3 million. The region encompasses an area of 500 km^2, and its topography can be characterised as complex (Figure 1.1). Table Mountain and the two oceans on the south and west coast of Cape Town are the main topographical features. As indicated by many studies, the areas meteorology is largely effected by these features (Keen, 1979; Smith, 1984; Jury et al., 1992).

Dutkiewicz et al. (1980) found that the complexity of the air movement in the Cape Town metropolitan area impeded the use of long-term dispersion models such as the Air Quality Display (AQDM) and the Climatological Dispersion Model (CDM). Other studies of the area's air quality have focused on the spatial and temporal variation of

pollutant measurements, as well as the meteorological conditions during air pollution episodes (Loewenheim, 1988; Jury et al., 1990). The winter's low mixing heights, in combination with low wind speeds ($u < 3$ m s^{-1}), were found to correlate with many air pollution episodes in the area.

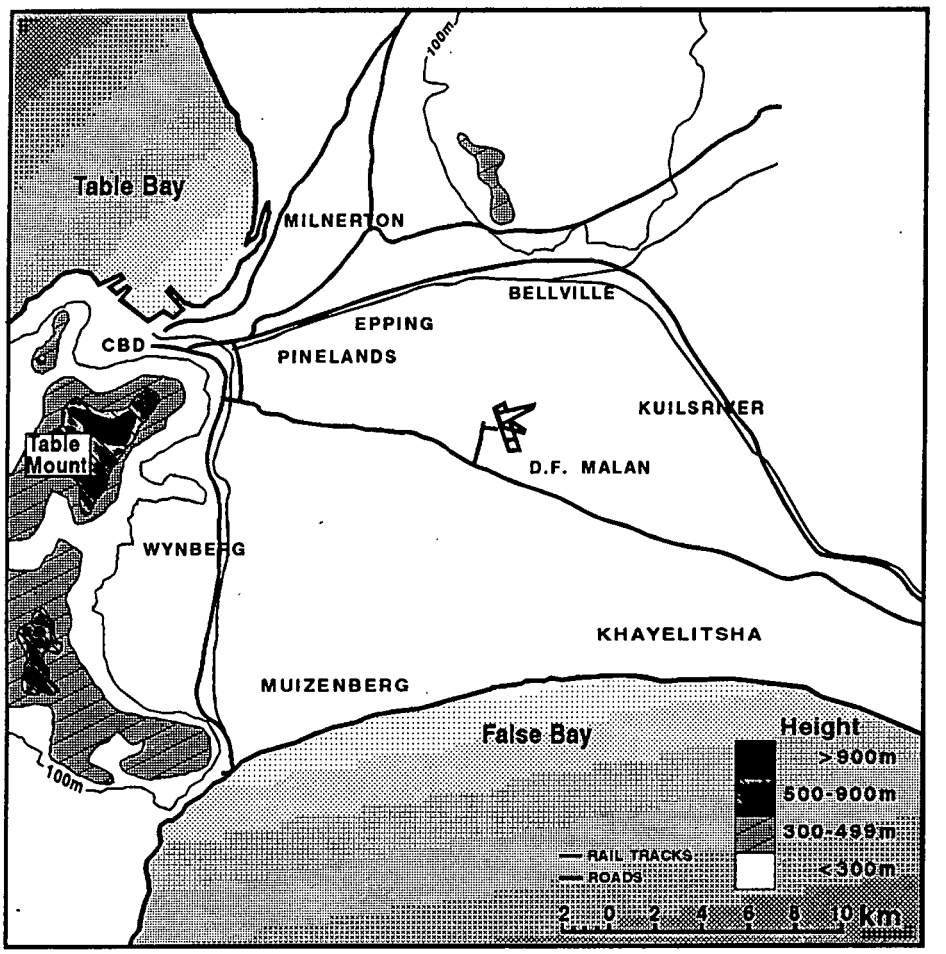

Figure 1.1 The Greater Cape Town (GCT) region with its surrounding topographical features, arterial roads and railway tracks.

Dispersion models require comprehensive emission data as input. The importance and effect of an accurate emission inventory on the model performance has been widely stressed (Turner, 1979; Ruff, 1983; Ku et al., 1987b; Hanna, 1988). The degree of detail to which the emission information is available, as well as the proper characterisation of the area and point sources is also significant. Air pollution pathway processes depend largely on the type of source the effluent is emitted from (i.e. point, area or line source).

Emission sources in the Greater Cape Town (GCT) region are comprised of a complicated combination of industrial and residential areas of different characteristics and emission strengths. To date, an adequately detailed emission inventory is not available for the GCT area. The only available source of emitters' information are the registration forms of appliances used in various municipal areas. This information, which is stored in a hard copy format, is inadequate for a dispersion modelling study.

Therefore, in the first part of the present study, a database code was developed for the emission inventory purposes from all stationary sources in the GCT area. This database is currently being used by the Cape Town City Council's Air Pollution Control, also for their registration purposes. The information collected in collaboration with the Air Pollution Control officers was used for the point source input into the ISCST2 dispersion model.

Ideally, local air pollution agencies such as the Departments of Health (DH) (municipal, national, etc.) should initiate the formulation of a policy for the development and update of emission inventories.

1.2 Dispersion Modelling and Air Pollution Control Strategies

The aim of every air pollution study is to quantify existing ambient air quality in order to set future abatement policies for sustainable development. Dispersion models are the unique tools which, if properly used, can provide, a deterministic source-receptor relationship. In this way, the fraction of impact of a particular source on the observed concentrations can be estimated, thus allowing for the development and implementation of appropriate air pollution control strategies. Figure 1.2 illustrates the various stages and elements of a comprehensive air pollution control strategy, with respect to air-quality models.

The emphasis of such strategies is on (Seinfeld, 1975):

- establishing emission control legislation which will achieve fixed air-quality standards
- evaluating the impacts of future control and emission changes
- selecting the locations of future sources and their contribution to the already existing concentration levels, in order to minimise their impact
- planning short-term emission reduction strategies, in order to avoid air pollution episodes in certain areas
- evaluating the contribution of present sources to air pollution levels

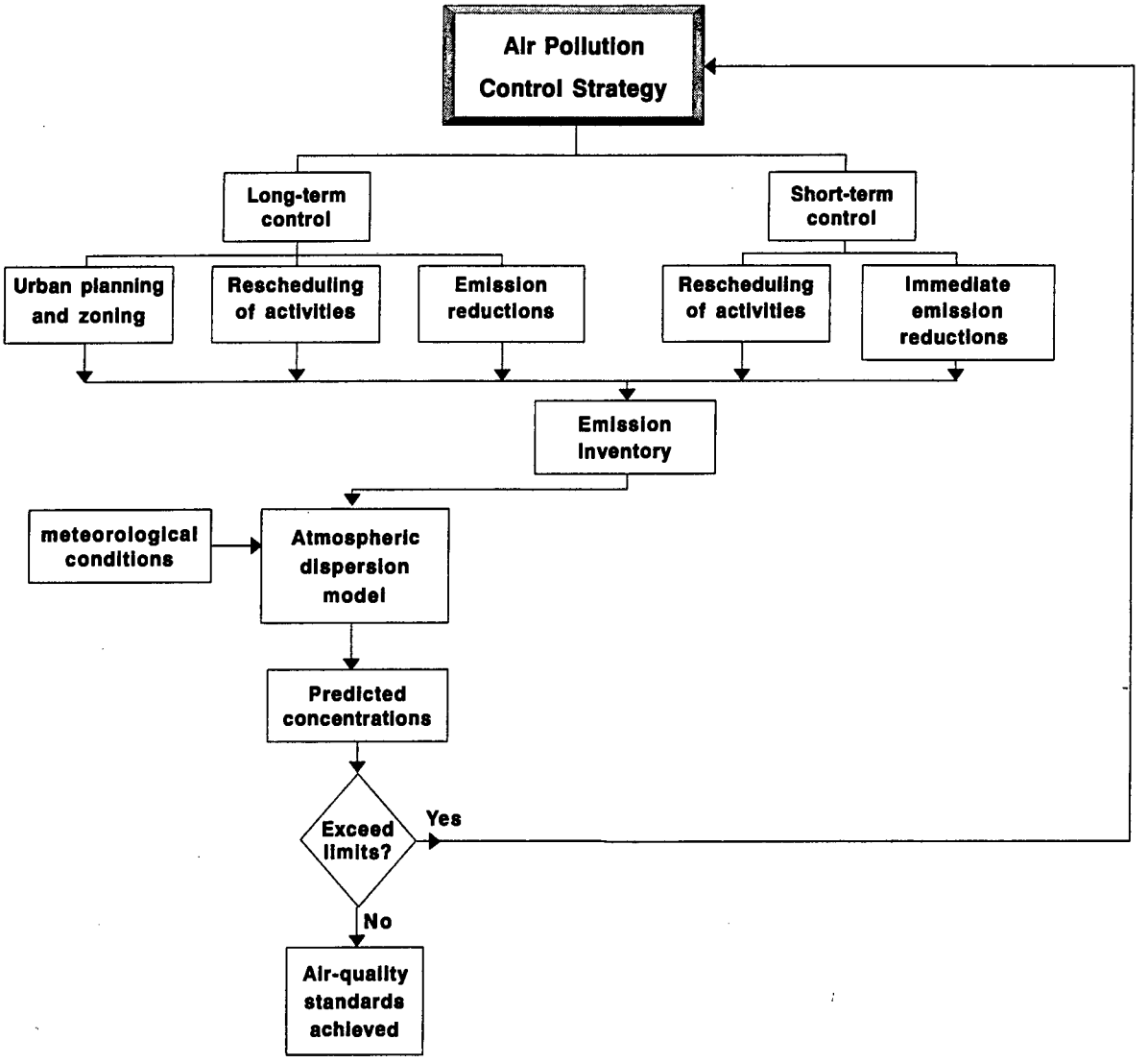

Figure 1.2 Various stages and elements of an air pollution control strategy, with respect to air-quality simulation models.

1.3 Modelling Air Pollution in Urban Areas

Urban air pollution dispersion models permit quantitative determination of ambient air concentrations in relation to emission sources and meteorological conditions. The most difficult part of an urban air pollution model is the assessment of the state of the atmosphere, due to the many changes that continually take place in it. Mathematical models used for air pollution studies range from simple empirical models to very complex numerical ones.

1.4 Gaussian Plume and Puff Models

The Gaussian plume models are based on the approximation that the concentration, downwind of a point source in the atmospheric boundary layer, has a Gaussian distribution, but with unequal dispersion coefficients in the horizontal and vertical directions. This is used to compensate for the fact that in the boundary layer the turbulence is neither isotropic nor homogeneous. The general form of the Gaussian plume equation for an elevated continuous point source is given by:

$$C(x,y,z;H) = \frac{Q}{2\pi\sigma_z\sigma_y U}\exp\left(-\frac{y^2}{2\sigma_y^2}\right)\left\{\exp\left[-\frac{(z-h_e)^2}{2\sigma_z^2}\right]+\exp\left[-\frac{(z+h_e)^2}{2\sigma_z^2}\right]\right\} \qquad \textbf{(1.1)}$$

where:

C : is the predicted pollutant concentration (g m^{-3})
x,y,z : receptor coordinates (m)
Q : pollutant emission rate (g s^{-1})
U : wind speed along the plume axis (m s^{-1})
σ_y, σ_z : crosswind and vertical dispersion coefficients (m) and
h_e : effective stack height (m) (i.e. stack height plus final plume rise).

The main assumptions of the Gaussian plume formulation are firstly, that the variability of concentrations, emissions and meteorological conditions can be treated as though they resulted from continuous sequences of different steady states (Hanna et al., 1982). Secondly, the horizontal wind field is assumed to be homogeneous. Lastly, the eddy diffusivities are taken to be constant along the principle axes.

Gaussian type models are commonly used for mathematical modelling of inert pollutants over urban areas (Seinfeld, 1986). Generally, the area's total emissions are subdivided into smaller sources. The solution of the basic equations, for each one of these sources, is obtained at a number of receptor points. Finally, the results are superimposed to yield the predicted concentration at a given receptor location.

A modification of the Gaussian model is the puff model. This type of formulation is not based on the quasi-steady state assumption for the governing parameters. It considers a series of instantaneous puffs which follow the wind trajectories and diffuse individually. Therefore, the puff model provides a better prediction of the actual spatial and temporal variation of the concentrations. Nevertheless, it requires an equally detailed spatial and temporal resolution of the wind and emission information. In most urban areas this type of data is often incomplete.

Many computer programs have been developed on the basis of the Gaussian plume formulation. One of the widest collections of air-quality models exists at the User's Network of Applied Modelling of Air Pollution (UNAMAP) at the U.S. Environmental Protection Agency (EPA). These models are divided into four general classes: 1) Gaussian, 2) numerical, 3) statistical or empirical and 4) physical. The most widely used models, recommended for estimating impacts of non-reactive pollutants, are the Gaussian models. Numerical models are recommended for applications involving reactive pollutants such as in photochemical smog. The U.S. EPA also provides guidelines related to the use and application of the UNAMAP models. In its guidelines these models are grouped into "preferred" and "alternative" models. Preferred are those which EPA have found to perform better than others in a given category, or chose on the basis of other factors such as fast use, public familiarity, cost or resource requirements and availability. One of the EPA "preferred" Gaussian models, which is also used in the present study, is the Industrial Source Complex (ISC) model.

1.5 Numerical Models

The atmospheric diffusion equation (1.1) provides a more general approach to the diffusion calculation than the Gaussian models. Nevertheless, analytical solutions of this equation can be obtained only for the steady-state and under simplifying assumptions for the velocity and the diffusivity coefficients. Available formulations have been discussed by Hanna et al. (1982) and Seinfeld (1986).

$$\frac{\partial C}{\partial t}+\frac{\partial (uC)}{\partial x}+\frac{\partial (vC)}{\partial y}+\frac{\partial (wC)}{\partial z}=\frac{\partial\left(K_x\frac{\partial C}{\partial x}\right)}{\partial x}+\frac{\partial\left(K_y\frac{\partial C}{\partial y}\right)}{\partial y}+\frac{\partial\left(K_z\frac{\partial C}{\partial z}\right)}{\partial z} \qquad \textbf{(1.2)}$$

where:

C	: is the estimated concentration
t	: time variable
x,y,z	: receptor coordinates on an X, Y, Z coordinate system
u,v,w	: wind components along the three main axes
K_x,K_y,K_z	: eddy diffusivity coefficients

With the increasing use of computers, numerical solutions of the atmospheric diffusion equation have been introduced. Time and space variability can be handled by carrying a large number of grid points in the computer.

Equation (1.1) was used by Ku et al, (1987a,b) to predict the air pollution above an urban area. The model incorporated the bulk Richardson number for the estimation of the atmospheric stability. The eddy diffusivity profile of the convective boundary layer was based on a numerical turbulence model by Lamb and Durran, 1978. They compared the numerical model results with the ones made by RAM (a Gaussian plume model). The performance of the former was not found to be significantly superior to the latter.

1.6 Air-Quality Model Selection

Several factors concerning the problem characteristics and output requirements should be considered when selecting a model. Some of these factors are:

- Domain characteristics of the area to be modelled. This includes topographical features such as hills, lakes and seas, as well as whether the area is urban or rural.
- Available air-quality measurements for the model evaluation, as well as the output averaging times of interest (i.e. short- or long-term).
- Type of pollutants to be modelled (i.e. reactive or non-reactive).
- Type of sources to be modelled (i.e. point, area or line sources) and specific features such as plume fumigation, the urban heat island or the building downwash effect.
- Recommendations or regulations of local air-quality authorities.
- Cost-effective analysis and available computational facilities.

The use of a model for air-quality control strategies requires model evaluation with local monitoring data. This assessment is important in order to determine the model's applicability and minimise prediction error. Only models that have been verified with past data should be used for future forecasting. However, evaluation is not an easy task, when sufficient monitoring and meteorological data are not available.

In the present study, the selection of the EPA's Industrial Source Complex 2 (ISC2) model was based on the following factors:

- Due to the large modelled area, a large number of sources should be accommodated by the model.
- No previous modelling studies could provide data for model inter-comparisons in the studied area. Therefore, the choice of a simple model, as the logical

starting point in air-quality modelling, was preferable to a more complicated one.

- The model should account for point as well as large area sources.
- The topography of the area at certain locations is complex. In view of this, it was initially decided to use a simple and cost-effective Gaussian model and assess the degree of accuracy obtainable at different locations and under different atmospheric conditions, before studying the predictions of a model which would account for such complex topography.
- The ISC model has been successfully applied by ESKOM for impact predictions by single power stations in the Eastern Transvaal Highveld region (Turner, 1993).

1.7 The Industrial Source Complex Short Term 2 (ISCST2) model

One of the multiple source Gaussian models in the EPA's "preferred" list, is the Industrial Source Complex. The ISC is a steady-state plume model that can be used to assess pollutant concentrations from a wide variety of sources associated with an industrial source complex (EPA, 1992). The model is available in two versions, one for short-term predictions (i.e. 1h, 24h to annual) and one for long-term (i.e. monthly, seasonal and annual averages). The original plume equation has been modified to account for building downwash, stack-tip downwash, dry deposition, as well as for point area and line sources. The model requires as input hourly meteorological data records to define the atmospheric conditions for plume rise, dispersion and diffusion. Pollutant concentrations from each point, area and line source are then calculated, and the results are superimposed at each of the user-defined receptor locations.

1.7.1 Point Source Calculations

The ISCST2 model calculates the hourly concentration at a downwind distance x and a crosswind distance y, from an elevated continuous point source as:

$$C(x,y,0) = \frac{QD_c}{2\pi\sigma_z\sigma_y u_s} \exp\left(-\frac{y^2}{2\sigma_y^2}\right) [V] \qquad \textbf{(1.3)}$$

where:

Q : pollutant emission rate
y : receptor crosswind distance

u_s : wind speed at release height
σ_y, σ_z : the lateral and vertical dispersion coefficients
D_c : decay term (accounts for pollutant removal processes)
V : vertical term

1.7.2 Area and Line Source Calculations

The model uses the "narrow plume hypothesis" to integrate Equation (1.3). Area sources are simulated by means of square areas with a uniform emission strength. Figure 1.3 illustrates the way in which an area source with irregular shape can be simulated into the ISCST2 model. The ground-level concentrations at a downwind distance x and crosswind distance y are calculated by:

$$C(x,y,0) = \frac{Q_A D_c E x_0}{4\sqrt{2}\sigma_z u_s} [V] \qquad \textbf{(1.4)}$$

where:

Q_A : area pollutant emission rate
x_0 : length of the side of the area source
u_s : wind speed at release height
σ_z : vertical dispersion coefficient
D_c : decay term
V : vertical term

E : error function term = $\text{erf}\left(\frac{r'_0+y}{\sqrt{2}\sigma_y}\right)+\text{erf}\left(\frac{r'_0-y}{\sqrt{2}\sigma_y}\right)$

r_0' : effective radius of area source = $x_0 / \sqrt{\pi}$

If a receptor location were situated within r_0' plus 1 meter of the centre of the area source, the above equation would not produce accurate results. Therefore, the ISCST2 model does not perform the calculation when the distance requirement is not met. This particular problem can be resolved by sub-dividing the area source into smaller squares (see Figure 1.3).

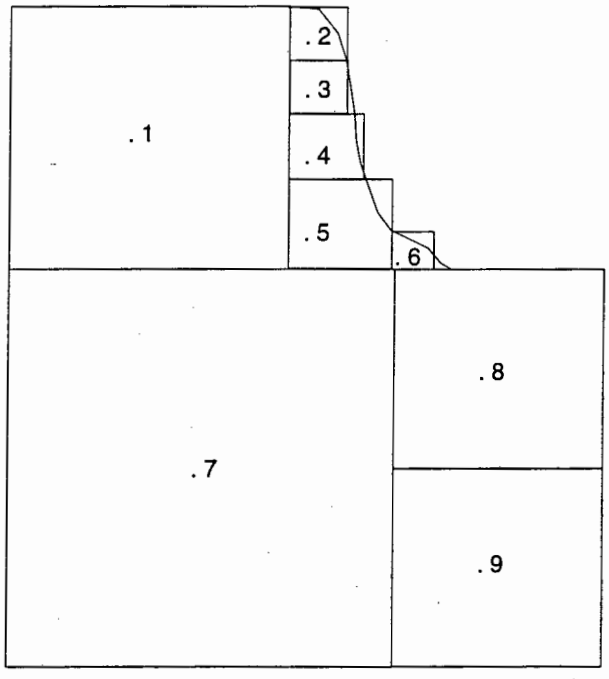

Figure 1.3 The procedure of sub-dividing an irregular shaped area with the use of 9 smaller square area sources.

1.7.3 Dispersion Parameters and Plume Rise

The dispersion parameters σ_y and σ_z are calculated as a function of the downwind distance and the atmospheric stability. Two dispersion options are available for the determination of these parameters. The first is the urban mode. It uses the formulas developed by Briggs (1973), which are based on experimental observations. The dispersion parameters for each atmospheric stability category are depicted in Table 1.1.

Table 1.1 Briggs formulas used for the urban dispersion coefficients σ_y and σ_z.

Pasquill class	σ_y (m)	σ_z (m)
A-B	$0.32x\ (1 + 0.0004x)^{-1/2}$	$0.24x\ (1 + 0.001x)^{1/2}$
C	$0.22x\ (1 + 0.0004x)^{-1/2}$	$0.2x$
D	$0.16x\ (1 + 0.0004x)^{-1/2}$	$0.14x\ (1 + 0.0003x)^{-1/2}$
E-F	$0.11x\ (1 + 0.0004x)^{-1/2}$	$0.08x\ (1 + 0.0015x)^{-1/2}$

A similar approach is adopted for the rural mode of the ISCST2. The lateral coefficient is obtained by (Turner 1970):

$$\sigma_y = a(x)\ \tan\{b[c - d\ \ln(x)]\} \qquad (1.5)$$

where: a, b are constants of 465.12 and 0.01745 respectively and c, d are obtained from tables (which are not repeated here), according to the atmospheric stability.

The vertical dispersion coefficient is obtained by the power law expression:

$$\sigma_z = A(x)^B \qquad (1.6)$$

where A, B are coefficients depending on the stability and distance from the source.

The above-mentioned dispersion coefficients are modified accordingly to account for building wake effects, as well as for area and line sources simulations. When the stack height is less than the building height plus the lesser of the building height or width, downwash methods of Scire and Schulman (1980) are followed. Otherwise, the Huger and Snyder (1976) methods are used.

For the plume rise (Δh) calculations the ISCST2 uses the Briggs plume rise equations. The model accounts for stack-tip and building downwash, as well as for buoyant and momentum plumes. A detailed description of these formulas can be found in Volume II of the ISC user's guide (EPA, 1992).

The Vertical Term of the Concentration Equations

The vertical term (V) in Equations (1.3) and (1.4) describes the effects on ambient concentrations of the mixing height and plume rise. It is assumed that the plume is reflected at the earth's surface and at the top of the mixing layer. If the effective stack height (h_e) exceeds the mixing height, the plume is assumed to penetrate the inversion, and the ground-level concentrations are set to zero. The vertical term can be written as:

$$V = \exp\left[-\frac{(z_r - h_e)^2}{2\sigma_z^2}\right] + \exp\left[-\frac{(z_r + h_e)^2}{2\sigma_z^2}\right] + \sum_{i=1}^{\infty}\left\{\exp\left[-\frac{H_1^2}{2\sigma_z^2}\right] + \exp\left[-\frac{H_2^2}{2\sigma_z^2}\right] + \exp\left[-\frac{H_3^2}{2\sigma_z^2}\right] + \exp\left[-\frac{H_4^2}{2\sigma_z^2}\right]\right\} \qquad (1.7)$$

where:

h_e = $h_s + \Delta h$
H_1 = $z_r - (2iz_i - h_e)$
H_2 = $z_r + (2iz_i - h_e)$
H_3 = $z_r - (2iz_i + h_e)$
H_4 = $z_r + (2iz_i + h_e)$
z_r : receptor height
z_i : mixing height
h_s : stack height

The infinite term in Equation (1.7) accounts for the ground and mixing height reflections. This method is called the image method because the reflections are caused by imaginary sources below the ground and above the inversion (see Figure 1.4). The presence of the second reflecting barrier causes the need for the infinite series in Equation (1.7). However, this series converges rapidly, and more than five sums are seldom required.

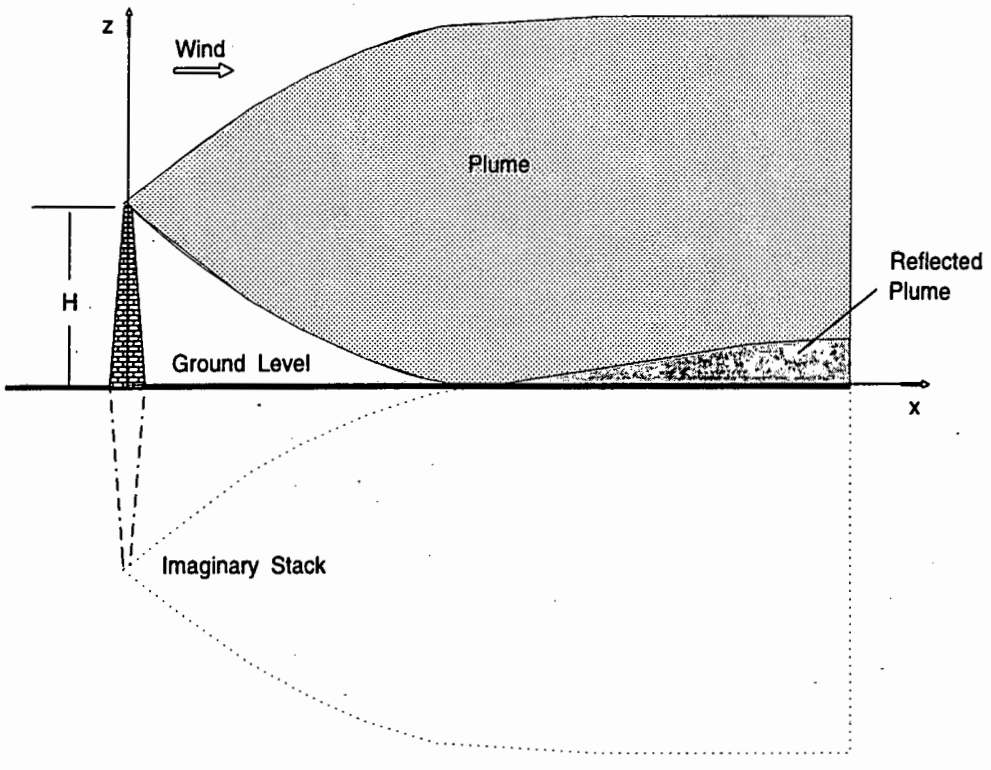

Figure 1.4 Illustration of a ground reflection simulated by the image method; i.e. an imaginary source, identical to the original one, is positioned at -H bellow the ground.

Yamartino, in order to reduce computational time at distant locations, proposed an approximation of the vertical term without loss of accuracy. The ISCST2 model adopts this method for downwind distances where the ratio σ_z/z_i is greater than or equal to 1.6. In this case the term V is obtained by:

$$V = \frac{\sigma_z\sqrt{2\pi}}{z_i} \tag{1.8}$$

1.7.4 Pollutant Decay and Velocity Profile

The decay term (D_c) in Equations (1.3) and (1.4) is a simple method to account for pollutant removal by physical processes. It takes into account the pollutant's half life $T_{1/2}$ (sec) to calculate the decay coefficient $\psi = 0.693/T_{1/2}$. The D_c term, for a downwind distance x, is obtained from:

$$D_c = \exp\left(-\psi\frac{x}{u_s}\right) \tag{1.9}$$

In an urban environment, the half life of sulphur dioxide is approximately 4 hours. Therefore, the urban mode of the ISCST model automatically assigns ψ the value of $4.8\text{x}10^{-5}$ s^{-1}.

The wind speed (u_s) at release height (h_s) is calculated with the power law equation from the measured wind speed (u_{ref}), at a reference height z_{ref} as:

$$u_s = u_{ref}\left(\frac{h_s}{z_{ref}}\right)^p \tag{1.10}$$

where p is the wind profile exponent.

The p parameter is a function of wind velocity and atmospheric stability. It can be provided externally by the user or can use the model's default values shown in Table 1.2. It should be noted that the power law method is less accurate than the wind profile obtained by the similarity theory but is a simple solution to the problem of wind variation with height.

Table 1.2 Wind profile exponent (p) values, as used by the default option in the ISCST2 model (EPA, 1992)

	Atmospheric stability				
	A-B	C	D	E	F
Urban p	0.15	0.20	0.25	0.30	0.30
Rural p	0.07	0.10	0.15	0.35	0.55

The urban options of the ISCST2 model were selected for the air pollution simulation of the Greater Cape Town region. The major objectives and scope of this simulation are outlined in the following section.

1.8 Scope and Aim of the Present Study

Air-quality related studies in the past have been focusing on the analysis of observational data. However, the spatial and temporal resolution of monitoring data is generally insufficient to represent the fate of the atmospheric pollutants, their dynamics and their response to perturbations. Only a well-tested and well-calibrated model is able to forecast the effect of pollution control strategies on ambient air-quality, in a cost-effective and reliable way.

The aim of the present study is to assess and evaluate the performance and applicability of a Gaussian plume model, such as the Industrial Source Complex 2, for the Greater Cape Town region. It is one of the first studies which attempts to quantify the pollution impact of all existing sources in the area.

The major objectives of this dissertation can be summarized as follows:

i) Examine and collect the available information necessary for a dispersion modelling study;

ii) Apply various methods to derive the meteorological parameters which are needed for modelling;

iii) Compile an emission inventory of all the major sources and source categories of the Greater Cape Town area;

iv) Apply the Industrial Source Complex Short Term 2 model to obtain hourly and daily pollution averages;

v) Evaluate the model performance at different locations and under different meteorological conditions;

vi) Highlight issues which need to be addressed in order to incorporate modelling in air-quality management for the Greater Cape Town region.

The required stages for the application and evaluation of the ISCST2 dispersion model, in relation to the above-mentioned objectives, are addressed in five separate chapters, as outlined below:

Chapter one introduces the rationale of dispersion modelling and addresses the issue of air-quality control strategies and dispersion modelling. It also provides a brief description of the model's main features and outlines the thesis' main objectives.

Chapter two describes the various methods which are used to calculate meteorological parameters for dispersion modelling. These parameters are then calculated from selected meteorological measurements. With this procedure, several data sets are analysed and prepared for input into the model.

Chapter three addresses the necessity for an accurate emission inventory and describes the methods utilised for the compilation of the inventory which is used in the present study. The findings of the fuel consumption and emissions in the Greater Cape Town region are summarised, according to source category and magisterial districts.

Chapter four analyses the model sensitivity to the various meteorological input parameters. The model evaluation is further assessed by cross-examination of the model predictions with observations at three monitoring sites. These predictions are also examined in terms of overall performance, as well as atmospheric condition and averaging period.

Chapter five summarises the basic findings and outlines the conclusions, as well as the recommendations which resulted from the present thesis.

In addition, several aspects of this study have been summarised in papers presented at the NACA conferences of 1993 and 1994 (Dracoulides and Dutkiewicz, 1993; Dracoulides, 1994).

Chapter TWO

AIR POLLUTION METEOROLOGICAL FACTORS

2 AIR POLLUTION METEOROLOGICAL FACTORS

2.1 Introduction

The atmosphere's air motion, as well as its turbulent condition, play an important role in air pollution modelling. The simulation of the different physical processes in the atmosphere is not an easy task. Usually, a model is designed to be appropriate for only specific atmospheric and landscape conditions. Over-simplified or unsuitable simulation of the atmosphere's physics could be the source of air pollution prediction errors. In ideal circumstances, the scatter in meteorological measurements, as caused by turbulence, dictates the degree of accuracy which models can obtain (Benarie, 1987; Fox, 1984). Therefore, there is an inherent uncertainty in the predictions, due to the random, stochastic nature of the turbulent atmospheric motion. The effect of the latter is so great that the magnitude of the stochastic fluctuations in predicted concentrations can, in some instances, reach the magnitude of the average concentration on the plume axis (Hanna, 1988). Meteorological properties near the earth's surface are very important, since most of the emitted pollutants are dispersed, transported and transformed in this vicinity (Seinfeld, 1986). These complicated processes are generally approached by simplifications such as the atmospheric stability class, the dispersion coefficients and the scaling of the atmospheric layer.

2.2 The Structure of the Planetary Boundary Layer

The first sublayer of the atmosphere, i.e. roughly the first 500 m, is called the planetary boundary layer (PBL) and governs the dispersion and transport of emitted pollutants. The main characteristic of this layer is the strong influence of the earth's surface on the layer's properties, such as the wind velocity, temperature profile and mixing height. Air motions within the PBL are influenced by frictional drag, moisture and energy exchange between the earth's surface and this layer.. This region of the atmosphere is also termed mixed layer, since shear-generated turbulence is sufficiently powerful to mix pollutants, as effective as the temperature gradient does. However, this is often not the case since under certain conditions the PBL becomes very stable, especially during night-time.

Turbulent diffusion primarily controls air mixing in the PBL. Molecular diffusion in this layer is significantly small. During day-time with clear skies turbulent diffusion can be greater than the molecular diffusion to the extent of seven orders of magnitude. The viscous effect caused by turbulence eddies is called eddy viscosity. This viscosity is not a permanent characteristic of the fluid, as opposed to density, but depends

upon the turbulent mixing of the fluid. The level of turbulence increases with wind speed, surface roughness and instability. It can be associated not only with mechanical features, but also with other elements, such as buoyant forces arising due to the surface's heat exchange with the PBL.

The Planetary Boundary Layer can be divided into three sublayers, according to their turbulence and structure characteristics:

- The laminar sublayer immediately adjacent to the ground is characterised by the prevailing molecular viscosities. Here turbulence is not fully developed and air flow is assumed to be laminar. The thickness of this layer is usually less than a centimetre and is equal to the roughness length z_0 (see Figure 2.1).

- The surface layer from z_0 to z_s has a depth of 10 to 100 m, which is the lowest 10% of the PBL (see Figure 2.1). Characteristic of the surface layer is that the momentum, heat and moisture fluxes are assumed to be constant with height. In this layer the Coriolis forces are taken to be negligible.

- The last sublayer is the Ekman layer and extends to a height of 300 to 1000 m, depending on the type of terrain and atmospheric condition. Deeper Ekman layer corresponds to a more irregular surface and an unstable atmosphere. Usually, the height of the PBL is restricted by an elevated temperature inversion at z_i with thickness d (see Figure 2.1). In the Ekman layer the wind speed and direction are governed by horizontal pressure gradients and shear stresses. Due to the Coriolis forces the wind direction tends to back with increasing height (in the southern hemisphere).

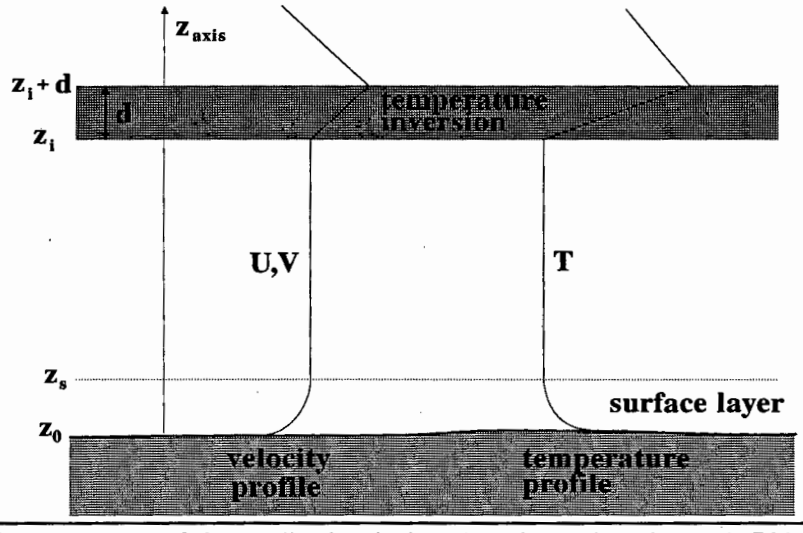

Figure 2.1 The structure of the well mixed planetary boundary layer (PBL).

The mixing potential, as well as the atmospheric properties controlling the dispersion and transport of pollutants, are categorised according to the turbulent condition of the PBL. When turbulence is vigorous the atmosphere is considered to be unstable. Stable conditions correspond to a low mixing stratified atmosphere. Under extremely stable conditions, there is a ground-based temperature inversion, and the depth affecting the dispersion of pollutants is the mixing height z_h or mixing layer. The z_h indicates the depth near the ground in which mixing is controlled by turbulence, and pollutants are likely to disperse within this height. In air pollution modelling the first elevated temperature inversion z_i and the z_h height are critical, since pollutants emitted lower than these heights will be trapped, producing high ground-level concentrations. Pollutants with effective release height above the inversion or mixing height are assumed not to contribute to the ground-level concentrations.

2.3 Atmospheric Stability

The turbulent condition of the lower atmosphere is primarily affected by the temperature profile. The lapse rate ($\Lambda = dT/dz$) of the atmosphere is the rate of temperature change with altitude. For adiabatic conditions, the lapse rate is symbolised by Γ and is described by the following equation.

$$\Gamma = \frac{g}{C_p} \qquad (2.1)$$

where C_p is the specific heat at constant pressure and g the acceleration of gravity.

The constant Γ denotes the dry adiabatic lapse rate. It defines the temperature change that a dry parcel of air would undergo if it moved adiabatically.

Since g=9.81 m s^{-2} and C_p=1004 J kg^{-1} K^{-1}, the dry adiabatic lapse rate is: Γ=9.8 °K km^{-1}

According to the relationship between the lapse rate Λ and the dry adiabatic rate, the atmospheric stability is defined as follows: (see Figure 2.2)

Unstable: $\Lambda > \Gamma$ corresponds to unstable atmosphere, where the lapse rate is termed superadiabatic.

Neutral: $\Lambda = \Gamma$ corresponds to neutral stability when the lapse rate is equal to the dry adiabatic value.

Stable: $\Lambda < \Gamma$ corresponds to stable atmosphere and the lapse rate is named subadiabatic.

In a superadiabatic atmosphere buoyancy forces enhance the vertical motion of the air. This means that a parcel of upward moving air is warmer than its surroundings and will continue to rise. Similarly, a parcel of air moving downward will be cooler than its surroundings and will continue to fall. This atmospheric condition is characterised as unstable. Under an unstable atmosphere air pollution mixing is favoured. When a parcel of air is moving under a neutral atmosphere it remains at its new position. Here vertical movement is not assisted or opposed by buoyant forces. Thus, the neutral stability neither favours nor disfavours atmospheric mixing. Under stable conditions the vertical movement of the air is suppressed by buoyant forces. Thus, any temperature change of an air parcel will cause it to rise or fall, but only for a short distance. When the subadiabatic rate is greater than the isothermal one, it is known as an inversion. The temperature gradient is positive, denoting a temperature profile increasing with height. Here buoyant forces strongly oppose the vertical displacement of air parcels. The atmosphere is very stable and characterised by horizontal stratification.

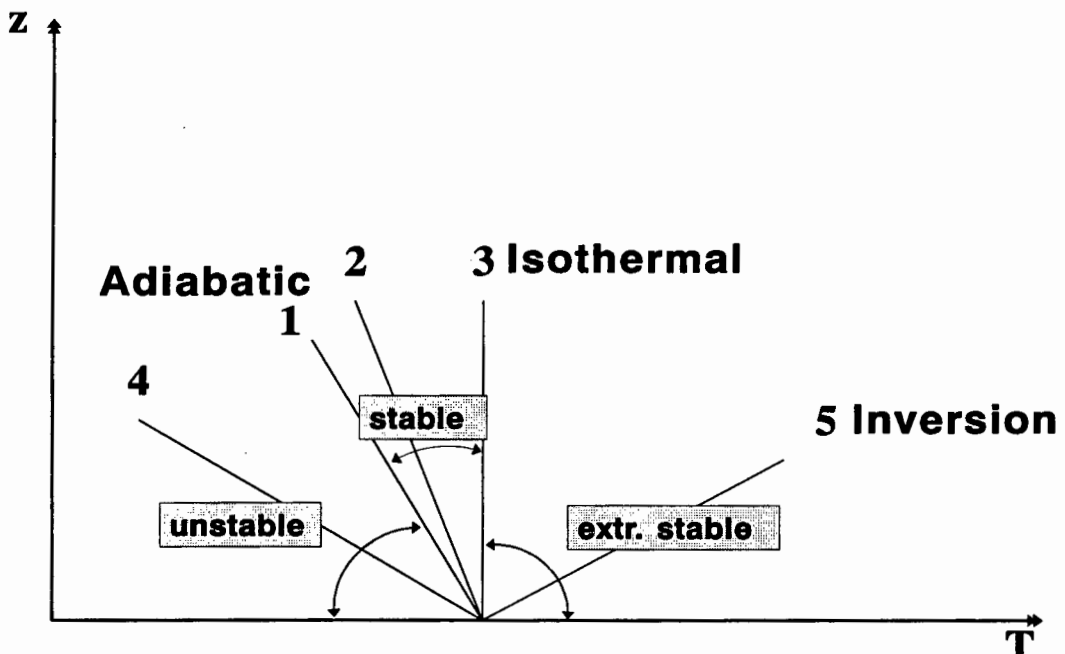

Figure 2.2 Atmospheric lapse rates. (1) Dry adiabatic lapse rate Γ=9.8 °K km^{-1}. (2) Subadiabatic (stable). (3) Isothermal corresponds to stable atmosphere. (4) Superadiabatic (unstable). (5) Inversion, temperature increase with height (very stable).

Atmospheric stability is one of the basic input parameters of dispersion modelling. The lateral (σ_x) and vertical (σ_z) dispersion can be quantified according to the turbulent condition (stability) of the atmosphere. Several methods, which are described bellow, exist for the atmospheric stability classification.

2.3.1 Pasquill Stability Classification

In order to categorise the turbulent state of the atmosphere, Pasquill (1961) introduced an empirical method which was later modified by Turner. This method is based on routinely available meteorological observations, such as wind speed, wind direction, sun insolation and opaque cloud cover. The atmospheric conditions are divided into six stability classes ranging from A to F (see Table 2.1).

The Pasquill stability classes (P) are based on experimental observations and do not account for the vertical structure of the PBL. They are appropriate for flat terrain and distances less than 10 kilometres between the source and the receptor (Weil, 1988). In addition, the P system is biased towards the neutral stability class, while higher up, the PBL can be stable or unstable (van Ulden and Holtslag, 1985; Weil and Brower, 1984). Nevertheless, the Pasquill scheme (P) is widely used due to its simplicity and the uncomplicated meteorological measurements employed.

The P classes can be also obtained using more complicated measurements, such as the sensible heat flux (Q_s), surface roughness length (z_0) and wind speed. Sutherland et al. (1986) developed a semi-empirical equation to determine the P classes for stable, neutral and unstable atmospheric conditions corresponding to surface roughness length from 0.1 to 100 cm. The Pasquill (P) atmospheric stability as a function of the modified Kazanski-Monin parameter (μ'), is written as:

$$P = A\, e^{\mu'} \qquad \textbf{(2.2)}$$

where A is a constant of 3.6 and (μ') the modified Kazanski-Monin parameter (see Appendix A). Knowing the modified Kazanski-Monin boundary values between stability classes for a certain location, the atmospheric condition could be classified by comparing the calculated (μ') to these boundary values.

The Pasquill stability classes can be also obtained directly from μ' by substituting it in Equation (2.2). The boundary values defining the transition between the successive P stability classes when derived from the Kazanski-Monin scheme, are slightly different to the ones obtained from the Golder nomograms. (Tagliazucca and Nanni, 1983).

Table 2.1 Meteorological conditions according to Pasquill dispersion classes:
A: extremely unstable B: moderately unstable
C: slightly unstable D: neutra
E: slightly stable F: moderately stable

	Insolation / Cloud Cover	Wind speed ($m\ sec^{-1}$)				
		<2	2 to 3	3 to 5	5 to 6	>6
Day	Strong*	A	A-B	B	C	C
	Moderate†	A-B	B	B-C	C-D	D
	Slight	B	C	C	D	D
Day or Night	Overcast	D	D	D	D	D
Night	>4/8	-	E	D	D	D
	≤4/8	-	F	E	D	D

* Strong insolation corresponds to solar elevation more than 60° above the horizon or insolation greater than 700 W m^{-2}.

† Moderate insolation corresponds to solar elevation of 35° to 60° or insolation between 350 and 700 W m^{-2}.

2.3.2 Richardson and Bulk Richardson Number Stability Classification

Another means of determining the atmospheric state is via the Richardson number (Ri):

$$Ri = \frac{g}{T} \frac{\frac{\partial \theta}{\partial z}}{(\frac{\partial \bar{u}}{\partial z})^2} \qquad (2.3)$$

This number postulates the ratio of the rate at which turbulence is consumed by buoyancy forces over the rate of produced turbulence by wind shear. T is the surface temperature, $\partial\theta/\partial z$ the potential temperature gradient and $\partial\bar{u}/\partial z$ the wind shear. The atmosphere is categorised according to the Richardson number as follows:

Unstable	Neutral	Stable
Ri < 0	Ri = 0	Ri > 0

Nevertheless, the Richardson number is often not available, since it requires accurate temperature and wind measurements at two levels (Irwin and Binkowsky, 1981).

Golder (1972) used the bulk Richardson number (Ri_B)

$$Ri_B = \frac{g}{T}\frac{\frac{\partial\theta}{\partial z}}{u^2}\bar{z}^2 \qquad (2.4)$$

to determine the atmospheric stability, since it requires wind measurements only at one level, and therefore, can be determined more accurately with less computational effort and less sophisticated instruments. Here $\bar{z}$ is taken to be the geometric mean height ($\sqrt{z_1 z_2}$), whilst z_1 and z_2 are the two levels where temperature is measured, g the acceleration of gravity and u the surface wind speed.

The relationship between the Ri_B number and the P stability categories was demonstrated in two nomograms for stable and unstable conditions by Zoumakis and Kelessis (1991) (see Figure 2.3).

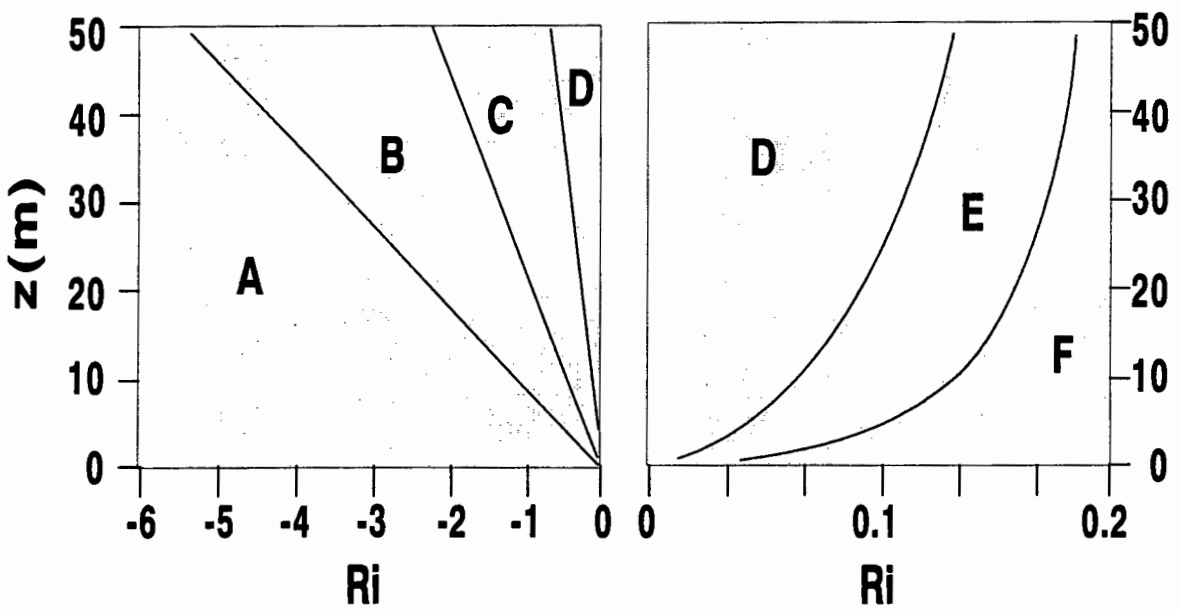

Figure 2.3 Atmospheric stability categories according to the bulk Richardson number (Ri_B), as a function of height (z) (Zoumakis and Kelessis, 1991)

The potential temperature gradient is needed in order to calculate the bulk Richardson number. This gradient measures the divergence of the actual temperature profile from the adiabatic one and is approximated by:

$$\frac{\partial \theta}{\partial z} \approx \frac{\partial T}{\partial z} + \Gamma \qquad (2.5)$$

where Γ is the dry adiabatic lapse rate.

2.3.3 Monin-Obukhov Stability Classification

According to the Monin-Obukhov similarity theory for steady state conditions and horizontal homogeneity, the Monin-Obukhov length is defined by:

$$L = -\frac{u_*^3 C_p \rho T}{kgH} \qquad (2.6)$$

where u_* is the friction velocity,
C_p the specific heat coefficient at constant pressure,
ρ is the air density,
T ambient temperature,
k the von Karman constant for air,
g acceleration of gravity and
H the sensible heat flux.

The Monin-Obukhov length represents the height above the earth's surface at which the production of turbulence by both buoyant and mechanical forces is equal. This length provides a measure of the stability in the atmospheric surface layer (see Table 2.2).

Table 2.2 Atmospheric stability classes based on the Monin-Obukhov length*.

L	L range	Atmospheric condition
Small negative	-100m < L < 0	Very unstable
Large negative	-10^5 m ≤ L ≤ -100m	Unstable
Very large (>0 or <0)	$\|L\| > 10^5$ m	Neutral
Large positive	10 m ≤ L ≤ 10^5 m	Stable
Small positive	0 < L < 10 m	Very stable

* Adapted by Seinfeld (1986)

Golder (1972) presented the relationship between the Monin-Obukhov length and the Pasquill stability classes as a function of the surface's roughness length. Golder's nomograms were used by Singal et al. (1989) to derive the inverse Monin-Obukhov length (1/L) from which the boundaries between the successive Pasquill-Gifford stability categories could be defined. These values corresponded to a surface with roughness length 13 cm (see Table 2.3). For surfaces with different roughness lengths, the boundary inverse Monin-Obukhov lengths can be obtained by a nomogram found in Tagliazucca and Nanni (1983). These boundaries for a typical urban environment with roughness length 50 cm are also shown in Table 2.3.

Table 2.3 The boundaries between the successive stability classes, as defined by the inverse Monin-Obukhov length for a surface with roughness length 13 cm* and 50 cm.

		Stability boundaries				
	z_0(cm)	A/B	B/C	C/D	D/E	E/F
1/L(m^{-1})	13	-0.092	-0.031	-0.007	0.006	0.032
Ri_B†	13	-0.323	-0.118	-0.027	0.024	0.089
1/L(m^{-1})‡	50	-0.0721	-0.0179	-0.0036	0.0030	0.0164

* Adapted from Singal et al. (1989)

† The bulk Richardson number is for temperature measurements at two levels 1.3 m and 52 m and wind measurements at 56 m.

‡ Values obtained from Tagliazucca and Nanni (1983) nomogram for surface roughness length 50 cm.

Using simple meteorological measurements the Monin-Obukhov length can be calculated as follows (Venkatram, 1988):

$$L = Au_*^2 \tag{2.7}$$

where

$$A = \frac{T}{g\theta_* k} \tag{2.8}$$

The potential temperature θ_* is

$$\theta_* = 0.09(1 - 0.5\,C^2) \qquad \textbf{(2.9)}$$

where C is the fractional cloud cover and $k \simeq 0.4$ the von Karman constant.

Van Ulden and Holtslag (1985) introduced another equation for the potential temperature θ_*, based on the energy exchange between the atmosphere and the earth's surface (see Appendix A).

Using the energy balance to determine the potential temperature and solving Equations (2.7) and (2.9) iteratively, we can obtain the friction velocity u. and the Monin-Obukhov length L from simple meteorological observations.

2.3.4 Wind Direction Standard Deviation and Temperature Difference Methods

When wind turbulence measurements are available it is preferable to estimate the vertical and lateral dispersion coefficients (Hanna, 1980), as well as the stability classes, from the standard deviation of the vertical and lateral wind component direction fluctuations, σ_θ (sigma theta) and σ_ϕ (sigma fi). The association of the P stability classes with σ_θ and σ_ϕ standard deviations is shown in Tables 2.4 and 2.5. Both measures depend greatly on the sampling and averaging times (Seinfeld, 1986). Sigma theta is usually measured at a 10 m level, using sampling times of not less than 10 minutes (Mitchell, 1982). Slade (1968) produced two nomograms for the σ_θ and σ_ϕ vertical profiles up to 130 m height. He used sampling times of approximately 10 minutes and averaging times of the order of a few seconds. When direct turbulence measurements are unavailable, Wratt (1987) showed how to calculate σ_θ and σ_ϕ using wind measurements and temperature profiles from meteorological towers.

Another method of determining the stability class of the atmosphere from direct turbulence measurements, is by examination of the standard deviation of the lateral and vertical wind fluctuations, σ_v and σ_w (see Table 2.5).

The turbulent condition of the atmosphere can be also tabulated, using the temperature gradient ($\Delta T/\Delta z$) of the first 100 m above the earth's surface (USNRC, 1972). Table 2.4 shows the boundaries of the successive stability categories for the temperature difference (delta T) method.

Table 2.4 Limits of atmospheric stability classes for the sigma theta (σ_θ), sigma fi (σ_ϕ) and delta T methods*.

Stability class	σ_θ (10m), degrees	σ_ϕ (10m)† degrees	$\Delta T/\Delta z$ (C°/100m)
A	$22.5<\sigma_\theta$	$14.8<\sigma_\phi$	$\Delta T/\Delta z<-1.9$
B	$17.5<\sigma_\theta<22.5$	$9.1<\sigma_\phi<14.8$	$-1.9<\Delta T/\Delta z<-1.7$
C	$12.5<\sigma_\theta<17.5$	$6.2<\sigma_\phi<9.1$	$-1.7<\Delta T/\Delta z<-1.5$
D	$7.5<\sigma_\theta<12.5$	$3.2<\sigma_\phi<6.2$	$-1.5<\Delta T/\Delta z<-0.5$
E	$3.75<\sigma_\theta<7.5$	$1.6<\sigma_\phi<3.2$	$-0.5<\Delta T/\Delta z<1.5$
F	$2.0<\sigma_\theta<3.75$	$1.0<\sigma_\phi<1.6$	$1.5<\Delta T/\Delta z<4.0$
G	$\sigma_\theta \leq 2.0$	$\sigma_\phi \leq 1.0$	$\Delta T/\Delta z \geq 4.0$

* Adapted from Sedefian and Bennett (1980)

† Values taken from a figure in Lyons and Scott (1990) as adapted from Slade (1968).

Table 2.5 Limits of atmospheric stability classes for the sigma theta (σ_θ), sigma fi (σ_ϕ), σ_v and σ_w methods*.

Stability class	σ_θ (10m), degrees	σ_ϕ (120m) degrees	σ_v (10m)	σ_w (10m)
A	$22.5<\sigma_\theta$	$12<\sigma_\phi$	$0.97<\sigma_v$	$1.0<\sigma_w$
B	$17.5<\sigma_\theta<22.5$	$10<\sigma_\phi<12$	$0.85<\sigma_v<0.97$	$0.9<\sigma_w<1.0$
C	$12.5<\sigma_\theta<17.5$	$7.8<\sigma_\phi<10$	$0.82<\sigma_v<0.85$	$0.8<\sigma_w<0.9$
D	$7.5<\sigma_\theta<12.5$	$5<\sigma_\phi<7.8$	$0.63<\sigma_v<0.82$	$0.5<\sigma_w<0.8$
E	$3.5<\sigma_\theta<7.5$	$2.4<\sigma_\phi<5$	$0.38<\sigma_v<0.63$	$0.2<\sigma_w<0.5$
F	$1.75<\sigma_\theta<3.5$	$1.2<\sigma_\phi<2.4$	$0.18<\sigma_v<0.38$	$0.1<\sigma_w<0.2$
G	$\sigma_\theta \leq 1.75$	$\sigma_\phi \leq 1.2$	$\sigma_v \leq 0.18$	$\sigma_w \leq 0.1$

* From Barclay (1993)

2.4 Applicability of the Stability Schemes for Dispersion Modelling

Through the years there have been many arguments as to the applicability and accuracy of the different stability classification schemes. The main shortcoming of the P method is based on the limitations dictated by the experimental derivation of this scheme. It is biased towards neutral stability and does not account for the

vertical structure of the PBL which it attempts to describe. Nevertheless, the P classification scheme is one of the most frequently used by dispersion models. This is due to its simplicity, as well as the capability of using routinely measured meteorological data from local weather stations.

The Metropolitan Tracer Experiment data analysed by Draxler (1987) revealed that the use of Pasquill-Gifford dispersion curves provided the best results when used with stability categories defined by the wind-direction fluctuation method. Nevertheless, for distances greater than 15 kilometres the Pasquill-Turner method performed equally well (Draxler, 1987).

Sedefian and Bennet (1980) compared different turbulence classification schemes, including the sigma theta, delta T, Richardson and Pasquill methods. Their results indicated a significantly poor correlation between the methods used on an hourly basis. Therefore, the atmospheric turbulence classification could result in considerable differences in concentration estimates depending on the stability scheme used.

Another source of dispersion prediction errors originates from utilising meteorological data of a weather station which, due to its off-site location, does not represent the studied area (Draxler, 1987). Prediction errors are observed especially in regions with complex terrain or close to coastal zones, where the wind direction is likely to shift significantly with height and distance. Therefore, there is a possibility of erroneous evaluation of the peak concentration sector and the dispersion parameters, as well as the concentration averages (Mitchell, 1982). Dispersion models which implement plume segmentation could solve the wind shift problem. This segmentation along the wind direction requires the use of a more detailed meteorological network and would improve the dispersion predictions, especially in source-receptor distances of more than 20 kilometres (Draxler, 1987).

2.5 Semi-empirical Parameters of PBL Used in Dispersion Modelling

Meteorological parameters for the planetary boundary layer are not often available from routine atmospheric measurements. These parameters can be estimated by semi-empirical methods and formulations from standard meteorological information available for the studied area (van Ulden and Holtslag, 1985). Venkatram (1988) demonstrated the estimation of the meteorological variables for use in dispersion modelling, utilising the same type of information used in the Pasquill-Gifford classification scheme.

2.5.1 The Roughness Length (z_0)

The roughness elements of a homogeneous or heterogeneous terrain, such as buildings, trees or bushes, decrease the wind momentum and affect the mechanically produced turbulence and wind profile (Irwin, 1979). These characteristics are represented by an "effective" roughness length z_0 which is generally a function of surface roughness. The parameter z_0 is affected by the wind direction (when different terrain features surround the region), and the wind speed. Typical values of z_0 are shown in Table 2.6, or are approximated by:

$$z_0 = \epsilon/30 \qquad \textbf{(2.10)}$$

where ϵ is the average height of the obstacles of the region.

Table 2.6 Roughness length (z_0) for various surfaces.

Surface type	Roughness length (m)
Sea, sand and snow	0.0002
Short grass	0.008 - 0.03
Long grass	0.02 - 0.06
Agricultural crops	0.04 - 0.18
Continuous bushland	0.35 - 0.45
Pine forest	0.8 - 1.6
Tropical forest	1.7 - 2.3
Dense low buildings	0.4 - 0.7
Regularly built city	0.7 - 1.5

With the use of wind measurements at two levels: z_1 and z_2 and assuming a logarithmic wind profile, the roughness length z_0 can be calculated by (Singal et al., 1989):

$$z_0 = \exp\left[\frac{(\frac{u_2}{u_1} lnz_1) - lnz_2}{\frac{u_2}{u_1} - 1}\right] \qquad \textbf{(2.11)}$$

2.5.2 The Mixing Height (z_h)

A parameter of great importance in air pollution modelling is the mixed layer at a height z_h. The pollutants emitted in the planetary boundary layer are likely to disperse within this layer. The depth of the mixed region is governed by properties such as wind speed, the atmospheric turbulent state and the heat flux to and from the earth's surface. Under unstable convective or neutral conditions the z_h is generally equal to the PBL height (z_p), or 10 per cent greater than z_p in order to account for entrainment at the top of the layer. Usually, under these conditions an elevated temperature inversion might exist at height z_i which, in these cases, would indicate the mixing layer.

2.5.2.1 Significant Levels

One technique to evaluate the z_h is by utilising radiosonde sounding records. Assuming the air to be an ideal gas, from the pressure height equation we obtain:

$$\frac{dp(z)}{dz} = \frac{pgM_a}{RT} \qquad \textbf{(2.12)}$$

We can integrate Equation (2.12), with an average constant temperature (T) between two heights, to yield

$$\Delta z = 29.28\, T \ln\left(\frac{p_0}{p}\right) \qquad \textbf{(2.13)}$$

where p_o is the pressure at ground level. With Equation (2.13) and the temperature and pressure values from the sounding's significant levels we can calculate the height of an existing elevated temperature inversion.

2.5.2.2 Holzworth Procedure

Holzworth (1972) identified the mixing height by extrapolating an adiabat from the maximum afternoon surface temperature to the morning temperature profile. The z_h is then taken as the intersection of the extrapolated and the morning temperature profiles. The adiabatically extrapolated temperature is the potential temperature (θ.) which can be written as:

$$\theta_* = T\left(\frac{P}{P_0}\right)^{\frac{(\gamma-1)}{\gamma}} \qquad (2.14)$$

where T is the measured temperature, P the measured pressure, γ the ratio of the specific heat at constant pressure over that at constant volume and P_0 a reference pressure usually chosen to be the 1000 mb. Therefore, the potential temperature is also given by:

$$\theta_* = T\left(\frac{1000}{P}\right)^{\left(\frac{R}{C_p}\right)} = T\left(\frac{1000}{P}\right)^{0.287} \qquad (2.15)$$

The potential temperature is firstly compared to the potential temperature of the successive temperatures of the sounding. The intersection between the two profiles is obtained by interpolation between the two successive levels at which the surface maximum potential temperature is first larger and then smaller compared to the potential temperature of the sounding levels. Then the interpolated temperature and pressure are used in the thickness Equation (2.13) in order to yield the mixing height.

2.5.2.3 Heat Exchange

The predawn values of the urban mixing height can be calculated by an empirical expression involving the lapse rate and the intensity of the urban heat island (Ludwig et al., 1970):

$$z_h = \frac{29.3\ T\ Q^{0.25}\left(0.298\frac{dT}{dP} - 0.0633\right)}{P\frac{dT}{dP} - 0.287\,T} \qquad (2.16)$$

Under a fully stationary neutral boundary layer the mixing height is given by (van Ulden and Holtslag, 1985):

$$z_h = \frac{c_n u_*}{f} \qquad (2.17)$$

where f is the Coriolis parameter, u_* the friction velocity and c_n=0.2 an empirical coefficient.

Under stable conditions a surface temperature inversion usually exists with thickness z_p (the thickness of the PBL layer). In this case the mixed layer z_h is much smaller than z_p and can be obtained by the following equation (Venkatram, 1988):

$$z_h = c_s \left(\frac{A u_*^3}{f} \right)^{1/2} \tag{2.18}$$

where f is the Coriolis parameter and u_* the friction velocity. The empirical coefficient $c_s \simeq 0.4$ is based on observations and is a function of the latitude and time of day (Garratt, 1982). The term A can be obtained from Equation (2.8) and the friction velocity u_* from Appendix A.

San José (1991) presented an equation for the unstable (L<0) mixed layer depth based on simple meteorological data over a mast. The unstable conditions were categorised as three classifications shown in Table 2.7. The expression for the height is:

$$z_h = |L| \left(\frac{1.3}{\alpha'} \right)^{\frac{1}{b'}} \left(\frac{1+3Q_f}{|L|} \right) \tag{2.19}$$

where the Q_f is a reduced sensible heat flux given by

$$Q_f = Q_s[1 - (pQ_s^2 + qQ_s)] \tag{2.20}$$

p=-10^{-5}, q=4x10^{-3} and Q_s the surface sensible heat flux obtained by

$$Q_s = -\theta_* \rho C_p u_* \tag{2.21}$$

The coefficients α' and b' used in Equation (2.19) are taken from Table 2.7, according to three atmospheric classifications.

From the above it is possible to evaluate the mixing height under all atmospheric conditions. In practice, however, an elevated inversion exists even when the atmosphere could be characterised as neutral or unstable. In these cases the mixing height is limited by the elevated inversion. For high wind speeds and low potential temperatures the Monin-Obukhov length becomes very large, thus, creating very large z_h values when the mixing height is calculated by Equation (2.17). Therefore,

these values should be limited by (2.18). The condition to be examined for this limitation is $|uJ(Lf)|<4$.

Table 2.7 Atmospheric categories for the parameters a' and b' used for the prediction of the unstable mixed layer depth*.

Class	L	a'	b'
A	-12 < L < -1	0.79961	0.32702
B	-40 < L < -12	0.80181	0.32989
C	L < -40	0.83411	0.37294

* Adapted from San José (1991).

The depth of the diurnal and nocturnal mixed layer can also be modelled from more complicated direct measurements of atmospheric properties, such as the temperature profile, wind speed and radiation fluxes. Melas (1990) addressed the limitations of estimating the mixing height using a Doppler sodar. Under convective atmospheric conditions, the sodar mixing height estimates had good agreement with measured values. A numerical model for the determination of the nocturnal stable boundary layer utilising a radiation scheme, is illustrated in Tjemkes and Duynkerke (1989). With the use of the one-dimensional equations of heat, kinetic energy and turbulence, the diurnal mixed layer heights can also be derived (Rayner and Watson, 1991).

Although the mixing height and the temperature inversion height are of basic importance to the meteorological input of an air pollution model, there is a low correlation between the mixing heights and the maximum hourly pollutant concentration. Pollution concentrations were found by Aron (1983) to correlate better with other parameters, such as height and temperature of the inversion's base and top, the previous day's concentration and the pressure gradient.

2.6 General South African Weather Patterns and Cape Town Meteorological Characteristics

Synoptic weather conditions have a strong influence on the local meteorological parameters used for dispersion predictions. The weather patterns over the South African subcontinent can be categorised into four typical synoptic maps, according to the resulting meteorology over the Cape Town region (see Figure 2.4). Usually during summer a ridging anticyclone forms over the South Atlantic, producing high south easterly winds (Figure 2.4 (a)). The atmosphere is well mixed and high in

turbulence, thus offering a good dilution potential for air pollutants. Figure 2.4 (b) displays a typical winter pre-frontal system which is associated with northerly air drainage flows, low temperatures and overcast conditions. The formation of a high pressure system over the western Cape, in association with another high over Natal and a cold front over the west coast, result in Berg wind recirculations over the western coastal area (c). Berg winds are more common during late winter and early spring (Preston-Whyte and Tyson, 1988). This pattern has been found to be associated with air pollution episodes over the Cape Town region (Jury et al., 1990). The last weather map (d) depicts stagnant air flow conditions produced by an anticyclone over the western Cape. This high pressure system produces light winds which frequently change direction. Under these conditions the subsiding air is warmed by compression, often establishing an elevated temperature inversion. The combination of light winds with a temperature inversion result in a high potential for air pollution episodes, as the atmosphere does not have adequate energy to dilute the pollutants and the inversion acts as a "lid" at the top of the planetary boundary layer.

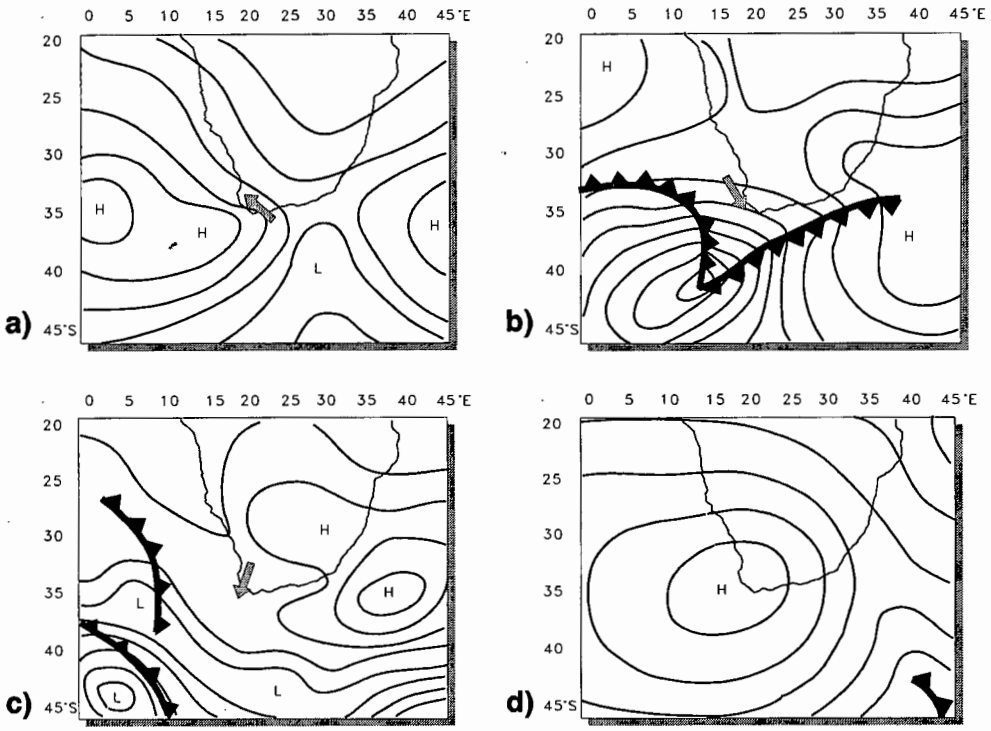

Figure 2.4 A schematic illustration of simplified weather maps according to the resulting winds over the Greater Cape Town: (a) high south easterly winds, (b) northerly air drainage flows, (c) Berg wind circulation over the west coast and (d) calm conditions with light variable winds.

Figure 2.5 (a), (b) shows the average base height of the subsistence inversions over South Africa during the winter and summer periods. It is evident how the semipermanent anticyclone over the South Atlantic and the elevated central plateau influence the base heights. The inversion bases decrease from over 2000 m in the interior to approximately 1000 m at the west coast. The monthly average heights of the first elevated inversion over Cape Town vary little throughout the year and their frequency of occurrence is approximately 65 per cent of the total (see Figure 2.5 (c)). A typical example of the averaged winter and summer subsidence inversion heights at D. F. Malan airport (Keen, 1979) is illustrated in Figure 2.5 (d). It is evident that due to low nocturnal surface temperatures during the winter, the subsidence inversions exist at an average of 600 m above sea level (a.s.l.), whilst in summer they rise to 1800 m (a.s.l.).

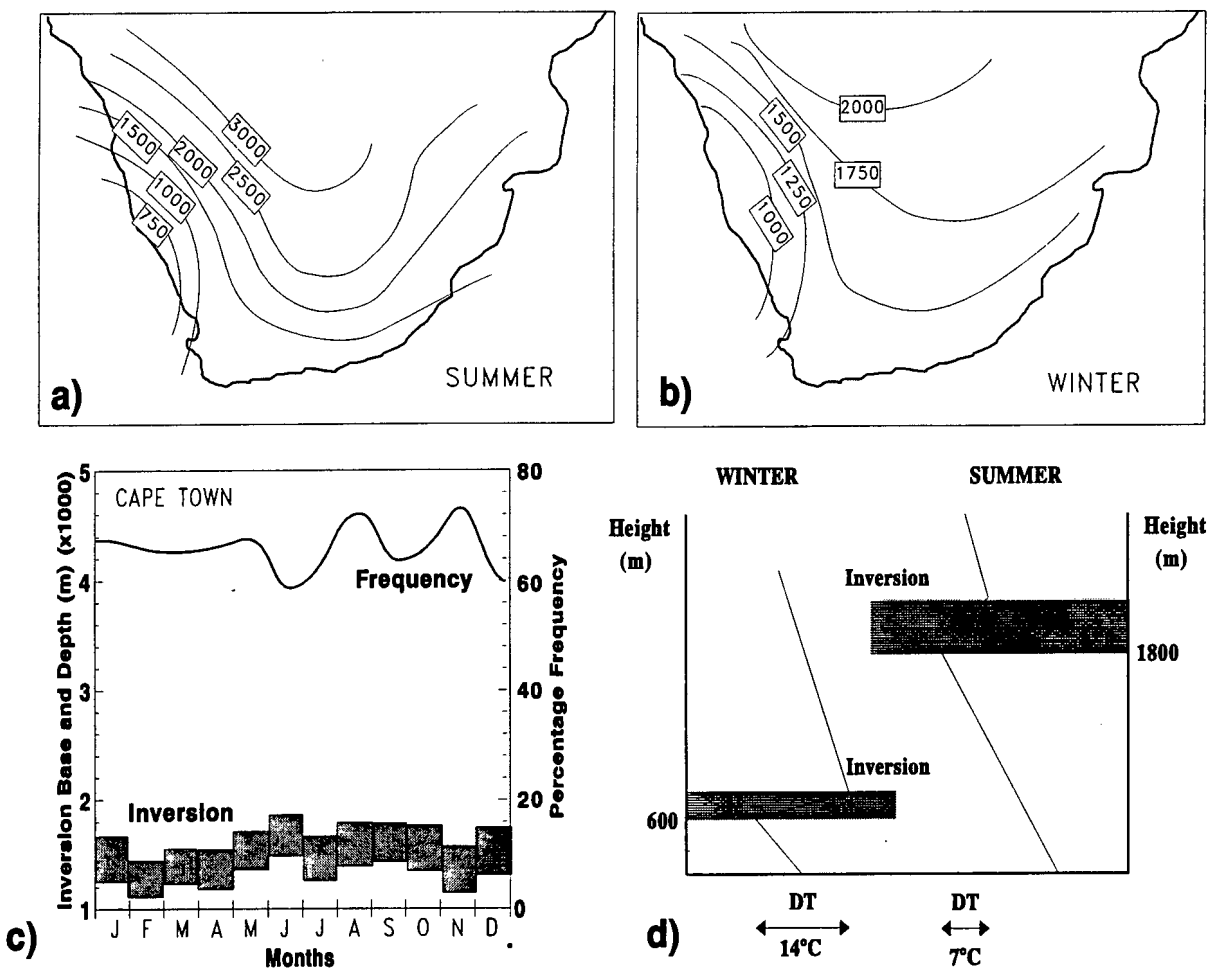

Figure 2.5 First elevated temperature inversion: (a) winter period, (b) summer period, (c) monthly average base height, depth and frequencies at Cape Town (after Preston-Whyte and Tyson, 1988) and (d) a typical example of averaged winter and summer subsidence inversions at D. F. Malan airport (data adapted from Keen, 1979).

2.7 Greater Cape Town Topographical Features

The Greater Cape Town area is situated in a coastal environment with complicated meteorology as a result of two opposing sea-land interfaces — that on the Atlantic and that on the False Bay. The effect of the two oceans during fine weather with low wind speeds occasionally leads to temperature inversion conditions in the coastal areas. However, during the winter the penetration of the sea breezes is seldom more than two to three kilometres. It is also considered unusual for the land breeze to last for more than two or three hours after sunrise.

In addition to the sea breeze situation there is also the effect of Table Mountain which, with a height of 1000 metres and with a shear face, has a significant effect on the air circulation in its vicinity. The effect of the mountain is so great that wind directions can vary by 180° within a vertical distance of 100 metres. In spite of these topographical effects it is possible to subdivide the area into a number of zones where classical diffusion equations may be expected to apply. These zones will be affected by the wind direction.

Surface temperature inversions over Cape Town have been found to correlate 70 per cent with high pollutant concentrations (Jury et al., 1990). They extend up to the 500 m level with a mean strength of 11° C. The top of a surface inversion and the base of an elevated inversion designate the height of the planetary boundary layer. However, this height, as mentioned earlier, is not always the mixing height used in dispersion modelling. The mixing height during a surface inversion is much smaller than the height of the PBL. Under surface inversion conditions, the latter is designated as the depth of the inversion layer. Under a typical nocturnal stable atmosphere the PBL height can be z_p=500 m but the mixing height only $z_h \simeq 100$ m. A meteorological study during several brown haze episodes in Cape Town indicated the association of the meteorological parameters with the high air pollution concentrations (Barclay, 1992).

2.8 Greater Cape Town Meteorological Features

Whilst the moderate to strong southeast wind in summer and the northwest wind in winter result in a strong mixing and thus low pollutant concentrations, low wind conditions and calm episodes give rise to potential high concentration episodes. An examination of several Cape Town air pollution episodes show that there is a strong surface inversion, starting as low as 100 metres and gradually increasing as the day progresses. Typically, in the greater Cape Town region the nocturnal surface inversions are between 100 m and 300 m deep, with a second elevated inversion at about 1400 m (Keen, 1979). This characteristic is liable to result in high ground level concentrations, as buoyant plums might penetrate the first inversion but they will be restricted by the second elevated inversion.

The vertical wind profile exhibits shear zones with opposite winds at higher levels, as a result of the topographic influences. These influences occur within 5 km of the peninsula mountains and often produce air channelling and acceleration of the low level winds. Under northerly winds, and far from Table mountain under southerly winds, the wind profile is fairly normal.

Sea breeze recirculation systems are developed along the west coast and False Bay. They are very important features, as they tend to recirculate and accumulate the pollutants emitted along the shorelines. Sea breezes occur approximately 50 to 60 times between September and May during the early morning hours (Keen, 1979). Pollutants emitted along the coastal zone first travel toward the interior following the sea breeze inflow. Then they are elevated to meet the outflow layer with seaward direction, where above the sea they reenter the inflow layer to close the circle and travel again inland. Under these conditions pollution is accumulated, especially beyond 2 to 3 km from the coast as a result of the recirculation pattern and due to the fumigation of the pollutants over the coast. However, heavy particles (>5 μm) are expected to fall-out above the sea as they are forced to descend, in order to reenter the inflow layer.

2.9 Collected Meteorological Data for the Study

The ISCST2 dispersion model requires an external file with meteorological parameters such as the wind direction, wind velocity, mixing height, stability category and ambient temperature. The mixing height and atmospheric stability are not readily available from weather bureau stations and have to be calculated. Meteorological pre-processors such as the EPA's RAMMET are usually used for these calculations.

In the present study several methods, including the ones used by some pre-processors, were utilised in order to calculate the stability category and mixing height as well as to assess their effect on the model accuracy. The original meteorological data for the years 1991 and 1992 were collected from D. F. Malan airport. The meteorological parameters of the year 1992 were selected for the particular purpose of including the Goodwood monitoring station in the evaluation. The Goodwood site began functioning only after the second half of 1992. This meant that the observed calculations were only available for the 2nd half of 1992. Thus, the meteorological information had to be restricted to the same period.

The data included hourly measurements of the wind direction and velocity, ambient temperature, cloud cover and the significant and standard pressure levels of sounding. Table 2.8 shows the selected days which were used for the ISCST2 evaluation. A total of 1272 and 936 hours were selected from the years 1991 and 1992 respectively. The 1991 data set consisted of 16 summer and 37 winter days.

All hours of the 1992 set belonged to the winter period. It should be indicated that the use of a continuous string of consecutive days was impossible, due to inconsistencies in the available data.

Table 2.8 The selected days for the evaluation of the ISCST2 model.

	Number of Days for Each Month					
	Febr.	June	July	August	Sept.	Total days
1991	16	11	15	11	—	53
1992	—	7	14	7	11	39

The D. F. Malan meteorological data sets were utilised for the calculation of the atmospheric stability and mixing height. The methods for the atmospheric stability computation were the Pasquill scheme, the inverse Monin-Obukhov length (1/L) and the Kazanski-Monin parameter ($\mu\sin\phi$). The friction velocity (u_*) was estimated, from one point meteorological observations, using an iteration procedure described in Appendix A. Stability schemes such as the wind direction standard deviation, as well as the temperature gradient methods were unable to be utilised, due to lack of direct turbulence observations and only one point of ambient temperature measurements.

Estimations of the mixing height were made utilising the significant pressure levels obtained twice a day from D. F. Malan sounding. A sine function interpolation scheme was employed for the hourly mixing heights on the basis of the early morning and afternoon mixing heights (see Figure A1.1 in Appendix A). The first method to calculate the morning and afternoon heights was based on the pressure equation. The second utilised the Holzworth procedure. The latter method is also used by the EPA's meteorological preprocessor RAMMET. The third procedure utilises different empirical equations corresponding to the atmospheric condition, and is based on the heat exchange between the earth's surface and the atmosphere. Combining the above methods, a total number of nine data sets were prepared as input to the model. Table 2.9 shows the assigned codenames for each one of the combinations.

The composite temporal variations of the stability classes produced by the three stability methods are depicted in Figure 2.6. This illustrates the relationship between the stability methods when applied to the same meteorological data (i.e. 53 selected days of the year 1991). It is evident that the Pasquill scheme generates more stable conditions at all hours and has the narrowest range (Figure 2.6). This could be explained from the fact that Pasquill method is biased towards the neutral (D) stability. The greatest discrepancies, between the Pasquill and the other two

methods, occur from two hours after the sunset to two hours before sunrise and during the unstable hours of the afternoon (i.e. 12h00 - 16h00). All three methods seem to produce similar results during the transitional hours of sunrise and sunset. The 1/L as well as the $\mu\sin\phi$ methods exhibit the same stability during most of the hours. The later method produces higher (i.e. stable) classes during the first five and last four hours of the day.

Similar differences between the three stability methods were also revealed, when the 16 summer and 37 winter days were analysed separately. Figures A1.2 and A1.3 in Appendix A illustrate the temporal variations of the stability classes for the winter and summer days respectively.

Table 2.9 The meteorological input data sets calculated from the different stability and mixing height methods. Each code represents a different combination.

Code*	Stability calculation method	Mixing height calculation method
P60	Pasquill classification	Significant levels at D. F. Malan
P61	Inverse Monin-Obukhov	Significant levels at D. F. Malan
P62	Inverse Monin-Obukhov	Holzworth procedure
P63	Pasquill classification	Holzworth procedure
P64	Pasquill classification	Heat exchange
P65	Inverse Monin-Obukhov	Heat exchange
P66	Kazanski-Monin parameter	Heat exchange
P67	Kazanski-Monin parameter	Holzworth procedure
P68	Kazanski-Monin parameter	Significant levels at D. F. Malan

* Code for the combination of meteorological calculations used in the model runs

The temporal variations for the three mixing height methods described earlier are depicted in Figure 2.7. The heights obtained by the significant pressure method (MHM) exhibit a similar shape to the heights derived from the Holzworth procedure (MHHZ). This is because both methods utilise the same sounding and interpolation scheme. Nevertheless, the MHHZ procedure produces approximately 25% lower mixing heights than the MHM at all hours of the day. The temporal variation of the heat exchange method (MRS) is not as smooth as the other two, since the hourly mixing heights are calculated from the wind velocity and the earth's energy balance at each hour. It is evident that the third procedure is the most conservative, producing the lowest mixing heights. Similar differences are illustrated in Figures A1.4 and A1.5 in Appendix A for the winter and summer days respectively.

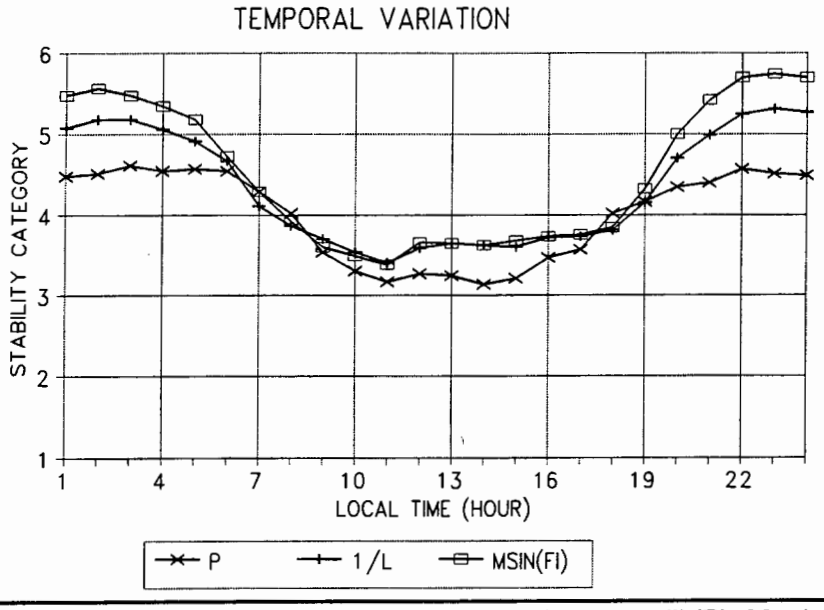

Figure 2.6 Temporal variation of stabilities produced by the Pasquill (P), Monin-Obukhov (1/L) and Kazanski-Monin ($\mu \sin\phi$) atmospheric classification schemes for the 53 selected days of the year 1991.

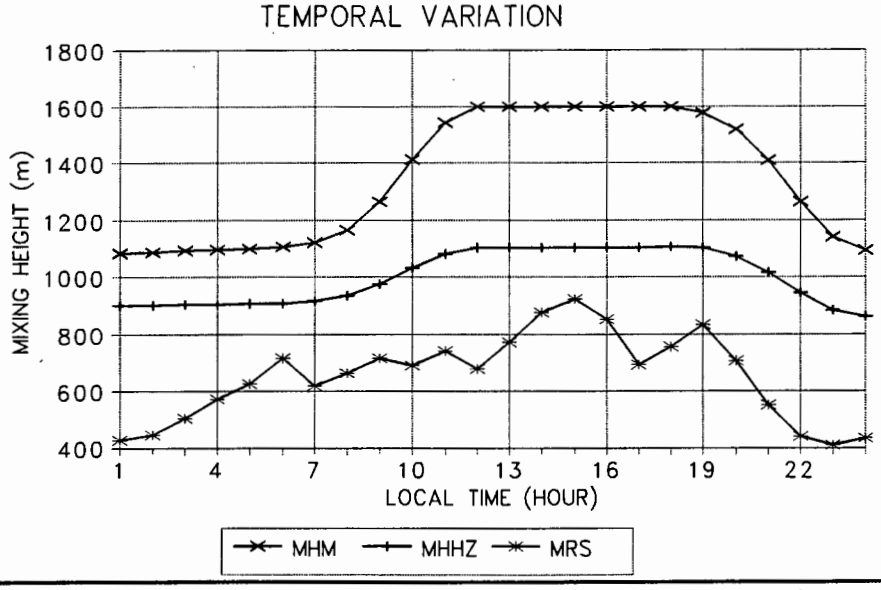

Figure 2.7 Temporal variation of the mixing height produced by the significant pressure levels (MHM), Holzworth procedure (MHHZ) and heat exchange (MRS) method for the 53 selected days of the year 1991.

The composite (winter and summer) frequency distribution of the stability classification schemes is summarised in Figure 2.8. The results from this comparison are similar to what has been found by many other studies (Draxler, 1987): i.e. that the Pasquill method is biased toward the neutral (D) stability and gives the highest frequency of this class. The frequency distribution of the 1/L and $\mu\sin\phi$ methods are more skewed towards stable conditions. This should be more realistic for the area and consistent with the Richardson number findings by Keen (1979).

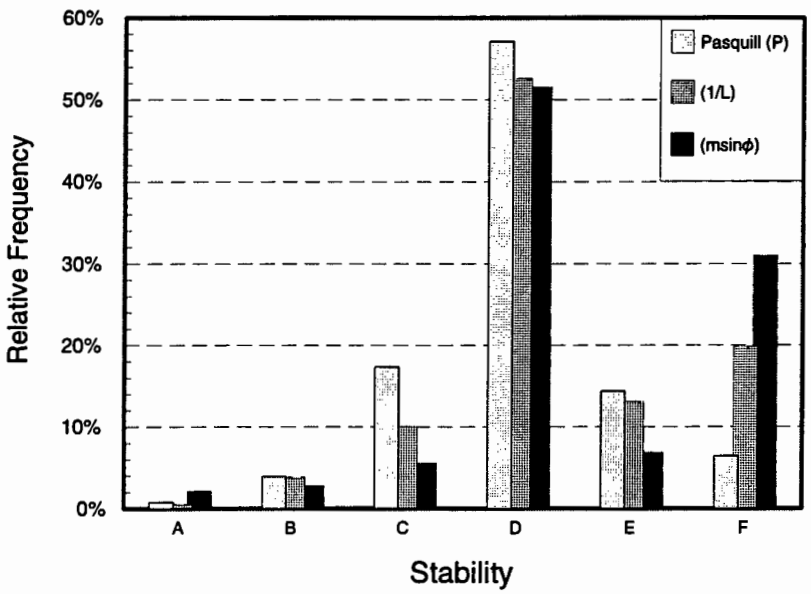

Figure 2.8 Relative frequency distribution of various stability classification schemes.

2.10 Summary

Meteorological observations from D. F. Malan have been collected for the years 1991 and 1992. From these data all the meteorological parameters necessary for the model runs have been computed. In addition, three stability and three mixing height methods have been utilised in order to generate nine input data sets and examine their influence on the model accuracy. The stability methods were the Pasquill scheme, inverse Monin-Obukhov length and the Kazanski-Monin parameter. It was found that Pasquill classification scheme over-estimates the number of neutral (D) atmospheric conditions.

For the mixing height estimations the first and second methods utilised the sounding at D. F. Malan and were based on the pressure equation and the Holzworth

procedure respectively. The third employed various empirical equations, according to the atmospheric condition and the earth's energy balance. All calculations were based on one point of meteorological measurements from D. F. Malan weather station. It is well known that meteorological conditions in the Greater Cape Town region follow complicated patterns, due to various topographical influences such as Table Mountain and the two oceans. It is therefore expected that the measured meteorological parameters at D. F. Malan do not represent the entire area under all atmospheric conditions. It would be an interesting exercise to quantify the effect of the stability and mixing height calculation schemes on the model performance, if the meteorological measurements were obtained at the same location as the monitoring stations.

Chapter THREE

EMISSION INVENTORY

3 EMISSION INVENTORY

3.1 Introduction

One of the first steps in attempting to predict concentrations of any pollutant released into the ecosystem, is the compilation of an emission inventory (EI). An emission inventory involves the systematic collection of information concerning the pollution emissions from all the sources in a particular area, over a certain time period. The boundaries of the area are fixed (Stern et al., 1973). A comprehensive EI forms the basis of many studies, such as source apportionment studies, monitoring network design, air pollution control strategies and dispersion modelling. The inventory is an on-going process due to possible changes in fuel consumption, number of sources and applied technology. Thus, it should be kept up to date and periodically modified in order to account for these changes.

The importance of accurate emission data, as related to air pollution dispersion modelling, has been widely stressed. A considerable source of errors in the predicted concentrations are related to inaccurate input emission data (Hanna, 1988). Even in the best tracer studies the emissions are known only within plus-minus 5 percent. An accurate emission inventory depends strongly on the emission factors used. These can vary up to 50 percent, depending upon the measurement techniques used (Stern et al., 1973). Such errors are directly passed on to the hourly model predictions. Other EI related errors occur due to inaccuracies in source coordinates, physical source heights, stack diameters and flue velocities. In short-term models the temporal variation of the emission rates can contribute significantly to model errors (Turner, 1879; Hanna et al. 1982). The detail of the spatial emission variation included in an emission inventory is also important in dispersion modelling. Grouping a number of small sources as an area source with one release height, could cause over-prediction at a downwind location due to the different release heights of the individual sources (Ruff, 1983). Therefore, irrespective of how accurately the atmospheric dispersion process is simulated, a considerable error will be carried along in the calculations if the emission inventory is not accurate enough. This kind of error is almost inevitable. Comprehensive data collection of all the emitters in such a large area as the Greater Cape Town is a major task.

The necessary data for dispersion modelling which should be included in an EI are the following:

- Source location (on a coordinate system)
- Type of fuel used
- Amount of fuel used per hour or day, month or year
- Daily fuel consumption rates or hours of function
- Stack height

- Stack diameter
- Flue exit velocity
- Flue exit temperature

3.2 Existing Source Emission Inventories

To date, there is no emission inventory for the Western Cape or the Greater Cape Town Region detailed enough to be used for dispersion modelling. The only exception is an inventory compiled by Dutkiewicz and Fuggle (1977) which was based on mailed questionnaires sent to different fuel consumers in the Greater Cape Town area. The result was a database with 603 records from which SO_2 and particulate matter was calculated. However, this information could not be used for the present study due to many changes in both the type of fuel used and the emission sources in the area since 1979.

Records of fuel burning appliances are kept by the Cape Town City Council's Air Pollution Control and Air Pollution Group of the Western Cape Regional Services Council. These records could, however, not be used for a dispersion modelling study since the information was appliance rather than emission oriented. In addition, except for the suburb and street name no coordinate reference system was used for the location. Therefore, a complete revision of the City Council's database is necessary in order to update the emission sources in the area and include the required information for an air pollution dispersion study.

3.3 Methods for Source Inventory Compilation

When only rough estimates of the major pollutants are needed and time and resources are limited, a rapid emission inventory is recommended by Wohlers et al. (1969). The method is based upon available fuel data for the different industries, according to the Standard Industrial Classification (SIC) code to which they belong. With this method only rough approximations of the emissions can be produced. Another weakness of the rapid inventory procedure is the necessity of emission factor adjustments for each industrial category, according to the specific local conditions.

A more elaborate procedure which requires more time, manpower and resources than the rapid survey is the detailed emission inventory (Rossano and Rolander, 1976). The latter is based on a detailed collection of source data. This information is then used to determine the physical characteristics of individual sources, their emissions during the various seasons of the year and to group all low strength emitting sources into areas according to their fuel consumption.

The point source information is collected via two-phase system registration forms sent

to the industries of the studied area. With phase one all the large emission sources are identified. Phase two follows up with a detailed questionnaire, obtaining information about the units used, physical data of the equipment, air pollution control devices, fuel used, fuel consumption and operation patterns.

The small sources are grouped as area sources within a grid system, according to categories such as industrial, commercial, residential, vehicular and land usage. The allocation of emission strength to each grid is based on a weighted rating system. Thereafter, the emission from each category is calculated from:

$$\begin{bmatrix} area\ grid \\ emission \end{bmatrix} = \left[\frac{grid\ rating}{total\ rating}\right] \times \begin{bmatrix} area\ total \\ category\ emission \end{bmatrix} \qquad (3.1)$$

The total emission for each grid is calculated by superimposing the emissions from each category obtained by Equation (3.1).

The grid rating can be achieved by employing either a subjective or an objective approach. The subjective rating is accomplished by one person who ranks the grids according to the strength of activity on a 1-10 scale. With the objective approach the rating system is based on a measurement such as census data or traffic volume patterns. The latter approach provides more accurate allocation of the emissions at a cost of more lengthy calculations. However, the subjective approach can give a reasonable estimation of the emissions compared to the objective (Rossano and Rolander, 1976). Also, it is not feasible to employ the objective approach with all the source categories. This applies particularly to emissions from the industrial and commercial sectors, due to the fact that usually no detailed reference values are available. Therefore, there are no values on which the grid rating system can be based. An example of such reference values used to allocate emissions from the residential sector could be the population densities. Generally, the choice of the rating approach depends on the availability of information and the level of accuracy required.

Area sources are usually spatially inhomogeneous. Therefore, in order to allocate emissions more accurately, a grid system with variable grid areas should be used. For example, by using a grid scheme which is constructed by the combination of two or more different square sizes, the total emission of an area can be allocated more accurately than by using only a uniform grid system (Raghavan et al., 1983). Singh et al. (1990) followed the objective approach for the domestic and vehicle emissions. They adopted a square grid system with two different area grids, so that the population p_i was inversely proportional to the area of every grid a_i. Each grid emission strength q_i was then given:

$$q_i = cons. \frac{1}{\alpha_i} \qquad (3.2)$$

If n_a and n_b are the number of grids having areas α_a and α_b respectively, then the total area emission Q_{tot} is:

$$Q_{tot} = \sum_{q_i} = const. \left(\frac{n_a}{\alpha_a} + \frac{n_b}{\alpha_b} \right) \qquad (3.3)$$

Knowing the Q_{tot}, the constant in Equation (3.3) can be calculated and the emission strength of each grid can be apportioned.

The compilation of an emission inventory has become a very important component of controlling emissions and assessing their effect on the immediate and global environment. The area encompassed by an EI can vary between a metropolitan area and a continent. A traffic emission inventory has been compiled for vehicle emissions by Alexopoulos et al. (1993) for Athens metropolitan area, including parameters such as population density, car intensity and average distance travelled. Even though this EI was based on sparse measurements, it could provide estimations of the spatial and temporal emissions variation in the area. The importance of information compatibility among emission inventories was stressed by Fontelle (1990). Towards this direction of compatibility the European emission inventory CORINAIR introduced a new methodology, in order to provide for a more coherent, consistent, transparent and comparable inventory. A more conventional approach was employed by Kato and Akimoto (1992) for the calculation of SO_2 and NO_x anthropogenic emissions in Asia. The study covered 25 Asian countries and was based on fuel consumption and on industrial processes.

3.4 Emission Inventory for the Greater Cape Town Area

The Greater Cape Town area, as defined for this study, consists of the municipalities of Cape Town, Milnerton, Parow, Bellville, Goodwood, Pinelands and Kuilsriver (see Figure 3.1). The total area covered by the study is approximately 440 km^2. Due to very limited municipal emission information which could be used for dispersion modelling, it was decided that updated data of the major pollution emitters should be obtained. Therefore, a considerable component of this study involved a complete revision and extension of the existing municipal appliance permit lists to compile a comprehensive emission inventory. The basis of the emission inventory comprises firstly, a database program from which the information can be downloaded into a dispersion model and secondly, a grid rating system which allocates emission strengths to small sources, such as residential, commercial, vehicular and those of small industry.

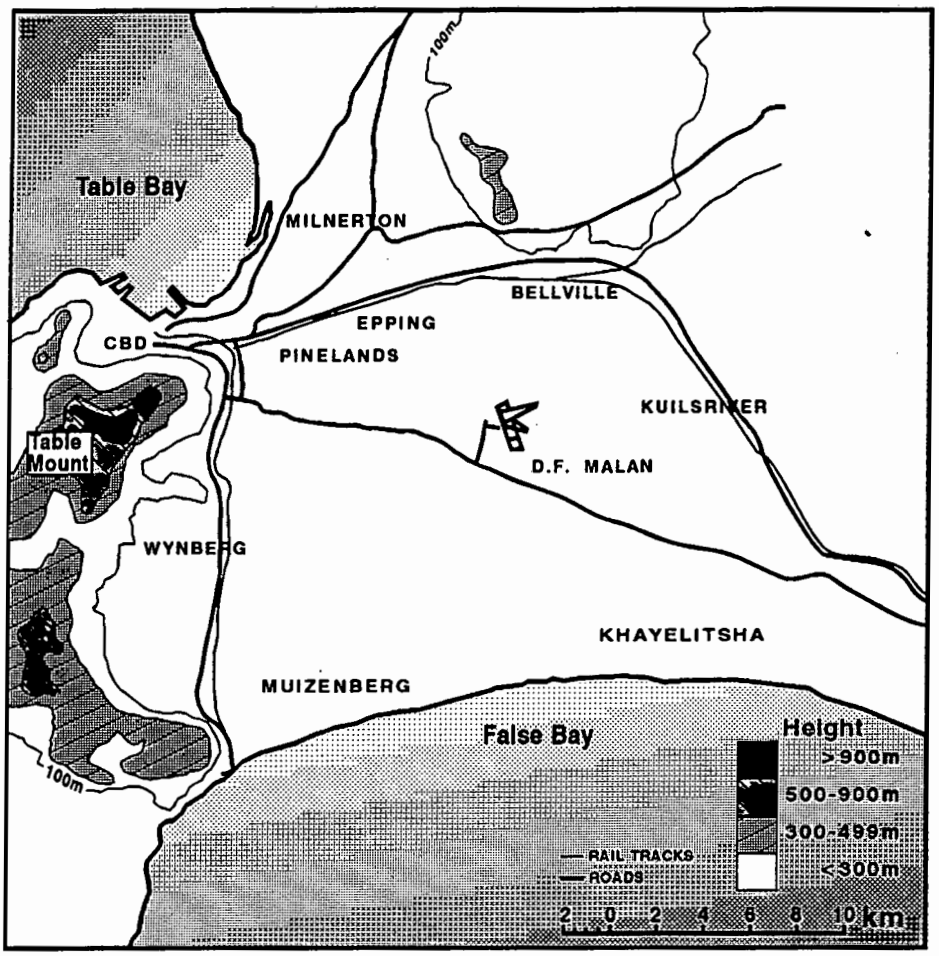

Figure 3.1 The Greater Cape Town region, as defined for this dispersion modelling study, consists of the municipalities of Cape Town, Milnerton, Parow, Bellville, Goodwood, Pinelands and Kuilsriver (approximately 440 km^2).

3.5 Data Collection

Due to the lack of readily available data of point sources for dispersion modelling, a new approach for the collection of data by the municipal Air Pollution Control officers was introduced. The data had to serve two purposes: firstly, the routine registration of utilised appliances and secondly, provision of information for dispersion modelling. A database program was developed, in order to collect all the necessary information and computerise the process of downloading the emissions into the model. All the emission sources of the Greater Cape Town area were grouped, according to their sulphur dioxide emission strength, into two categories. Individual sources with emissions greater than 400 kg per month were grouped in the first category and

treated individually as point sources. The second category consisted of all the remaining low strength sources which were grouped into area sources, using a variable square grid. With the collaboration of the Cape Town's Air Pollution Control officers all the major industries were identified. The collection and updating of information from these sources was prioritised. For the data collection a new form (see Appendix C) was designed which also depicts the entries in the database. A total of 187 point sources were registered and their information was entered into the inventory database.

The emissions from the area sources were calculated by adopting both objective and subjective approaches for the allocation of fuel consumption. The subjective approach was used with the industrial fuel consumption. A rating system from 1-3 was adopted, and an air pollution control officer assisted the ranking, according to industrial activity in each grid. The fuel consumed by the domestic sector, as well as the transport sector, was apportioned according to the population densities of the area. Townships such as Khayelitsha, Langa, Gugulethu, Nyanga and Crossroads were treated separately, since the fuel consumption patterns are different from the urban residential sector (see Appendix C). A total of 263 area sources were allocated to the entire Greater Cape Town region.

3.6 Emissions for Greater Cape Town

The fuel consumed according to sectors and type of fuel is shown in Table 3.1 (see Appendix C for more detailed emissions). The emissions can be calculated from the fuel used at each point source and grid area by utilising the procedure described in Appendix C.

Table 3.2 shows the emissions according to sector and pollutant. A monthly total of 2251 metric tons SO_2 is emitted in the Greater Cape Town area, of which 90 percent is contributed by the industrial sector. Of this industrial SO_2, 50 percent is emitted by point sources (i.e. large industries). Since the location and physical characteristics of these sources are accurately known, it is expected that their contribution to the concentration would be more accurately predicted than from the area sources where their physical characteristics and location are averaged. This is the main reason why SO_2 is the pollutant selected for the model's evaluation. Other reasons are that SO_2 is considered to be an inert gas with a half life decay adequately described by a logarithmic function, and it has no significant gravitational settling velocity. Particulate matter emissions are approximately 5768 metric tons, and 79 percent comes from industry. Vehicular emissions contribute 64 percent of the NO_x from a total monthly emission of 2398 metric tons (see Figure 3.2).

Table 3.1 1991 monthly consumption of coal, diesel, HFO, petrol, LPG and wood in the sectors: industrial, residential and vehicular.

	Total Industrial	Residential[a]	Vehicular	TOTAL
Coal (kt/m)	45.8	0.2	—	46.0
Diesel (Ml/m)	15.9	—	7.6	23.5
HFO (Ml/m)	15.7	—	—	15.7
Petrol (Ml/m)	—	—	65.9	65.9
Gas (Ml/m)	13.7	4.2	—	18.0
Paraffin (Ml/m)	—	2.7	—	2.7
Wood (kt/m)	—	0.9	—	0.9

[a] Residential fuel sales include also the township consumption.

Table 3.2 1991 monthly emissions of SO_2, NO_x and particulate matter according to sector: industrial, residential, vehicular, and aviation.

Pollutant	Industrial	Residential	Vehicular	Aviation	TOTAL
SO_2 (t/m)	2036	27	183	5	2251
NO_x (t/m)	799	17	1534	48	2398
Part. (t/m)	4570	20	1174	3	5768

The locations of the residential and main industrial areas are shown in the following regional map (Figure 3.3). Emission distribution for the area sources was based on this map and the emission inventory techniques described earlier.

The air pollution load in the Greater Cape Town region was calculated, according to the fuel consumed by these sources and applying the appropriate emission factors. Figures 3.5 to 3.10 show the spatial distribution of the point and area emissions for SO_2, NO_x and particulate matter.

A significant factor is the accumulation of sources with large emission strength along the east-west axis, following the railway tracks through Maitland, N'Dabeni, Epping and Bellville and along the north-south tracks through Wynberg, Plumstead and Diepriver.

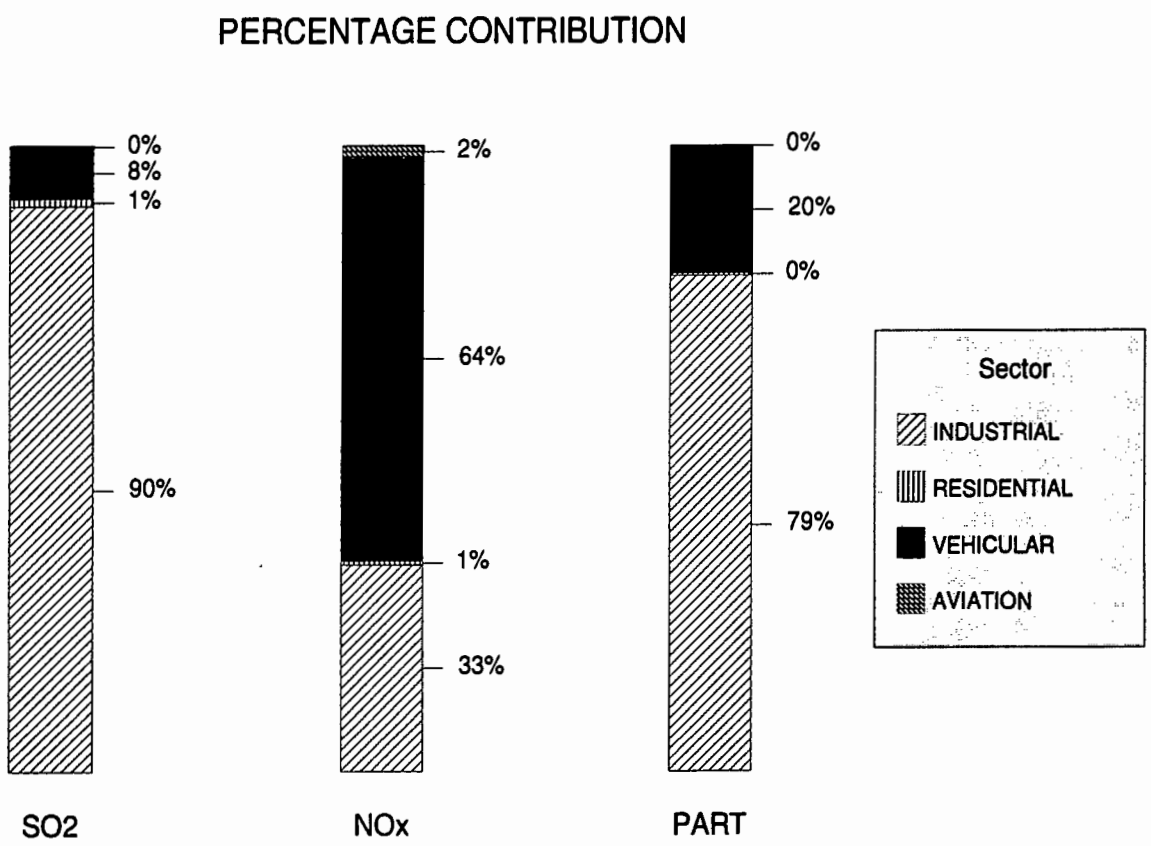

Figure 3.2 Emission contribution percentages of SO_2 NO_x and particulate matter for the year 1991 according to emitting sectors: industrial, residential vehicular and aviation.

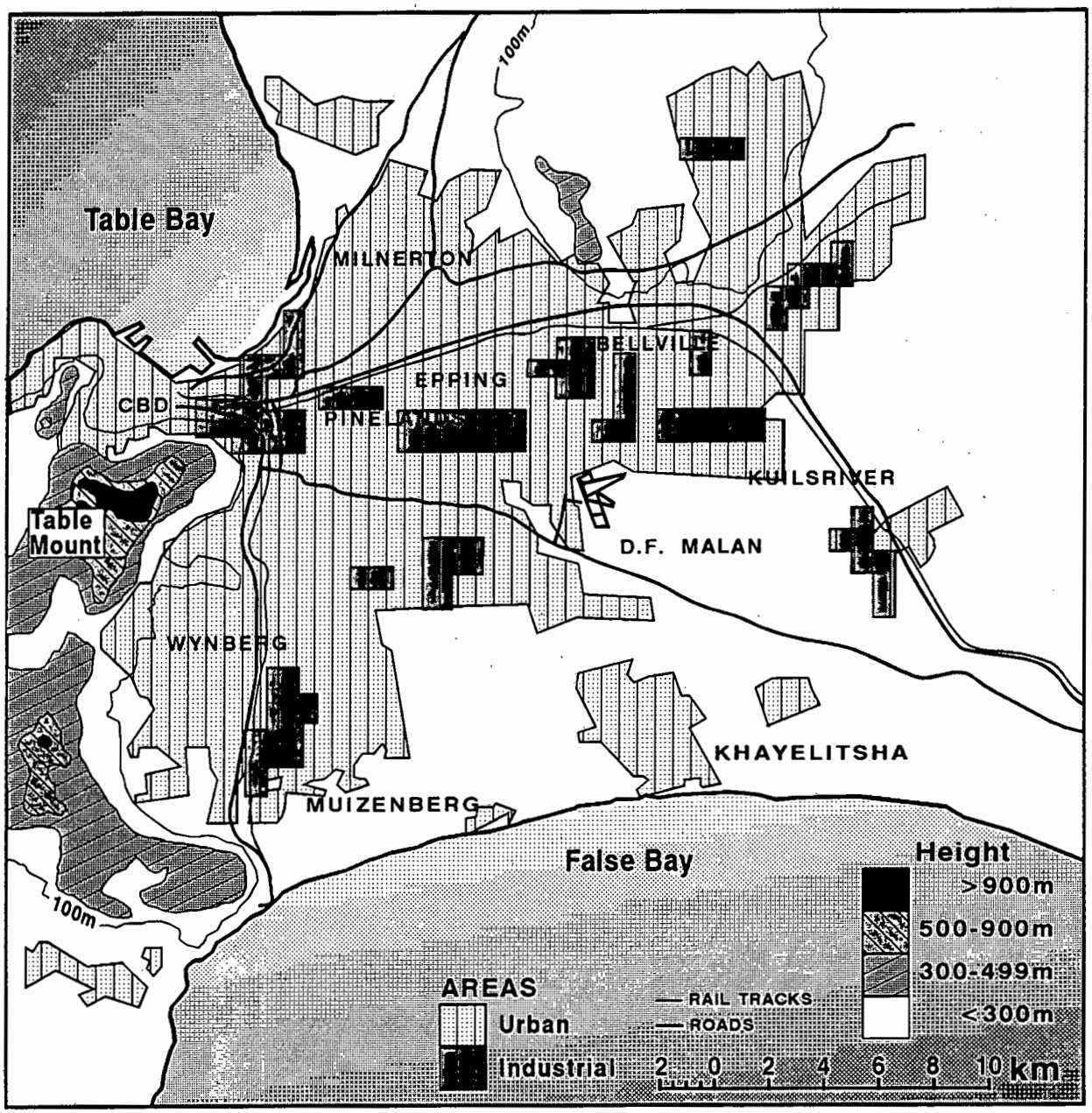

Figure 3.3 Urban and main industrial areas of the Greater Cape Town region.

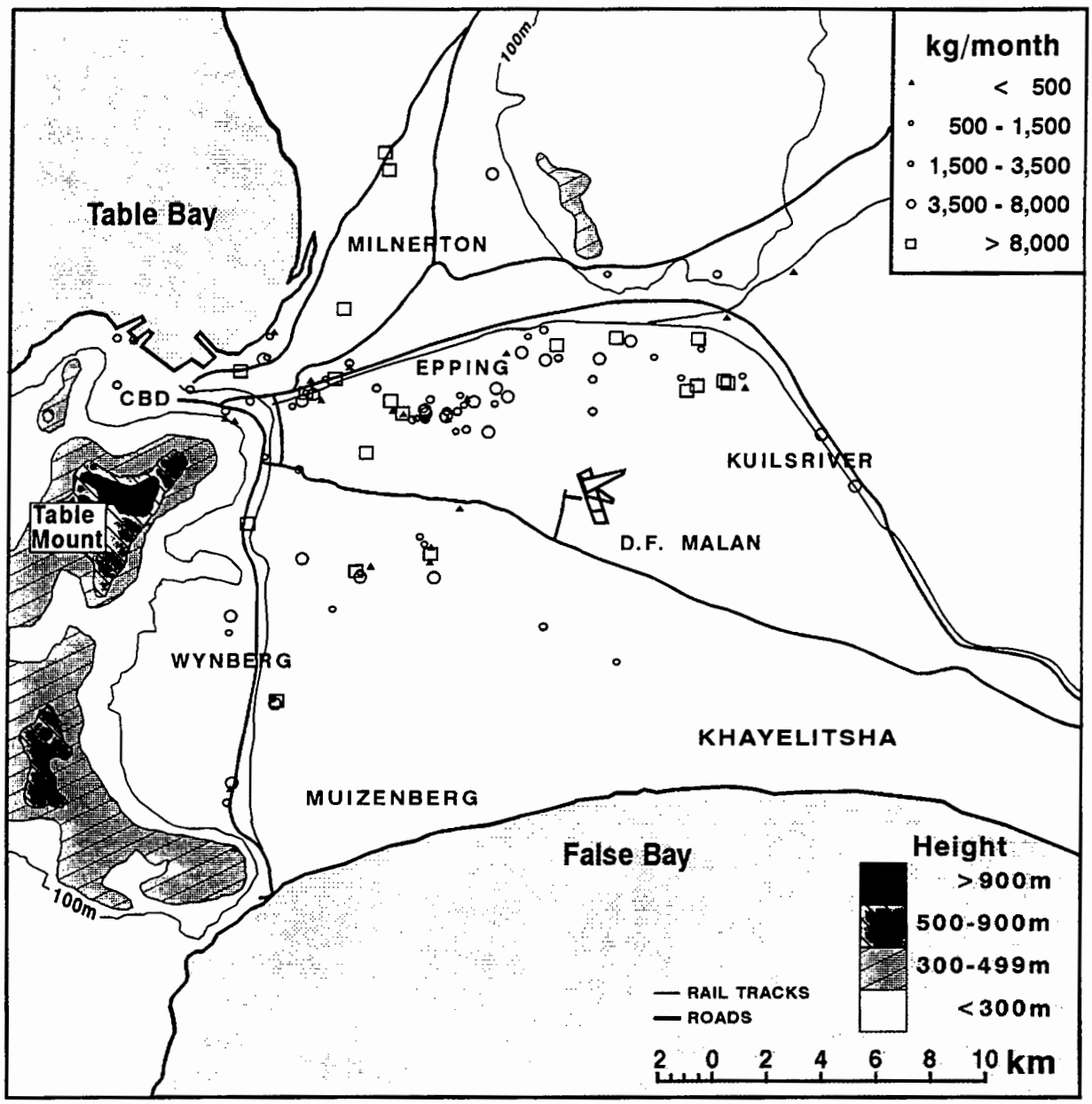

Figure 3.4 Sulphur dioxide (SO_2) point emissions for the Greater Cape Town region.

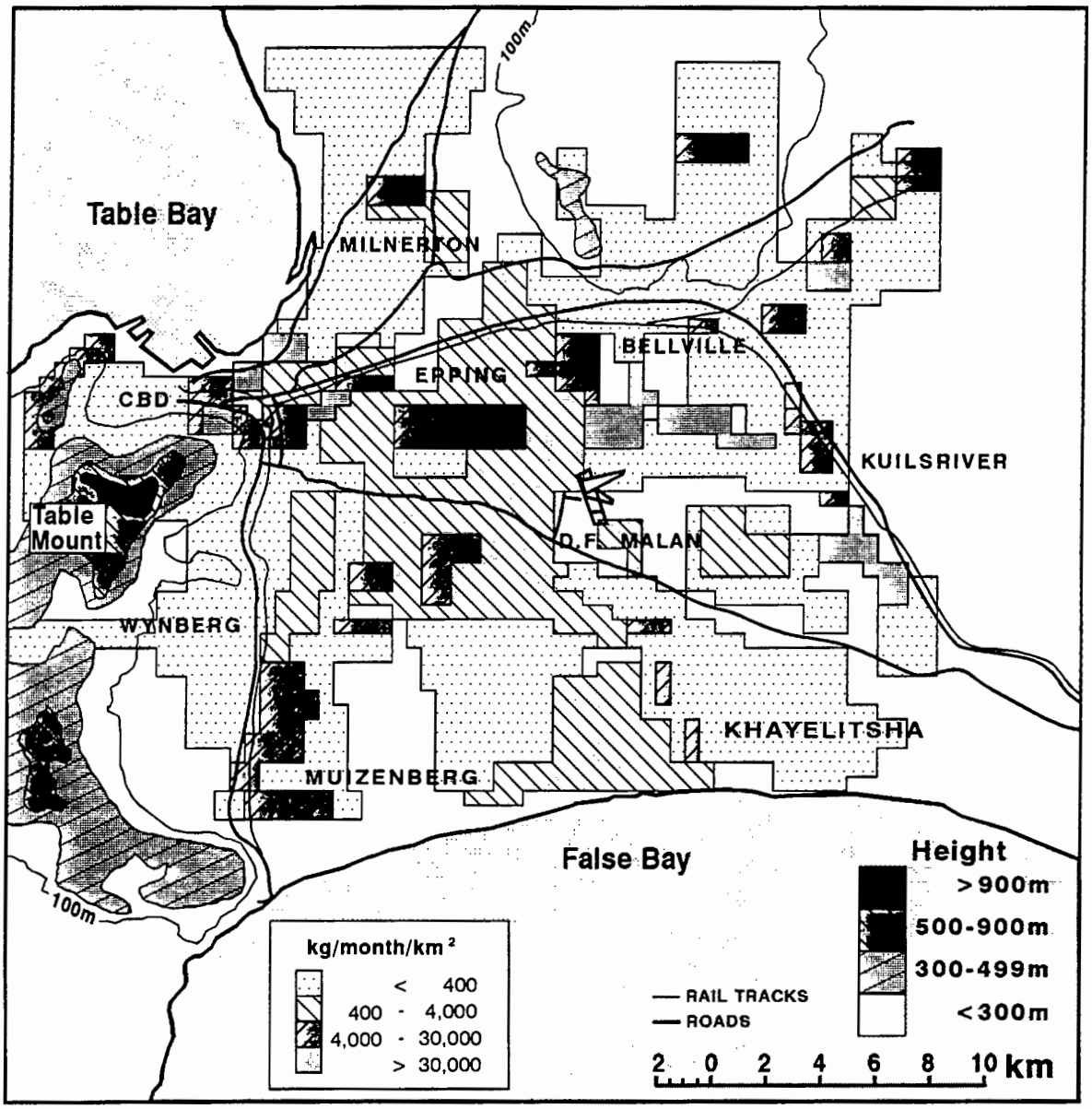

Figure 3.5 Sulphur dioxide (SO_2) area emissions for the Greater Cape Town region.

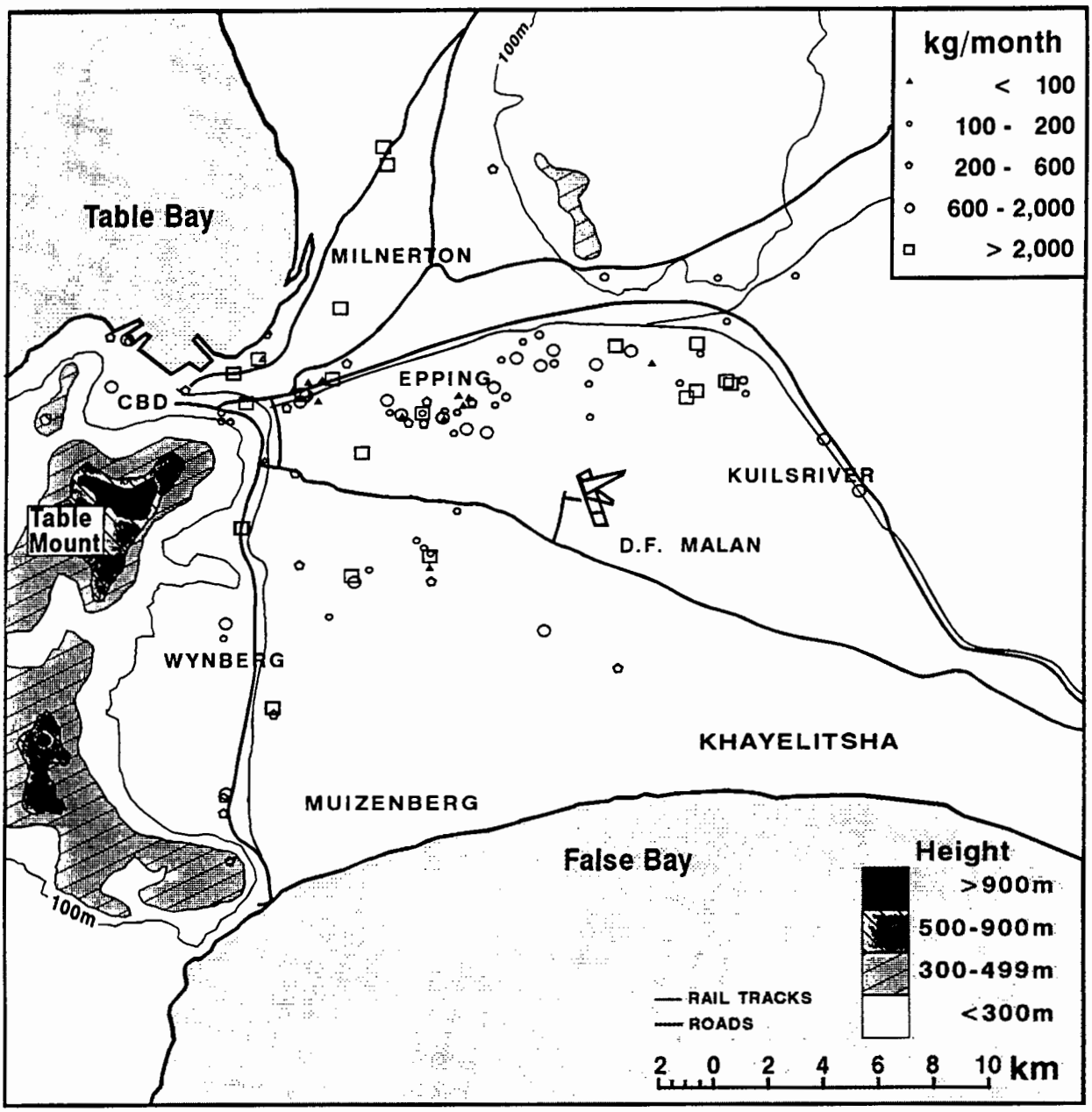

Figure 3.6 Nitrogen oxides (NO_x) point emissions for the Greater Cape Town region.

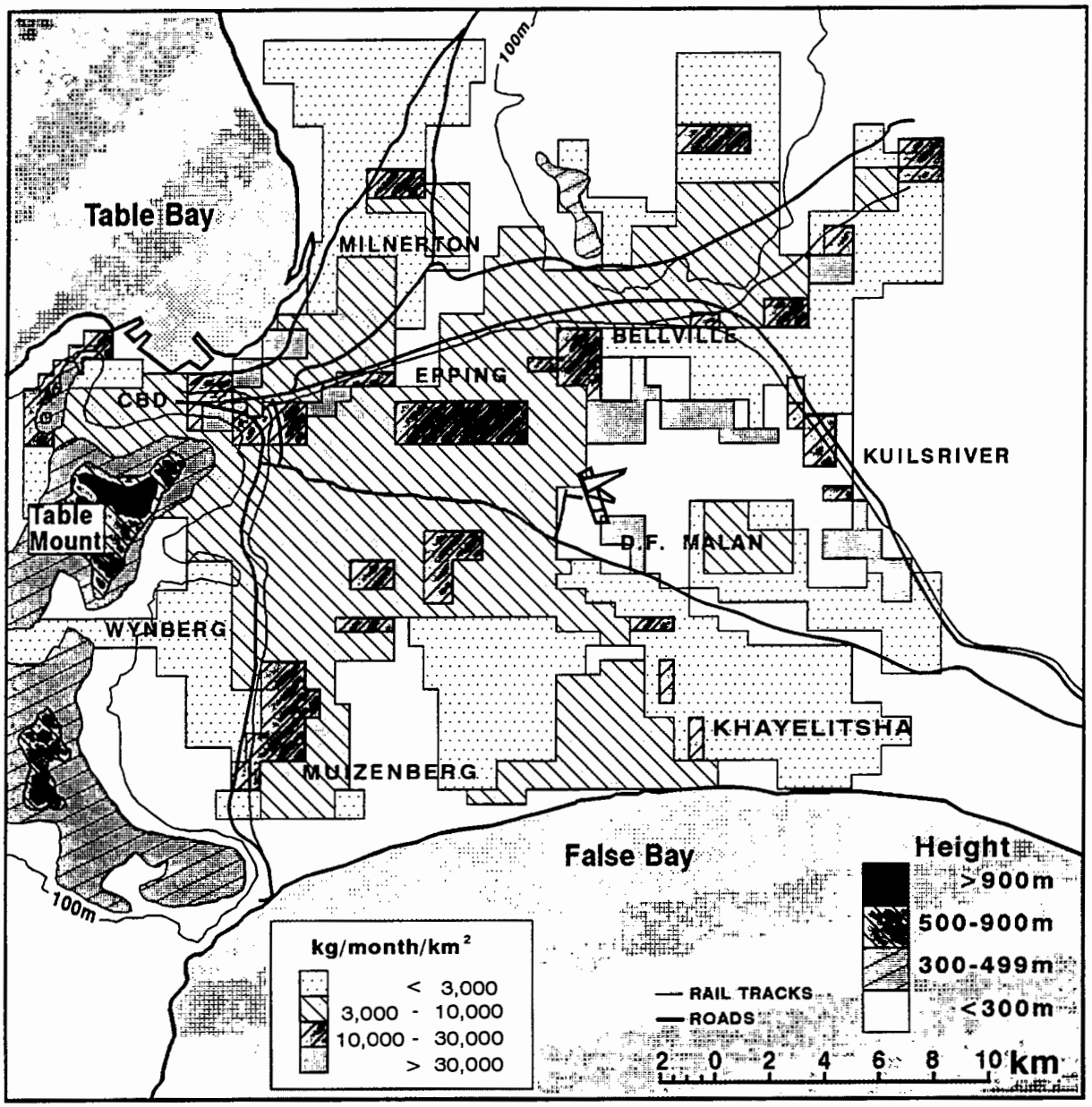

Figure 3.7 Nitrogen oxides (NO_x) area emissions for the Greater Cape Town region.

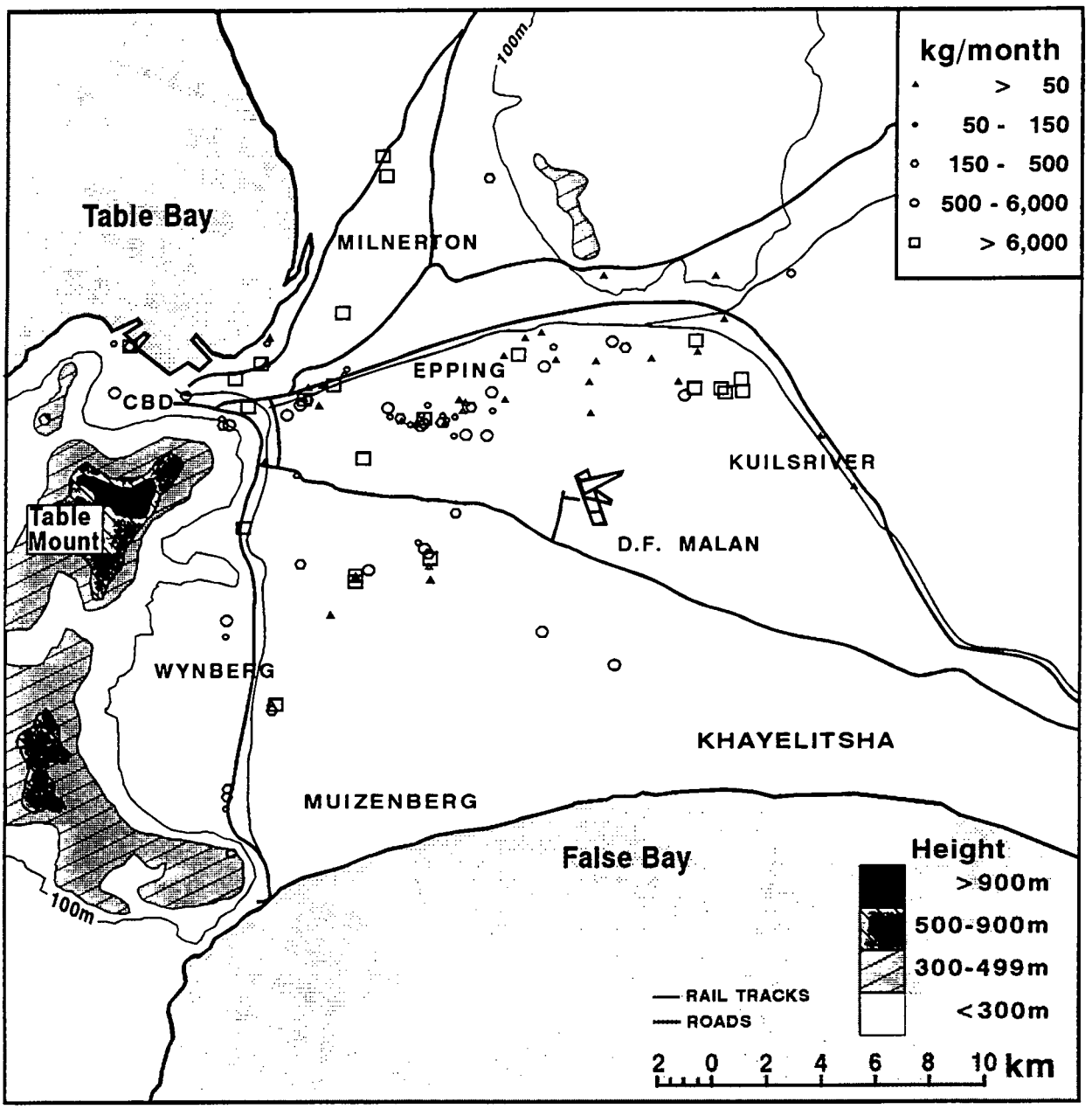

Figure 3.8 Particulate matter point emissions for the Greater Cape Town region.

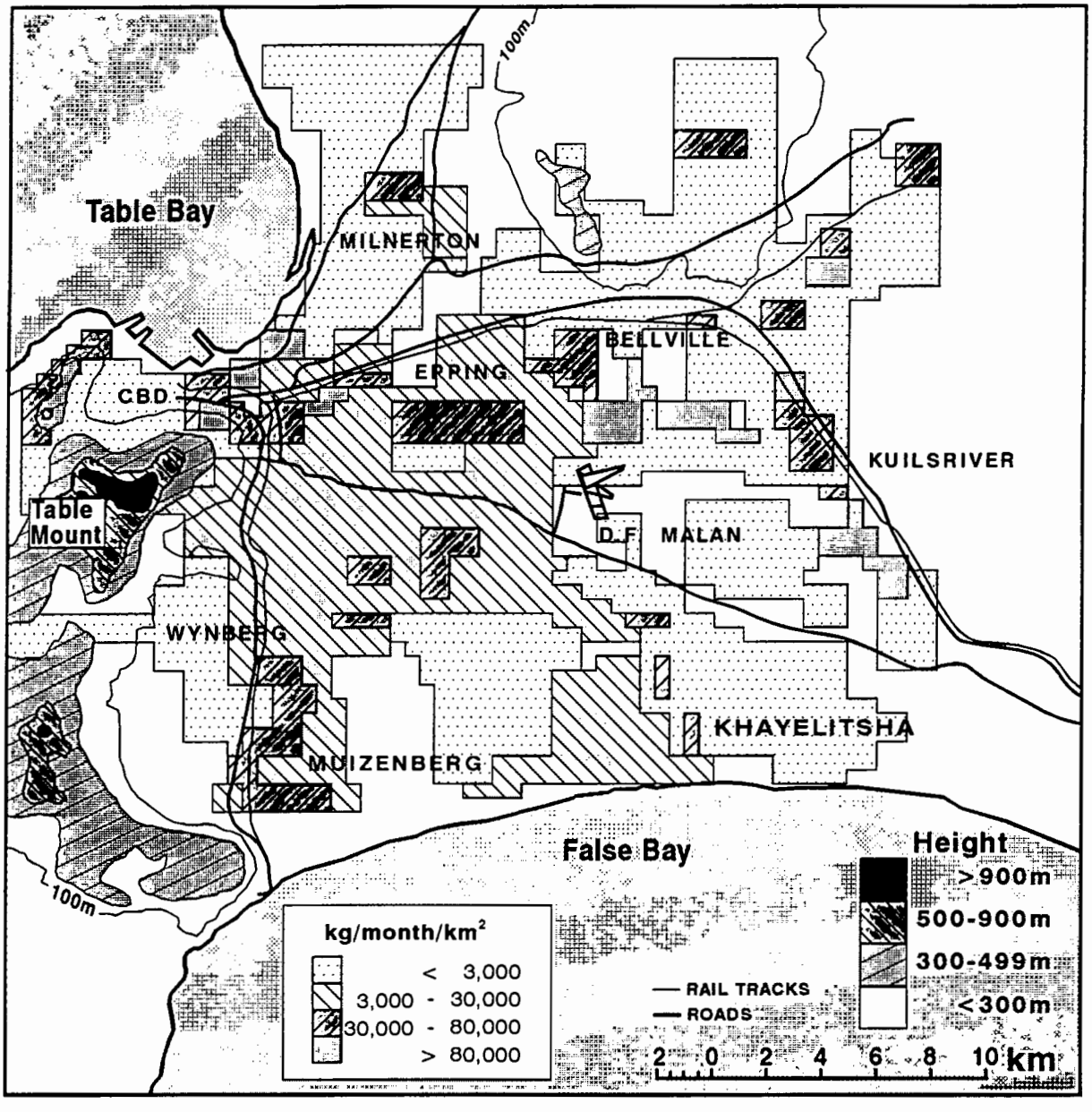

Figure 3.9 Particulate matter area emissions for the Greater Cape Town region.

From the function hours of the industries, as recorded in the database, it was possible to determine the diurnal variation of SO_2 and particulate matter emitted by all the point sources (see Figure 3.10). The sulphur dioxide emissions follow a daily cycle of being approximately 30 percent higher during the day than the night-time. Particulate matter follows the same cycle but with smaller variation.

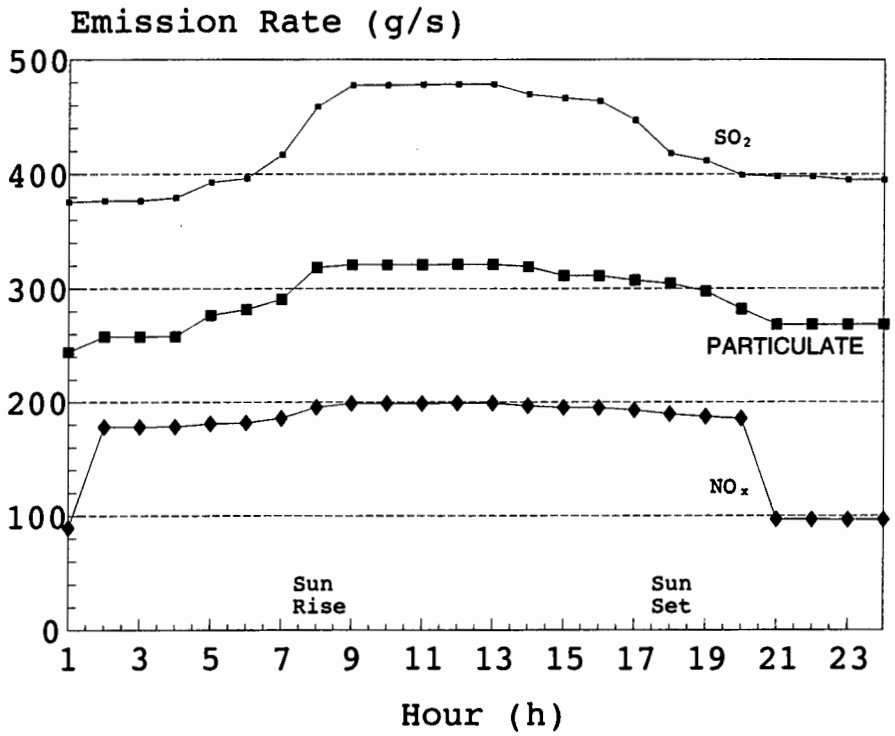

Figure 3.10 Diurnal variation of SO_2, NO_x and particulate matter emitted by the large industrial point sources of the Greater Cape Town region.

The fuel consumption information provided for the point and area sources did not allow for the calculation of the seasonal (winter-summer) variation of the emissions, nor emissions from different industrial processes. A more detailed emission inventory database could have solved this problem. The accomplishment of such a comprehensive emission inventory could be the focus of another study on its own and is beyond the scope of the present one.

3.7 Data Formulation for Use in Dispersion Modelling

In most cases, the information available in an emission inventory must be manipulated in order to be introduced into a dispersion model. Due to the model-oriented design of the inventory database, a minimum data modification was necessary for this study, mainly to accommodate the required hourly emission for the ISCST2 model.

The options and emission data used by the ISCST2 model are entered with an ASCII (American Standard Code for Information Interchange) file format. Each point source entry consists of:

- Source location (on the National Grid system LO 19)
- Pollutant emission ($g \cdot sec^{-1}$)
- Emission diurnal variations (24h scale)
- Stack height (m)
- Stack diameter (m)
- Flue exit velocity ($m \cdot sec^{-1}$)
- Flue exit temperature (°K)

Area sources are entered as:

- Lower left corner location of the area (on the LO 19 grid system)
- Length of side of square area source (m)
- Pollutant emission ($g \cdot sec^{-1} \cdot m^{-2}$)
- Emission diurnal variations (24h scale)
- Average release height (m)

Two more input options are provided by the ISCST2 model which are, however, not used due to lack of input data:

- Building downwash (height and width dimensions of a possible building near the stack)
- Emission variations by season and hour-of-day

The first of these two options is important when a nearby building effects the plume dispersion, which in turn would effect the downwind location of the plume's impact point with the ground and thus the predicted concentrations. The seasonal variation is also a parameter which could influence the accuracy of the predictions. This kind of variation is observed especially in domestic and vehicular sources.

Since modelling is the most inexpensive way to investigate different pollution scenarios in order to develop air pollution control policies, the formulation of uniform state inventory policy is strongly recommended. The initial information and the manpower needed for the compilation and data collection of such comprehensive inventories is already available at state departments, such as the Department of Health and the Department of Manpower. Organizing steps should be taken towards the direction of registering information with a focus on air pollution studies.

3.8 Summary

An emission inventory database in DBase IV was compiled, in order to register and download, into a dispersion model, all the large industrial sources of the Greater Cape Town region. The rest of the sources were divided into sectors such as residential, industrial, vehicular and townships. Emissions from each sector were apportioned on a grid system using the subjective and objective methods. A total of approximately 2251, 2398 and 5768 tons of SO_2, NO_x and particulate matter respectively is discharged monthly in the area. There is a significant accumulation of pollution sources along an east-west axis, following the railway tracks through Maitland, Epping and Bellville. Finally, for the establishment of an air pollution control and planning policy, the need for a comprehensive emission inventory study for the Greater Cape Town area is stressed.

Chapter FOUR

MODEL PERFORMANCE AND EVALUATION

4 MODEL PERFORMANCE AND EVALUATION

4.1 Introduction

Atmospheric dispersion models are widely used for air quality assessment and development of air pollution control strategies. In order to determine if a model is applicable to a particular area and its atmospheric conditions, the model's reliability and prediction accuracy has to be evaluated. Model evaluation is the quantification of the model's performance, using real data from real emissions and atmospheric scenarios. The main statistical measurements of this performance have been summarised in two workshops by Fox (1981, 1984). Willmott (1982) stressed that this evaluation should be further enhanced by data-display graphics, sensitivity analysis and comparisons with other models.

In this section the evaluation of the Industrial Source Complex Short Term 2 (ISCST2) model is presented. Emissions of the Greater Cape Town area and meteorological data of the year 1991 were implemented as the model input. The statistical measurements resulted from both paired and unpaired analyses of the predictions (P) and observations (O) at three monitoring stations in the area. Several graphic illustrations depict the degree to which the model's predictions comply with observations at the three locations.

4.2 Unpaired Statistical Measurements

The unpaired statistics describe the populations of the predictions (P) and observations (O) separately. The statistics involved in the unpaired analysis of the two populations are the average, the standard deviation and the cumulative frequency distribution. The first two measures display the populations' average tendencies. The comparison of the predictions' average ($\overline{P}$) with the average of the observations ($\overline{O}$) reveals the overall under-prediction or over-prediction of the model. Comparing the standard deviations, one can obtain a relative indication of how well the observed variability is reproduced by the model. Furthermore, these two summary measurements can be cross-examined by several statistical tests. A Wilcoxon statistical test could indicate if there is a significant difference between the $\overline{P}$ and $\overline{O}$ (Fox, 1981). The variances could be compared by utilizing a t-test statistic, as well as checking the confidence intervals of the ratio of the two variances.

The cumulative frequency distributions can reveal those part(s) of the distribution at which the model might over- or under-predict. For regulatory applications the model should not under-predict, especially not at the upper tail (i.e. percentiles greater than 90%). The importance of the unpaired analysis, and in particular of the average and

standard deviation, is stressed by Willmott (1982). He states that the $\overline{P}$ and $\overline{O}$ provide a better description of the model's performance than some of the statistical measurements, such as the average of the difference ($\overline{d}$) or the variance of the difference (s_d^2).

4.3 Paired Statistical Measurements

Paired statistical analysis is the basic tool for dispersion modelling evaluation. The corresponding predictions (P) and observations (O) are treated as pairs. The difference (d) between the P and O is calculated as: $d = P\text{-}O$. For the paired analysis of the model's performance, several statistical measurements were recommended at the Woods Hole EPA/AMS Workshop (Fox, 1981). Most of these statistical measures are given below.

4.3.1 Mean Difference

The mean difference ($\overline{d}$) is an estimate of the overall bias of the model in predicting the pollution levels and is defined as:

$$\overline{d} = \frac{1}{N} \sum_{n=1}^{N} d_n \qquad \textbf{(4.1)}$$

where N is the sample size of the differences.

4.3.2 Variance of the Difference

The second moment of the distribution of the differences is the variance of the difference (s_d^2) and is computed by:

$$s_d^2 = \frac{1}{N-1} \sum_{n=1}^{N} (d_n - \overline{d}) \qquad \textbf{(4.2)}$$

This measures the average noise in the data, i.e. the variability of the differences around $\overline{d}$. The square root of the variance is the standard deviation.

The average difference ($\overline{d}$) and the s_d^2 do not contribute more diagnostic value to the

model evaluation than the $\overline{P}$ and $\overline{O}$ from which they are computed (Willmott, 1982). Due to this reason, there is a tendency to omit these two statistics in favour of other measurements of difference which are presented below.

4.3.3 Root Mean Square Error

A measure of the actual error size produced by a model is the root mean square error (RMSE). The RMSE is the square root of the mean square error (MSE). It is computed so as to create an easier means of comparison, since its units are the same as the units of P and O. The root mean square error may be written as:

$$\text{RMSE} = [\frac{N-1}{N} s_d^2 + (\overline{d})^2]^{1/2} \qquad \textbf{(4.3)}$$

Furthermore, it is important to know how much of this error is systematic (RMSE_s) and how much unsystematic (RMSE_u). Systematic error results from the model's formulation, the parameters used or from improper emission and meteorological data. Its value accumulates by a consistent recurrence of the same error, which could be easily rectified by improving the model or correcting the input data. A "good" model should have the (RMSE_s) approaching zero. This would mean that the model functions at its best possible performance for the particular application. The unsystematic error (RMSE_u) originates by a number of small effects, such as the imprecision of a constant. These errors are unsystematic because they cause positive or negative variation in the final predicted value. The RMSE_u is interpreted as a measure of potential accuracy which can be achieved by the model. This error should approach the RMSE (Willmott, 1982).

The systematic and unsystematic root mean square errors are given by:

$$\text{RMSE}_s = [\frac{1}{N}\sum_{n=1}^{N} (\hat{P}_n - O_n)^2]^{1/2} \qquad \textbf{(4.4)}$$

$$\text{RMSE}_u = [\frac{1}{N}\sum_{n=1}^{N} (P_n - \hat{P}_n)^2]^{1/2} \qquad \textbf{(4.5)}$$

where $\hat{P}$ is obtained from the relation $\hat{P} = a + bO_n$; where a is the intercept and b the slope of the regression line between the predictions and observations.

4.3.4 Mean Absolute Error

Another measure of overall performance is the mean absolute error ($|\bar{d}|$) (Fox, 1981). It is more robust than the RMSE, since it is less sensitive to extreme values. The mean absolute error takes the form:

$$|\bar{d}| = \frac{1}{N}\sum_{n=1}^{N} |P_n - O_n| \qquad (4.6)$$

4.3.5 Normalized Mean Square Error

The scatter of the data can be also measured by the normalized mean square error (NMSE) (Hanna, 1988). For example, if the NMSE is 1.0, then the typical difference between the predictions and the observations is approximately equal to the mean. The NMSE is calculated from the MSE by normalizing it with the predicted ($\bar{P}$) and observed ($\bar{O}$) averages as follows:

$$\text{NMSE} = \frac{\frac{1}{N}\sum_{n=1}^{N} (P_n - O_n)^2}{\bar{P}\,\bar{O}} \qquad (4.7)$$

4.3.6 Index of Agreement

Instead of the correlation coefficients (r and r^2) which can be misleading in interpreting a model's accuracy, Willmott (1982) suggested the use of the root mean square error, together with the index of agreement (D). The reason that r^2 is not as reliable as D is that the later is sensitive to the relative size of the average difference, as well as certain changes in proportionality (Rao et al., 1989). The index of agreement demonstrates the degree to which P approaches O, both in magnitude and in sign. It offers an uncomplicated way for cross-comparison of different models, since it is constrained between zero and one. An index value of one would indicate an error-free model with perfect agreement between the predictions and the observations. The index of agreement can be written as:

$$D = 1 - \frac{\sum_{n=1}^{N} (P_n - O_n)^2}{\sum_{n=1}^{N} (|P_n'| + |M_n'|)^2} \quad \textbf{(4.8)}$$

where $P_n' = P_n - \overline{O}$ and $O_n' = O_n - \overline{O}$.

Due to the fact that D becomes unstable when the denominator approaches zero, it should not be interpreted separately but in combination with the root mean square errors ($RMSE_s$ and $RMSE_u$) and other measures of difference (Stunder and SethuRaman, 1985).

4.3.7 Fractional Bias

Another statistic widely used for model evaluation is the fractional bias (FB). It measures the degree to which the average predicted concentration ($\overline{P}$) approaches the observed ($\overline{O}$). The fractional bias is calculated as (Cox and Tikvart, 1985):

$$FB = \frac{2(\overline{P} - \overline{O})}{\overline{P} + \overline{O}} \quad \textbf{(4.9)}$$

The FB has the desirable characteristics of being bounded and symmetrical. Its values range from 2, for extreme over-prediction, to -2, for extreme under-prediction. For example, if a model's predictions are within a factor of 2 from the observations, the fractional bias would range from 0.67 to -0.67. A limitation for FB exists when both concentrations are zero. This results in the fractional bias being undefined and therefore should not be the only measure used for a model evaluation.

4.4 Resampling Procedures

In order to assess the reliability of the calculated statistical measures, it is necessary to know their confidence limits. This is important in order to establish if the index of agreement is significantly different from zero or whether the confidence limits of the fractional bias include the zero value. In two EPA-AMS workshops on air quality model performance (Fox, 1981, 1984) it was proposed, that for evaluation purposes, the data be transformed to the normal distribution. This was suggested because all

confidence intervals for the statistical measurements refer to the normal distribution. Air-quality data do not usually follow the normal distribution, nor can they always be transformed to one. Alternative methods to resolve the problem are the bootstrap and the jackknife resampling techniques, since these do not depend on the distribution function (Efron, 1982).

4.4.1 Bootstrap Resampling

In this section the bootstrap resampling procedure, as described in detail by Efron and Gong (1982), will be outlined . This technique allows for the estimation of the reliability of a statistical parameter, without the assumption of any underlying distribution function concerning the data.

Assuming a data set of N=500 pairs of predicted and observed concentrations, the bootstrap procedure randomly draws a new set of 500 pairs from the original one. This set is called a bootstrap sample. By using a computer the same procedure is repeated a large number of times, in order to obtain approximately N_b=1000 bootstrap samples. Every time a value from the original data set is drawn for the bootstrap sample, the previous one has been already replaced back into the original data set. Therefore, it is possible for a bootstrap sample to include a value from the original data set more than once or not at all. For each bootstrap sample the statistical measure is recalculated. The cumulative distribution function of the N_b statistical values provides the statistic's confidence intervals.

Rao et al. (1985) applied the bootstrap procedure to the residuals (d) between maximum predicted and observed concentrations, to demonstrate the bias of the model at different percentiles. Ku et al. (1987b) applied the same procedure to the mean difference and root mean square error, in order to determine the degree of difference between two models' predictions. Hanna (1988, 1989) reviewed the bootstrap and jackknife resampling techniques and analysed their variations. He argued that the resampling technique, as described above, could lead to erroneous conclusions at the tails of the distribution function. This could be caused by the possibility of drawing bootstrap sample(s) containing only one value of the original data set. Although such a bootstrap sample is not likely to happen, it is not impossible. That bootstrap procedure was named "seductive bootstrap".

One way to resolve the unrealistic density function at the tails is to perform a blocked bootstrap procedure (Tukey, 1987). The blocking is performed by dividing the original data set into two or more blocks from which each value for the bootstrap sample will be drawn. The blocking of the data should be performed with the aim of creating data subsets with similar characteristics. Examples of such subsets are the measurements from monitoring stations grouped at varying distances from the source, or according to season. Cox and Tikvart (1990) applied the blocked bootstrap procedure in order to estimate the 95% confidence intervals of the absolute

fractional bias. They blocked the original data set according to season and drew from each block 3-day clusters of data, in order to maintain the day-to-day meteorological persistence.

4.5 The ISCST2 Model Evaluation

Hourly SO_2 concentration measurements at three monitoring stations were employed for the evaluation of the Industrial Source Complex Short Term 2 (ISCST2) model. The first monitoring station (S1) was located at Labiance, Bellville. The second station (S2) was at Cape Town's Central Business District (CBD), and the third (S3) at the Goodwood Showgrounds (see Figure 4.1).

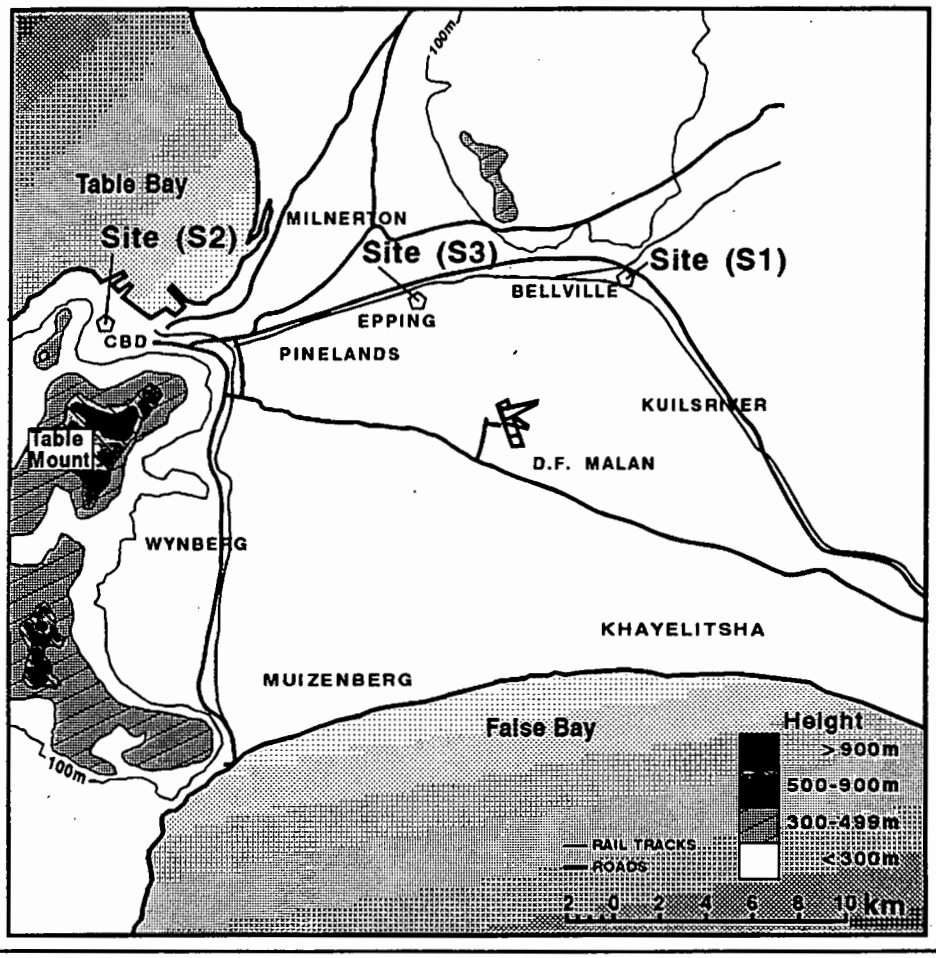

Figure 4.1 Locations of the three monitoring stations in the Greater Cape Town area. The first site (S1) is situated at Bellville, the second (S2) at Cape Town's CBD and the third (S3) at Goodwood.

The area in which the first monitoring station (S1) was situated can be characterised as an urban area with rolling terrains. The second monitoring station in Cape Town's CBD is surrounded by Table Mountain and Table Bay. This region can be described as one with a complex terrain. The area's meteorology is also strongly effected by the land and sea-breeze systems, especially in the early morning hours. The topography and meteorological characteristics of the third station (S3) are less complicated than the CBD. However, the sea and land-breezes are still expected to influence the meteorology, since the site is only 6 kilometres away from the coast line.

Meteorological parameters needed for the model runs were collected from D. F. Malan airport. These data included the wind direction, wind velocity, cloud cover, standard level sounding and significant level sounding. The days for which hourly observed concentrations and the meteorological measurements were available are depicted in Table 4.1. For the year 1991 a total of 1272 hours were selected. Of this data, 16 days were for the summer and 37 for the winter period. The total selected hours for the year 1992 were 936. All of the latter belonged to the winter period, since the monitoring station was transferred from Bellville to Goodwood in June. It should be indicated that the use of a continuous string of more than ten consecutive days was not possible, due to inconsistencies in the available meteorological and observational data.

Table 4.1 The selected days for the evaluation of the ISCST2 model.

	Number of Days for Each Month					
	Feb.	June	July	August	Sept.	Total days
1991	16	11	15	11	—	53
1992	—	7	14	7	11	39

Even though the emission inventory was constructed for the year 1991, comparison of the model's predictions with the 1992 Goodwood observations served the purpose of assessing model performance at these three locations. Predictions at the S3 site were expected to be lower due to the fact that the total fuel sales for the area were increased by approximately 15% from 1991 to 1992. Therefore, the actual emissions from the area sources, corresponding to the observed concentrations, were higher than the ones used.

4.5.1 Examination of Different Meteorological Inputs into the Model

The meteorological data are entered into the ISCST2 model with an external ASCII file. As outlined in Chapter 2 several methods were used to calculate the meteorological parameters. Table 4.2 shows the different combinations of the stability and mixing height methods which were used to produce nine input data sets for the ISCST2 model.

Table 4.2 The meteorological input data sets calculated from the different stability and mixing height methods. Each code represents a different combination.

Code*	Stability calculation method	Mixing height calculation method
P60	Pasquill classification	Significant levels at D. F. Malan
P61	Inverse Monin-Obukhov	Significant levels at D. F. Malan
P62	Inverse Monin-Obukhov	Holzworth procedure
P63	Pasquill classification	Holzworth procedure
P64	Pasquill classification	Heat exchange
P65	Inverse Monin-Obukhov	Heat exchange
P66	Kazanski-Monin parameter	Heat exchange
P67	Kazanski-Monin parameter	Holzworth procedure
P68	Kazanski-Monin parameter	Significant levels at D. F. Malan

* Code for the combination of meteorological calculations used in the model runs

Examination of the paired and unpaired statistics at each monitoring site for all the meteorological combinations, did not reveal any significant differences in the model's predictions. This was also confirmed by the bootstrap resampling procedure applied to the predicted and observed 24h averages (Appendix D). At the 95% confidence level the combinations did not produce predictions significantly different from each other. This was due to the fact that, at monitoring stations (S2) and (S3), predictions were lower than the observations by a factor of 2-4, thus not allowing for small differences to be distinguished.

At Bellville station (S1), where predictions correlate better with observations, it was noted that the predictions had the same interval patterns when the same stability method was used. In contrast to the stabilities, the 95% confidence intervals from the various mixing height methods were randomly variable to each other. Therefore, the model predictions seem to be more sensitive to the stability than the mixing height input.

Overall, for the three monitoring sites, the Pasquill scheme and the inverse Monin-Obukhov method produced the best results in comparison with the other combinations when the mixing height was calculated by the Holzworth procedure (see Appendix D). It was also clear that the mixing height calculated with the heat exchange method was the most conservative, thus producing lowest heights and highest concentrations at all three monitoring sites. The Holzworth procedure for the mixing height seemed to produce the most accurate predictions for all the monitoring stations and stability methods.

The paired and unpaired model evaluation, as discussed in the following sections, involves the creation of several data subsets. In order to limit the number of these subsets and since two combinations clearly performed better than the rest, the data sets P62 and P63 are to be kept for the paired and unpaired statistical analyses.

4.5.2 Overall Model Performance

The overall evaluation of the model's performance was based on comparisons of hourly SO_2 concentrations with predictions from three monitoring stations at Bellville, CBD and Goodwood. For each monitoring station, two sets of predictions were produced. The first was a result of the combination of the Pasquill scheme and the Holzworth procedure. The second involved the combination of the latter with the Monin-Obukhov stability method.

Figure 4.2 (a)-(c) presents the auto-correlations of the observed and predicted concentrations at the three monitoring stations. The correlations of the concentrations at all stations fall off rapidly within the first few lags. At the Bellville (S1) and Goodwood (S3) sites, the correlations of the model predictions fall off more rapidly than those for the measured concentrations. Therefore, observed concentrations exhibit a higher degree of serial correlation or persistence than the predictions at locations with no complex topography and meteorology, such as Bellville and Goodwood.

At Cape Town's CBD site, the correlations of the observed and predicted concentrations have the same drop rate. There is no persistence in the observed and predicted values at this location, as shown by the very low coefficients after the 12^{th} lag. A possible explanation to the above could be the rapid recirculating patterns and rapid changes of the wind in the lee of Table Mountain.

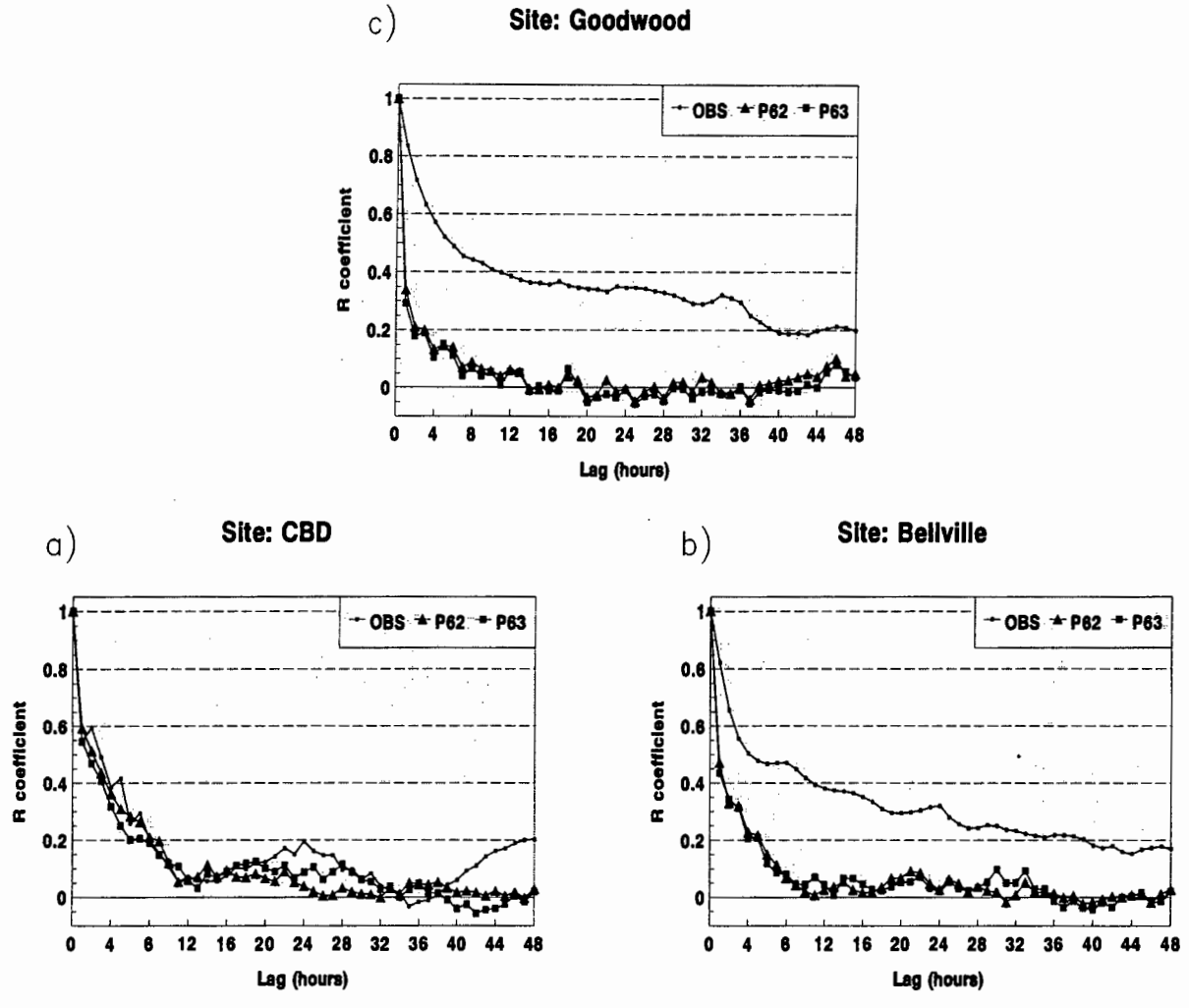

Figure 4.2 Auto-correlations of the observations (Obs) and predictions (P62 and P63) at the monitoring stations: a) CBD (S2), b) Bellville (S1) and c) Goodwood (S3).

In order to assess if a consistent bias is introduced into the model by the emission sources or the meteorological parameters, the temporal variations of the emissions, mixing height, stability categories and concentrations are evaluated. The temporal variations are calculated by averaging each variable for each hour of the day.

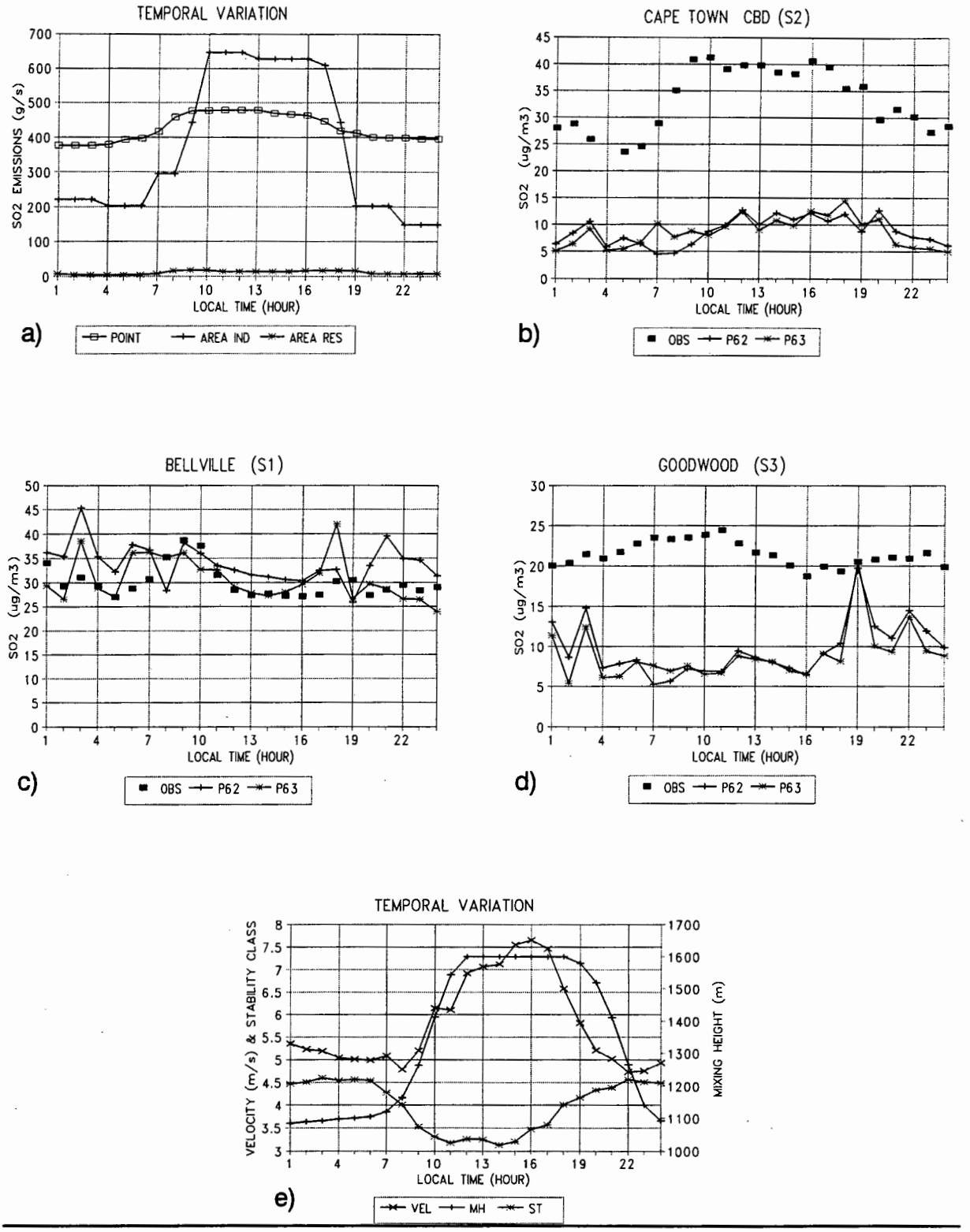

Figure 4.3 The temporal variations of: a) area and point emissions for the Greater Cape Town region. The variations of the observed (Obs) and predicted (P62 and P63) SO_2 concentrations for: b) CBD site (S2), c) Bellville site (S1), d) Goodwood site (S3) and e) the hourly averaged wind velocity, mixing height and stability classes for the days selected for the model evaluation.

The time-averaged area and point emissions are depicted in Figure 4.3 (a). The mean area source emissions are about 45% of the total. The coefficient of variation, which is the standard deviation divided by the mean, is 9% and 54% for the point and area emissions respectively. Therefore, the daily variation of the area emissions is much greater than the one observed by the point sources.

The area source emission strength peaks at two hours after sunrise (8h00), to remain approximately the same during the next 6 hours. It then decreases rapidly to reach a minimum at 12 hours after sunrise. A similar trend is evident for the point source emissions (Figure 4.3 (a)).

In order to evaluate how the predictions compare with the observations, the time-averaged concentrations were calculated. Figure 4.3 (b)–(d) shows the mean concentrations of the predictions and observations for the three monitoring stations as a function of the local time. At the CBD monitoring station (S2) the model consistently under-predicts at all hours. However, it follows the general trend of the observed concentrations (see Figure 4.3 (b)). The terrain surrounding station S2 and the area's meteorological conditions are complicated, due to the sheltering effects of Table Mountain and the land and sea-breezes of Table Bay. A steady-state Gaussian model such as ISCST2, is not able to simulate accurately such complex conditions.

At Goodwood monitoring station (S3), the model predictions are biased toward under-prediction (Figure 4.3 (d)). The larger deviation between predicted and measured concentrations is evident during the 6 hours following the sunrise at 8h00. At this location, the observed concentrations show a peak between one hour before sunrise to 3-4 hours after sunrise. It should be noted that a possible explanation for the general bias at site S3 is the use of emissions for the year 1991 instead of the year 1992, as already mentioned in Chapter 3.

The best results, as expected, were produced for Bellville station (S1) (Figure 4.3 (c)). The model seems to over-predict at the hours before sunrise and after sunset. Predictions with the Pasquill stability characterization (P63) seem to compare better with observed concentrations at the hours after the sunset and between 10h00 and 16h00. At all three sites predictions show a peak at 3h00 and 18h00. The peak at 18h00 could originate from the atmospheric stability calculation for the transient hour of day to night-time. Another possible explanation for these peaks could be unrepresentative hourly emissions in the emission inventory. According to this inventory, the hours of emission are represented by the hours of function for each industry, which may not correspond to all the sources.

From Figure 4.3 (e) it is evident that the maximum dilution potential of the atmosphere is at 15h00, as the mixing height and wind velocity are maximal and atmospheric stability is unstable. Around 15h00 the area and point emissions are also maximum. Therefore, in terms of phase relationship, the predicted ground level concentrations correspond primarily to the meteorological parameters. At all sites the

observed concentrations reach maximum values about 1-2 hours after sunrise. During these hours convective turbulence starts to break-up the ground-based elevated inversions. Emissions from elevated point sources which have been trapped aloft by stable layers, are now entrained towards the ground. This plume fumigation process is possibly responsible for the observed concentration peaks.

The point and area sources have different characteristics and therefore the ISCST2 model treats them differently. In order to assess the contribution of each source type to the predicted concentrations, two separate runs were performed. The first included only the area sources whereas the second only the points. From these runs, the temporal variations of the predicted concentrations at Bellville and Goodwood were calculated separately for the area and the point sources, as illustrated in Figure 4.4 (a) and (b).

During the unstable hours of the day, between sunrise and sunset, the emissions are 50% higher from area sources than from point sources. The temporal variations reveal that the predicted concentrations from the area sources do not increase proportionally to the emissions. On the contrary, area predictions are higher during the stable hours of the day (i.e. before sunrise (8h00) and after sunset (18h00)). Therefore, area sources have greater influence on the ground-level concentrations during the night-time and low mixing heights. Point sources are the main contributors to the ground-level concentrations during the hours between sunrise and sunset.

If more sources would have been characterised as point sources with the use of a more accurate emission inventory, the predicted concentrations would possibly have shown a better phase relationship with the observations.

4.5.3 Paired Statistical Analysis

The time averaged variations of the SO_2 concentrations showed a better agreement between observations and predictions, when the Pasquill stability scheme was combined with the Holzworth procedure for mixing heights. Statistical analyses were applied to the concentration pairs at all monitoring stations, in order to quantify these discrepancies. Examination of these statistics, as presented in Tables 4.3 - 4.5, show that the two stability methods do not produce significantly different predictions.

A closer look at monitoring station S2 reveals that, even though the Pasquill data set (P63) predicts the observed maximum value of 79 $\mu g/m^3$ and standard deviation of 13.6 $\mu g/m^3$ more closely than the Monin-Obukhov data set (P62), the P63 mean difference is slightly greater than the one produced by the P62 data set (see Table 4.3). The index of agreement (D), which describes the percentage of potential error in predicting concentrations, denotes that there is only a 0.3% difference between the D_{P63} and D_{P62}.

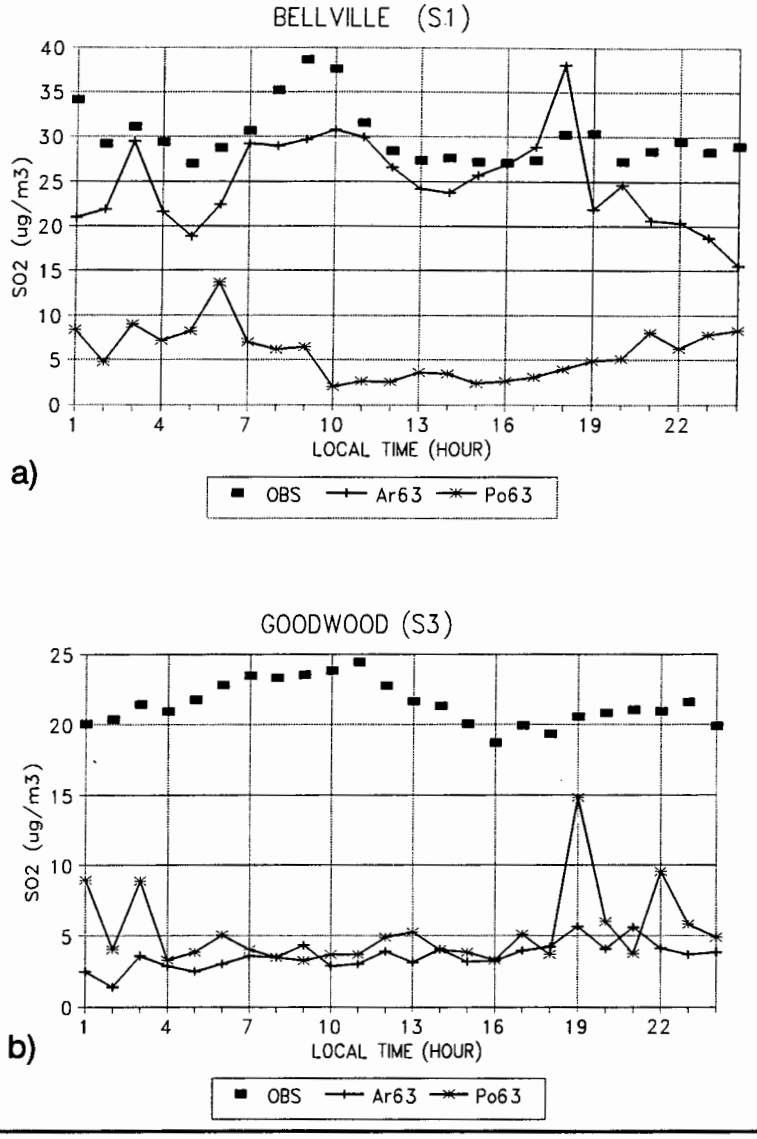

Figure 4.4 Temporal variations of observed (Obs) and predicted SO_2 concentrations calculated with separate runs for the area (Ar63) and point (Po63) sources: a) Bellville site (S1) and b) Goodwood site (S2).

The RMSE suggests that, on the average, P62 is 0.4 $\mu g/m^3$ closer to the observations than P63. Nevertheless, this is counterbalanced by the intercept and slope which reveal that P62 has a poorer linear fit to the O than P63. Consistent with the slope and intercept is the MSE_s which suggests that P62 under-predicts 2% more systematically than P63. This may have been introduced by the Monin-Obukhov stability method used by P62. In general, due to the large under-prediction at the CBD site, the calculated statistical values do not reveal any substantial differences between the two stability methods. The prediction accuracy, as described by the

above-mentioned statistical measures , is slightly higher when the Pasquill stability method is used.

Table 4.3 Summary of paired and unpaired statistics for the monitoring station at Cape Town's CBD (S2).

	Observations	Predictions	
		P62	P63
Sample size	607	607	607
Range[a]	5-79	0-66	0-74
Mean[a]	33.5	9.5	9.4
Standard deviation (STD)[a]	13.6	9.9	11.2
Average P/O		0.33	0.32
STD of P/O		0.46	0.48
Mean difference[a]		-24.1	-24.2
Intercept		4.7	3.9
Slope		0.14	0.16
Fractional bias (FB)		-1.119	-1.128
Index of agreement (D)		0.420	0.423
NMSE		2.56	2.66
RMSE[a]		28.5	28.9
$RMSE_u$		9.6	11.0
$RMSE_s$		26.8	26.7
MSE_u/MSE		12%	14%
MSE_s/MSE		88%	86%

[a] The units of range, mean, STD, mean difference and RMSE are $\mu g/m^3$

At Bellville monitoring station (S1), the mean observed concentration of 29.2 $\mu g/m^3$ is predicted 11% more accurately by the $\overline{P}_{P63}$ (Table 4.4). Both stability methods P62 and P63 over-predict the mean concentration, and their mean difference from the observed is 4.6 and 1.5 $\mu g/m^3$ respectively. The variability of the observed concentrations, as revealed by the STD, is also over-estimated by both methods. Nevertheless, the maximum predicted concentrations are within a factor of two of the observed. The fractional bias also indicates that predictions are within a factor of two from the observations, with FB_{P63} being closer to FB=0.0 than FB_{P62}. Similarly, the regression parameters (slope and intercept) suggest that P63 has a better fit to the observations than P62. The MSE_s is 6% lower for the P63 data set. Lower systematic error means that the model predicts closer to its accuracy limits. Even though the general performance of P63 is better than P62, the former produced

higher RMSE. This is due to the fact that RMSE is sensitive to the presence of extreme $|P_i - O_i|$ values. Examination of the range and STD of the two sets shows that there are more extreme values in the P63 predictions, thus explaining the higher RMSE.

Table 4.4 Summary of paired and unpaired statistics for the monitoring station at Bellville (S1).

	Observations	Predictions	
		P62	P63
Sample size	1272	1272	1272
Range[a]	5-160	1-279	1-299
Mean[a]	29.2	33.8	30.7
Standard deviation (STD)[a]	18.1	31.2	33.8
Average P/O		1.47	1.31
STD of P/O		1.77	1.71
Mean difference[a]		4.6	1.5
Intercept		22.8	17.2
Slope		0.37	0.46
Fractional bias (FB)		0.145	0.051
Index of agreement (D)		0.422	0.435
NMSE		1.11	1.32
RMSE[a]		32.9	34.3
$RMSE_u$		30.6	32.8
$RMSE_s$		12.2	9.8
MSE_u/MSE		86%	92%
MSE_s/MSE		14%	8%

[a] The units of range, mean, STD, mean difference and RMSE are $\mu g/m^3$

For the Goodwood monitoring station, the statistics in Table 4.5 show no distinct difference between predictions using the two stability methods. The mean of P62 is 0.8 $\mu g/m^3$ closer to the $\overline{O}$ than the P62 mean. The fractional bias calculated from the P62 data set is closer to the perfect value of zero. But the index of agreements (D) suggests that P63 is about 0.5% more accurate than P62. Consistent with D, the linear regression coefficients reveal that the Pasquill data set has a better fit to the observations than the Monin-Obukhov set. An overall comment as to the effect of the stability method on the model's accuracy is that the Pasquill method produces better, or in worst cases, similar results to the ones produced by the Monin-Obukhov method.

Table 4 5 Summary of paired and unpaired statistics for the monitoring station at Goodwood (S2).

	Observations	Predictions	
		P62	P63
Sample size	769	769	769
Range[a]	1-72	0-175	0-163
Mean[a]	21.4	9.8	9.0
Standard deviation (STD)[a]	12.6	16.8	16.2
Average P/O		0.78	0.7
STD of P/O		2.98	2.58
Mean difference[a]		-11.6	-12.4
Intercept		8.5	7.5
Slope		0.06	0.07
Fractional bias (FB)		-0.748	-0.816
Index of agreement (D)		0.403	0.408
NMSE		2.67	2.87
RMSE[a]		23.6	23.5
$RMSE_u$		16.8	16.1
$RMSE_s$		16.6	17.1
MSE_u/MSE		50%	47%
MSE_s/MSE		50%	53%

[a] The units of range, mean, STD, mean difference and RMSE are $\mu g/m^3$

Therefore, for a steady state Gaussian model such as the ISCST2, the Pasquill stability method combined with the Holzworth procedure for the mixing heights produces more accurate results than when the stability is obtained from the inverse Monin-Obukhov length (1/L). Nevertheless, it would be of interest to examine the accuracy of the predictions when the latter stability method is obtained by direct turbulence measurements or wind velocities at two different levels, instead of being calculated from one point measurements.

4.5.4 Model Performance According to Stability Category and Wind Velocity

In order to examine how the model performs under different atmospheric conditions, the data set P63 was categorised according to the stability category. The first category was the unstable one which comprised the Pasquill-Gifford classes A-C. The second group consisted of the neutral class (D) and the third of the stable classes E and F.

The statistical values of the paired analysis for each group at monitoring station S1 are depicted in Table 4.6. The results of this analysis show that the model under-predicts under unstable and neutral conditions and over-predicts at stable conditions. The index of agreement indicates that the model is approximately 12% more accurate under unstable conditions than under stable atmospheric conditions. This finding is also reinforced by the fractional bias of -0.17 and the high percentage of the unsystematic mean square error of 89%. For the stable conditions the FB is 0.83 and the MSE_u/MSE is 51%.

A similar analysis of the monitoring stations S2 and S1 revealed that the model under-estimates the concentrations under all stabilities and produces the highest predictions under stable conditions (Tables D1.2 and D1.3 in Appendix D). The index of agreement at site S2 indicates, similarly to the Bellville site, that under unstable conditions the model predicts about 10% more accurately than under stable atmospheric conditions.

Table 4.6 Summary of paired statistics according to atmospheric stability for the monitoring station at Bellville (S1) (unstable 1-3, neutral 4, and stable 5-6).

	1-3 (Unstable)		4 (Neutral)		5-6 (Stable)	
	Obs.	Pred.	Obs.	Pred.	Obs.	Pred.
Sample size	258	258	679	679	162	162
Range[a]	8-96	6-279	5-160	1-145	5-107	4-299
Mean[a]	32.3	27.2	27.3	20.7	32.5	78.4
Standard deviation (STD)[a]	15.7	26.8	18.3	17.5	19.5	50.9
Average P/O	0.94		0.98		3.23	
Mean difference[a]	-5.0		-6.6		46.0	
Intercept	10.8		17.3		46.4	
Slope	0.51		0.12		0.99	
Fractional bias (FB)	-0.17		-0.27		0.83	
Index of agreement (D)	0.495		0.409		0.374	
NMSE	0.84		1.07		1.70	
RMSE[a]	27.2		24.5		65.8	
$RMSE_u$	25.6		17.4		47.1	
$RMSE_s$	9.2		17.3		46.0	
MSE_u/MSE	89%		50%		51%	
MSE_s/MSE	11%		50%		49%	

[a] The units of range, mean, STD, mean difference and RMSE are $\mu g/m^3$

When the same data set (P63) is grouped according to wind velocity (≤ 3 m s^{-1}, 3-6 m s^{-1}, ≥ 6 m s^{-1}), the poorest agreement between predictions and observations is evident under low wind speeds (≤ 3 m s^{-1}). At Bellville monitoring station (S1), the model predictions over-estimate the observed concentrations under low wind speeds (see Table 4.7). Similarly, predictions at the other two sites (S2, S3) are highest at the low speed group (Tables D1.4 and D1.5 in Appendix D). Nevertheless, consistent with the 1h analysis, the observed concentrations at sites S2 and S3 are under-estimated for all wind categories.

Table 4.7 Summary of paired statistics according to wind velocity (u) for the monitoring station at Bellville (S1) (≤ 3 m s^{-1} , 3-6 m s^{-1}, and ≥ 6 m s^{-1}).

	u ≤ 3m s^{-1}		3m s^{-1}< u <6m s^{-1}		u ≥ 6m s^{-1}	
	Obs.	Pred.	Obs.	Pred.	Obs.	Pred.
Sample size	192	192	398	398	509	509
Range[a]	5-107	10-299	6-117	2-188	5-160	1-69
Mean[a]	34.9	72.9	29.8	29.6	26.6	15.7
Standard deviation (STD)[a]	19.4	52.3	17.4	23.6	17.5	9.6
Average P/O	2.85		1.26		0.76	
Mean difference[a]	38.0		-0.2		-10.9	
Intercept	45.1		24.3		13.7	
Slope	0.8		0.18		0.08	
Fractional bias (FB)	0.71		-0.01		-0.51	
Index of agreement (D)	0.365		0.404		0.399	
NMSE	1.56		0.85		1.13	
RMSE[a]	62.9		27.5		21.7	
$RMSE_u$	45.0		23.4		9.5	
$RMSE_s$	38.2		14.3		19.5	
MSE_u/MSE	63%		73%		19%	
MSE_s/MSE	37%		27%		81%	

[a] The units of range, mean, STD, mean difference and RMSE are $\mu g/m^3$

4.5.5 Examination of the Maximum Concentrations

When the regulatory use of models is of interest, comparison of the magnitudes of the maximum predicted and observed concentrations is important. Air-quality standards are based on a concentration level which should not be exceeded for a particular time span. Models are used to assess the compliance with these standards and estimate the impact of new sources on the existing pollution levels.

Table 4.8 shows the calculated statistical measures for the one hour maximum observed and predicted concentrations, which were selected from the P63 data set. Since the hourly variation of the SO_2 emissions in the emission inventory were not detailed enough to allow for the comparison of the maximum observed concentration with its corresponding predicted value, the maximum concentrations for each day were selected independently of the time of occurance during the day.

The ISCST2 model includes an option for regulatory purposes. With this option the concentration during an hour with calm wind conditions (u=0.0) is set to zero, and the specified averages for the day are calculated from the remaining hours. Therefore, hours with calm wind conditions were excluded from the hourly model evaluation. Due to the above mentioned regulatory option, the upper boundary of the selected observed concentrations which were used for the hourly model evaluation, could not include concentrations measured during hours with calm wind conditions. This is not the case for the evaluation of the maximum concentrations, since the concentrations are selected independently of the hour of occurance during the day. Therefore, the observed range in the tables with the evaluation of the maximum concentrations could be wider than the one observed for the hourly evaluation. The above discrepancy is evident at site S2 were the hourly upper boundary concentration is 79 $\mu g/m^3$ (see Table 4.3), when the maximum upper limit is 89 $\mu g/m^3$ (see Table 4.8).

Analysis of the maximum observed and predicted concentrations, independent of the time of occurance during the day, demonstrates that the model reproduces the range, and particularly the upper boundary of the concentrations, approximately within a factor of two at all three sites (see Table 4.8). In particular, predictions at CBD (S2) monitoring station systematically under-estimate the maximum concentrations, as suggested by the systematic fraction of the mean square error (MSE_s/MSE=67%). The fractional bias of -0.61 indicates that, on average, the predicted maximum concentrations are within a factor of two from the measured ones.

A better performance is evident at the Goodwood site (S3) (see Table 4.8). In contrast to the general under-prediction shown by the one hour concentrations at this location, the predicted maxima are, on average, 21% higher than the observed. The unsystematic fraction of the MSE reveals that the model performs closer to its potential accuracy at the Goodwood (S3) location, since 81% of the mean square error is unsystematic. The closest fractional bias (FB) to the desired value of 0.0 is also the one at site S3.

At Bellville monitoring station (S1) the observed maxima are over-estimated approximately by a factor of two (Table 4.8). The mean maximum predicted concentration is 106 $\mu g/m^3$ when the mean observed is 56 $\mu g/m^3$. The systematic fraction of the MSE is high (42%). This indicates a possible systematic cause for the over-prediction, such as the emission strengths.

The fractional bias is within the ±0.67 range at all three monitoring stations. When the FB is out of these limits, predictions are considered to be over- or

under-estimated by a factor greater than two. In general, the model seems to perform poorly at Cape Town's CBD site (S1), since the maximum concentrations are under-estimated. The magnitude of over-prediction at the Bellville site (S1) could possibly be explained by the lack of detailed emission information available for the Bellville area. The portion of the SO_2 emissions in the Bellville magisterial district, which was allocated to point sources was approximately 25% of the total, whilst it was 40% for Goodwood and 55% for Cape Town.

From Figure 4.5 (a)-(c) it is evident that at locations such as Bellville and Goodwood the model would predict the maximum concentration with a tendency towards over-prediction. The same finding is also indicated by the bootstrap analysis which is discussed in detail later. The maximum concentrations are of most importance when a model is to be used for regulatory purposes. Therefore, the requirement for the ISCST2 not to under-estimate these concentrations is met at the two monitoring sites S1 and S3.

Table 4.8 Summary of statistics for the one hour maximum observed and predicted concentrations independent of time of occurance during the day. These subsets were selected from data set P63 for the monitoring stations at CBD (S2), Bellville (S1) and Goodwood (S2).

	CBD (S2)		Bellville (S1)		Goodwood (S3)	
	Obs.	Pred.	Obs.	Pred.	Obs.	Pred.
Sample size	33	33	53	53	39	39
Range[a]	21-89	5-74	18-160	19-299	10-72	5-163
Mean[a]	53.8	28.7	55.8	106.3	38.4	48.4
Standard deviation (STD)[a]	16.3	20.1	32.25	65.2	14.2	35.3
Average P/O	0.57		2.29		1.49	
Mean difference[a]	-25.1		50.5		10.0	
Intercept	14.3		85.4		47.9	
Slope	0.27		0.37		0.01	
Fractional bias (FB)	-0.61		0.62		0.23	
Index of agreement (D)	0.422		0.353		0.298	
NMSE	0.75		1.19		0.83	
RMSE[a]	34.0		84.0		39.3	
$RMSE_u$	19.6		64.0		35.3	
$RMSE_s$	27.8		54.4		17.2	
MSE_u/MSE	33%		58%		81%	
MSE_s/MSE	67%		42%		19%	

[a] The units of range, mean, STD, mean difference and RMSE are $\mu g/m^3$

The same data subset with the maximum concentrations was used to calculate the cumulative frequency distributions at each monitoring station (Figure 4.6). It is

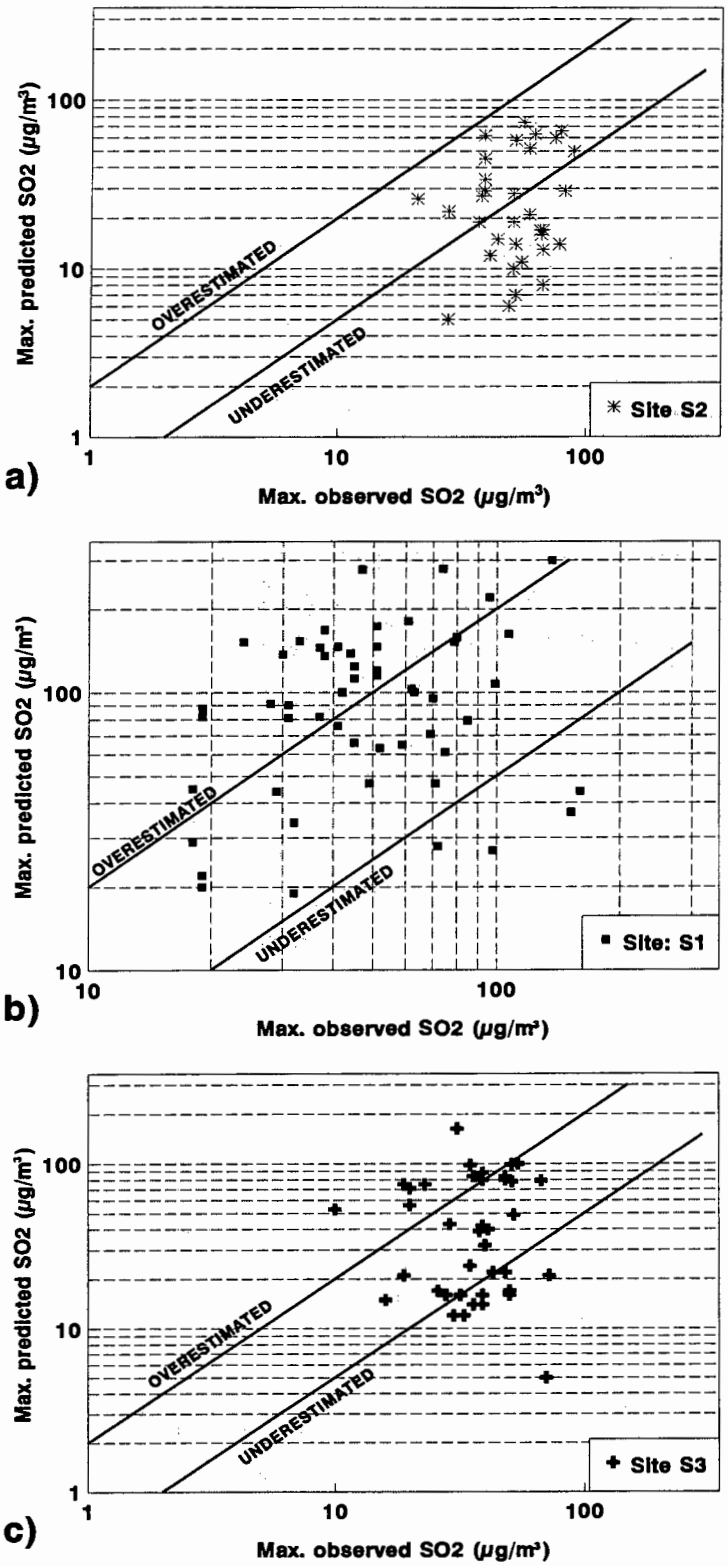

Figure 4.5 The daily maximum predicted and observed concentrations independent of time of occurance during the day for the monitoring stations of: a) CBD (S2), b) Bellville (S1) and c) Goodwood (S3). The solid lines represent the over- and under-estimation by a factor of two.

evident, consistent with the bootstrap analysis, that at site S2 the model under-estimates the observed concentrations at all percentiles. The opposite occurs at site S1 where the maximum predictions are higher than the maximum observed concentrations at all probabilities. The crossover of the frequency distributions at site S3 indicates that ISCST2 tends to under-predict at the low concentrations and over-predict at the higher percentiles (i.e. above the 0.6 quartile). The latter are more important from a regulatory point of view.

Included in Figure 4.6 are also the cumulative distributions from the P62 data set. There is no significant difference between the distributions from the Pasquill and the inverse Monin-Obukhov length methods. Pasquill scheme is based on meteorological variables such as wind velocity, solar radiation and cloudiness. The correspondence between these variables and the dispersion characteristics is qualitative. Thus, it would not be surprising if the model would not perform well at a location with complicated meteorology such as the CBD. Therefore, the fact that Pasquill scheme seems to follow the observed distribution better than the Monin-Obukhov method could be fortuitous.

4.5.6 Bootstrap Resampling Analysis

In order to estimate the reliability of the model's prediction at the three monitoring stations, the blocked bootstrap resampling procedure was applied to several statistical measurements. A FORTRAN code was developed for the application of the blocked bootstrap on the 1h and 24h averages.

The daily averages are blocked according to the season (i.e. winter, spring, summer, autumn). Examination of the auto-correlogram of the stability classes and wind velocities revealed 24h and 48h cycles. In order to maintain the day-to-day meteorological persistence in the 1h bootstrap data set, the blocking was performed in two manners. The first was the same as the one used for the 24h averages. The second blocking procedure allowed the selection of 2-day clusters within each season block. The input to the bootstrap generator is the ISCST2 meteorological input file and the observed and predicted concentrations. The code correlates the dates to the concentrations, performs the blocking and calculates the mean observed and mean predicted concentrations, mean difference, absolute difference, index of agreement, fractional bias, normalised mean square error, variance of difference and root mean square error of the difference. The same process is repeated by the program 1000 times to obtain the bootstrap sample, which consists of 1000 values of the computed statistical parameters. These values are then used for the distribution function and confidence limits of each parameter.

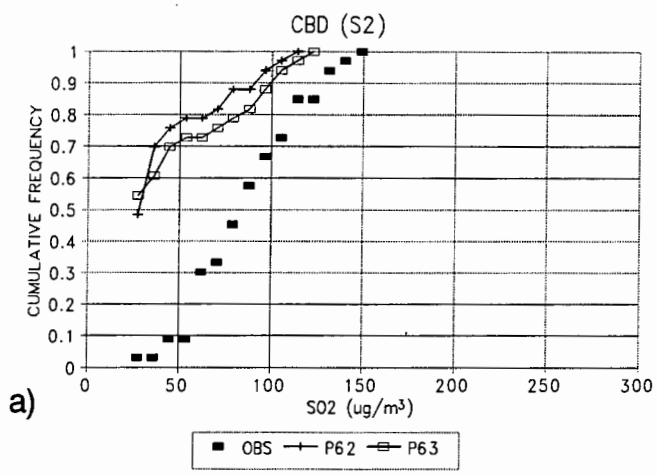

a)

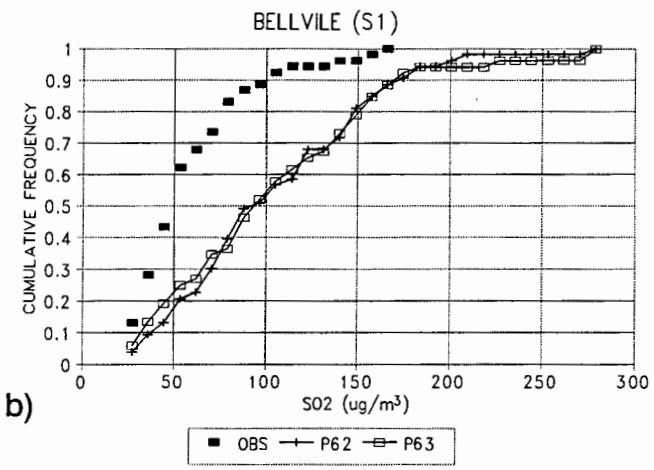

b)

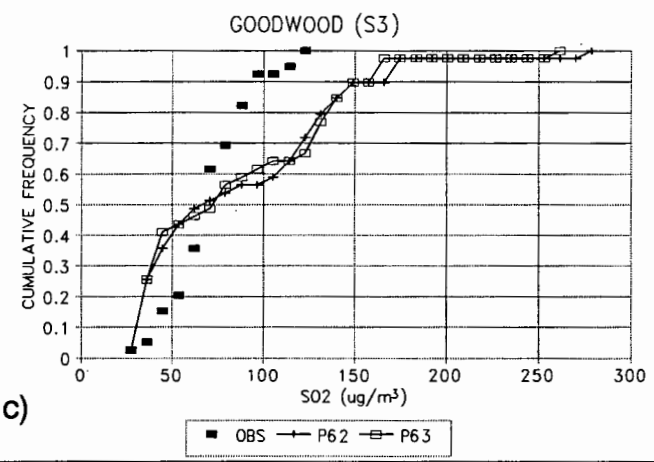

c)

Figure 4.6 Cumulative frequency distributions of the maximum observed and predicted concentrations selected from the data sets P62 and P63 at monitoring sites: a) Cape Town's CBD (S2), b) Bellville (S1) and c) Goodwood (S3).

The bootstrap generator was applied on all data sets (P60-P68) and monitoring stations (see Appendix D). In this section, the bootstrap results for the 1h and 24h averages, as well as the maximum concentrations from the data set P63 are presented. Figure 4.7 (a)-(c) depicts the 95% confidence intervals of the index agreement, fractional bias and mean difference, as calculated from the 1h concentrations. Figure 4.8 (a)-(c) displays the bootstrap results for the same parameters from the 24h averaged concentrations. Figure 4.9 (a)-(c) illustrates the same results for the hourly maximum concentrations independent of time of occurrence during the day. Each of these results are grouped according to the monitoring stations at CBD (S2), Bellville (S1) and Goodwood (S3). The upper and lower boundaries represent the 95% confidence bounds for each parameter. These bounds were computed by adding and subtracting twice the standard deviation to and from the parameter's actual value.

The FB intervals of the 1h concentrations indicate that the model performance is significantly different at site S1 than at the other two sites (Figure 4.7 (b)). When the FB confidence interval overlaps zero, the predictions will be in good agreement with observed concentrations 95% of the time, with repeated use of the model. The same performance is revealed by the mean difference (Figure 4.7 (c)).

The 24h averages, consistent with the 1h analysis, reveal a similar difference in performance at Bellville from the rests monitoring stations (Figure 4.8). The model seems to perform within the acceptable accuracy limits only at the Bellville site (S1). If the confidence intervals of the fractional bias and mean difference do not overlap zero, this indicates a statistically significant difference between the observed and the predicted concentrations. The model at Goodwood site is at the limit of under-estimating the observations by a factor of two. At Cape Town's CBD the under-estimation is greater than a factor of three.

From a regulatory point of view, the model should be able to accurately estimate the highest concentrations which may occur at a certain location. The bootstrap analysis of the maximum concentrations (Figure 4.9 (a)-(c)) reveals that the model over-estimates the observations at sites S1 and S3. Nevertheless, the confidence intervals of the fractional bias and mean difference at site S3 overlap with zero. The maximum concentrations at CBD site (S2) are still under-estimated, indicating a bias towards under-prediction. The magnitude of the predicted maximum concentrations, as revealed by the bootstrap analysis, is within a factor of two from the maximum observations at all three monitoring stations. Therefore, it would be reasonable to use the ISCST2 model for regulatory purposes, particularly for areas further away from the coast line, such as Goodwood and Bellville.

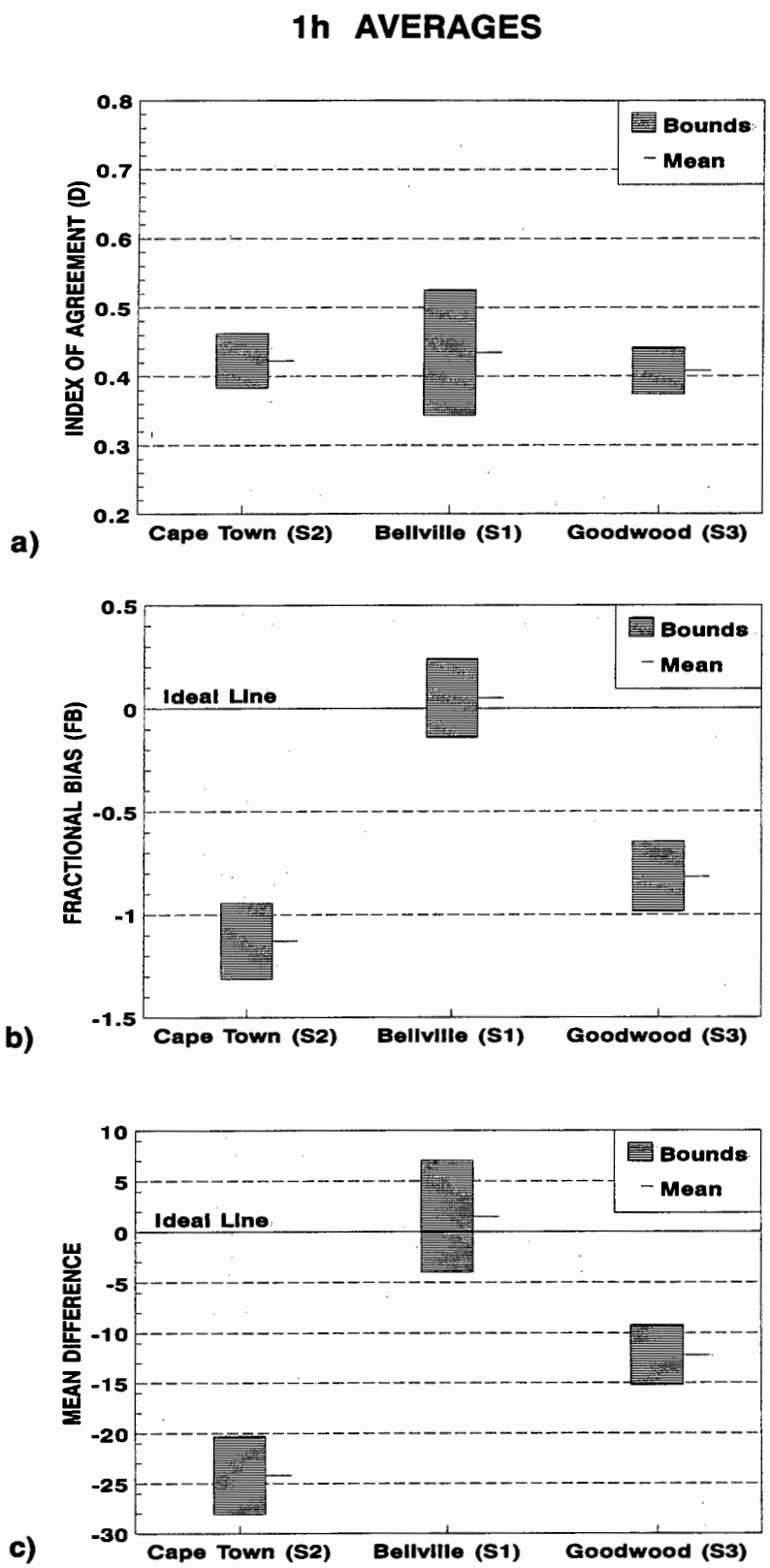

Figure 4.7 The 95% bootstrap confidence intervals for the: a) index of agreement, b) fractional bias and c) mean difference. The calculations were based on 1h observed and predicted concentrations and the results were grouped according to monitoring site.

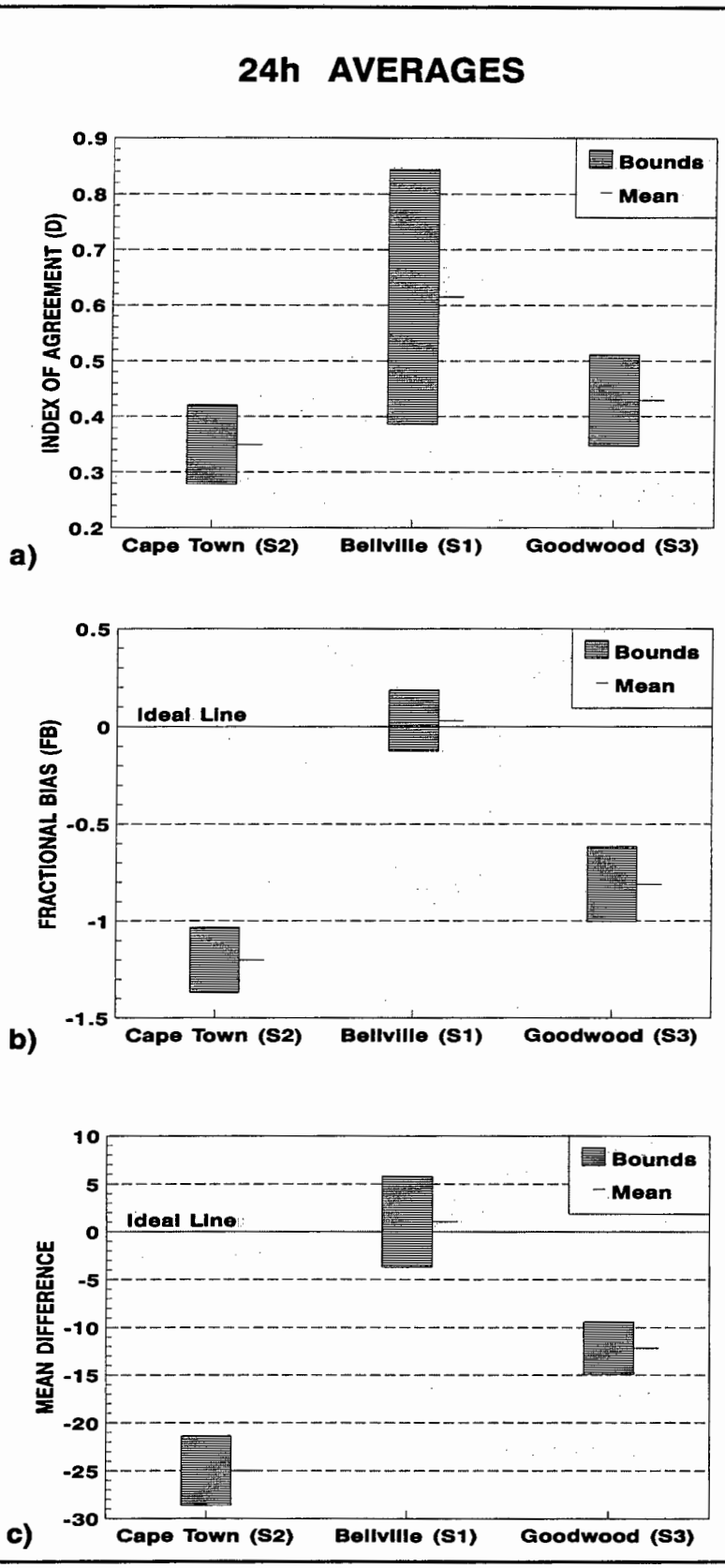

Figure 4.8 The 95% bootstrap confidence intervals for the: a) index of agreement, b) fractional bias and c) mean difference. The calculations were based on 24h averaged observed and predicted concentrations and the results were grouped according to monitoring site.

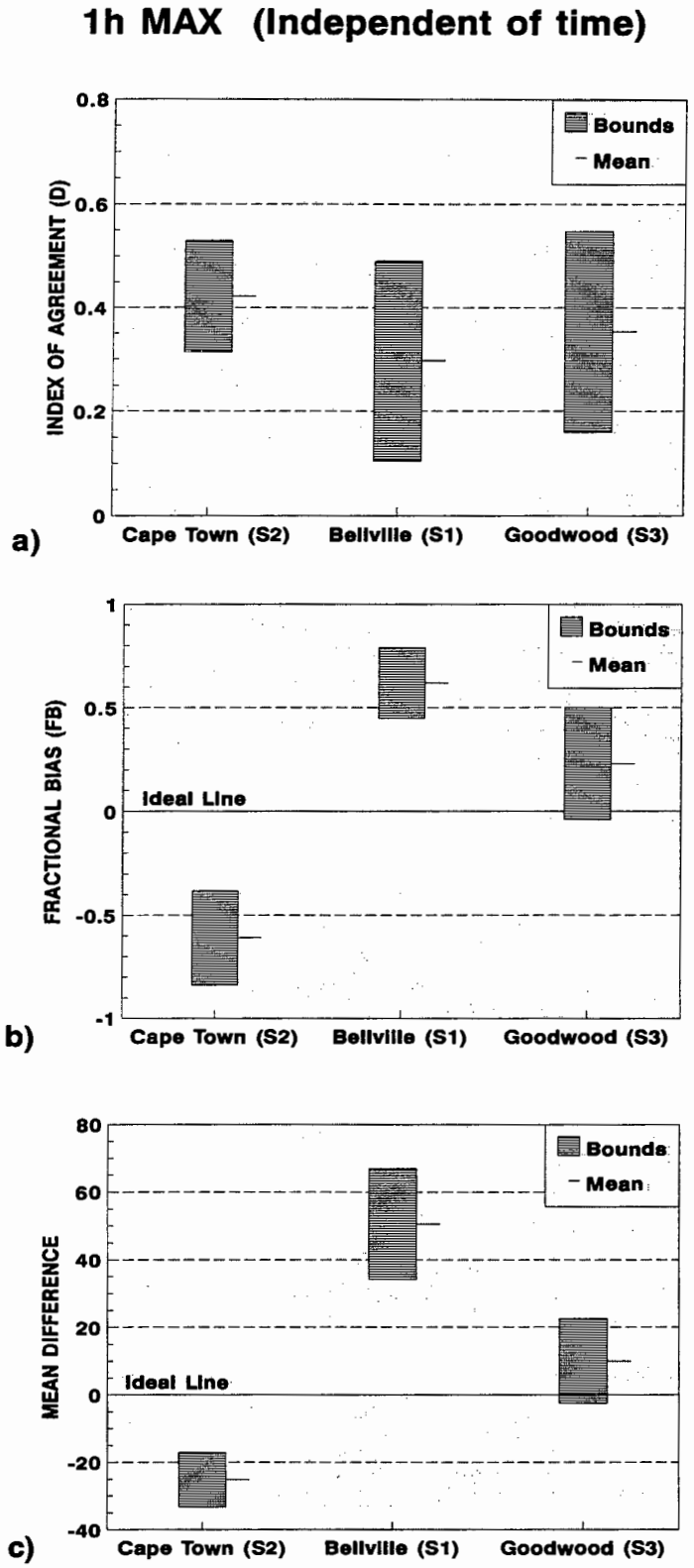

Figure 4.9 The 95% bootstrap confidence intervals for the: a) index of agreement, b) fractional bias and c) mean difference. The calculations were based on maximum observed and predicted concentrations independent of time of occurance during the day. The results were grouped according to monitoring site.

4.6 Summary and Conclusions

The performance of the Industrial Source Complex Short Term 2 (ISCST2) model was evaluated with the use of hourly SO_2 concentration measurements at three monitoring stations. The first monitoring station (S1) was at Labiance, Bellville; the second (S2) at Cape Town's CBD and the third (S3) at Goodwood, showgrounds. Both paired and unpaired analyses were performed in order to compare the model performance at each station. The paired statistics used were recommended at the Woods Hole EPA/AMS Workshop. In addition, other measures such as the fractional bias, the index of agreement, the systematic and unsystematic fractions of the mean square error were also included. Several methods from which the meteorological parameters were estimated produced various model inputs, in order to compare their effect on the model accuracy.

The best overall prediction performance of the ISCST2 model was evident at Bellville monitoring station (S1). At the Goodwood and the CBD sites the observations were under-estimated by a factor of two and four respectively. Nevertheless, examination of the maximum concentrations, selected independently of the time in which they occur during the day, revealed best model performance at site S2. The maximum concentrations at Bellville were over-estimated, and under-estimated at CBD; but at both locations the predictions were within a factor of two from the observations.

Furthermore, the observed and predicted concentrations were grouped according to the atmospheric stability category and wind speed, so as to assess the model's performance under different meteorological conditions. It was found to perform better under unstable and neutral conditions than under stable atmospheric conditions. When the data were grouped according to wind velocity, the poorest performance occurred at the lowest wind category (i.e. $u \leq 3m\ s^{-1}$).

The temporal variations of the concentrations, as well as the emissions and meteorological parameters, provide some insight as to how complex the relationship between the ground-level concentrations, the area and point sources and the meteorological conditions really is. These results reveal the importance of the area sources during the stable hours of the day (i.e. night-time) and low mixing heights. Point sources dominate the concentrations during day-time and are responsible for the peak values. These results also suggest that besides the correct estimation of the emission rates, the proper characterisation and distinction between area and point sources is of great importance for the accurate simulation of ground-level concentrations.

The bootstrap procedure was employed to determine the uncertainty of statistical measures, such as the index of agreement, fractional bias and mean difference. Analysis of the bootstrap results showed that the differences among the predictions at the three locations are statistically significant at the 95% confidence level.

At Bellville site (S1) the model predicts the 24h averages within a factor of two, whilst the confidence intervals of the fractional bias and mean difference overlap zero. At Goodwood and CBD sites, the bootstrap analysis suggested that the under-prediction is significant at the 95% confidence level.

Application of the bootstap procedure on the maximum concentrations revealed that the model is able to predict the maxima within a factor of two at all three monitoring stations. However, at the 95% confidence level, the CBD observed concentrations are under-estimated, whereas they are over-estimated at the Bellville site. These results are statistically significant at both locations (S1, S2) since the intervals of the FB and mean difference do not overlap zero. The best predictions of the maximum concentrations was evident at Goodwood site, as the above mentioned intervals overlap zero.

Chapter FIVE

SUMMARY AND CONCLUSIONS

5 SUMMARY AND CONCLUSIONS

This thesis considers air pollution modelling aspects for the Greater Cape Town region. An EPA Gaussian plume model, the Industrial Source Complex 2, has been applied and evaluated with observed sulphur dioxide concentrations at three monitoring stations in the area.

The meteorological data used in this study were collected form D. F. Malan airport measurements for the years 1991 and 1992. The model requires additional meteorological parameters, such as the mixing height and the atmospheric stability class. Since these are not readily available they needed to be calculated. For this purpose, three mixing and three stability class methods were utilised, in order to examine their effect on the model's accuracy.

The general emissions of SO_2, NO_x and particulate matter in the Greater Cape Town area were calculated from the fuel consumption at each magisterial district, according to different source categories. A database code was developed in order to store, as well as provide easy access to, emission information from all the large emitters in the area. This emission inventory is currently being used by the Cape Town City Council's Air Pollution Control and can provide updated information of the SO_2, NO_x and particulate matter emitted from the industrial and commercial sectors in the area. The general emissions, as well as those obtained from the inventory database, comprised the area and point source emission input to the ISCST2 model.

The performance of the ISCST2 model was evaluated with the use of 53 days of hourly SO_2 concentrations at three monitoring sites. These monitoring stations were situated at Bellville, Cape Town's CBD and Goodwood. The model performance was quantified by utilising several statistical measures as proposed in the EPA/AMS Workshop, as well as by additional parameters such as the fractional bias and the index of agreement. Their confidence intervals were examined with the use of the bootstrap resampling technique. In order to assess the model accuracy under different atmospheric conditions at each location, the paired observed and predicted concentrations were grouped according to different atmospheric stabilities and wind velocities. The conclusions reached in the present thesis, from all the above-mentioned analyses, are discussed in the following sections.

5.1 Use of Different Meteorological Methods

As mentioned earlier, nine meteorological input data sets were used with the ISCST2 model. The bootstrap analysis of the model's predictions did not reveal any significant differences between these meteorological methods. However, the model was more sensitive to stability than to the mixing height input.

Even though the Pasquill method was found to be biased towards the neutral (D) atmospheric stability, it produced more accurate results. This can be explained firstly, by the fact that the Pasquill method is more robust towards atmospheric changes. Secondly, the Monin-Obukhov, as well as the Kazanski-Monin methods were calculated from one point measurements. The friction velocity, on which these two methods are based, is calculated more accurately when two point wind velocities and temperatures are available.

Therefore, utilising routine measurements, in order to derive the micro-meteorological parameters with more advanced methods, does not contribute significantly to the model's accuracy. However, it should be noted that the above applies when a central location, such as D. F. Malan airport, is used for the meteorological description of the area. If more stations, as well as two point and turbulence measurements would have been available, the Pasquill method would be expected to produce the poorest results.

A recommendation for further study could thus be the assessment of the effects of these methods on the model performance, when the meteorological observations are obtained at the same location as the monitoring sites.

5.2 Inventory of Emissions

From the emission inventory for the Greater Cape Town (GCT) region, as summarised in Figure 5.1, it is evident that industry accounts for 90 and 80 percent of the sulphur dioxide and particulate matter respectively.

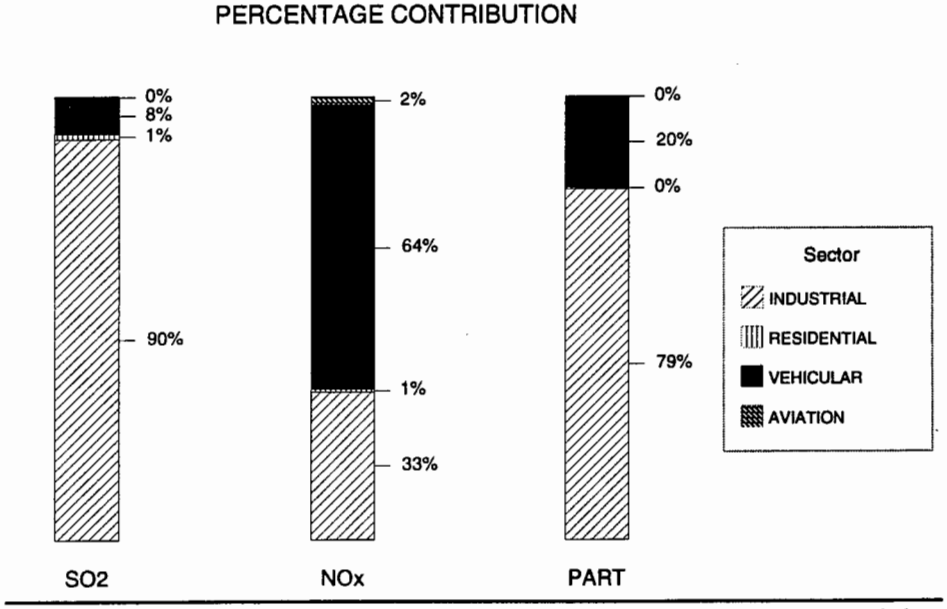

Figure 5.1 Emission percentages according to pollutant and emitting sector.

The transportation sector is responsible for 66 percent of the total nitrogen oxides and 20 percent of the particulate emissions. In general, traffic emissions follow different patterns to those from the domestic sector. Therefore, the spatial and particularly the temporal variation of the traffic emissions, cannot be accurately simulated on the basis of population densities. This indicates the need for a traffic related simulation program to be employed for these type of sources. An alternative could be the compilation of an inventory on the basis of car densities at different hours and locations in the GCT area.

In general, an accurate emission inventory should not only focus on the correct amount of the emissions, but also on the proper characterisation of the sources. The dispersion and diffusion of emitted pollutants by non-buoyant area sources is treated differently to that of the point sources.

Point sources account for the hourly peak concentration values and are mostly responsible for the ground-level concentrations during the unstable hours of the day (i.e. from sunrise 8h00 to sunset 18h00). Area sources, due to their low release height, contribute significantly to the ground-level concentrations during the stable hours of the day.

During the collection stage of the emission information, it was noticed that the readily available data were inappropriate for use in dispersion modelling. The manpower and general structure for the collection of this information already exists at departments such as the Cape Town City Council's Air Pollution Control. The only requirement is the formulation of the method and format with which the data could be collected, as part of the regular air-quality inspections.

5.3 General 1h and 24h Model Performance

The ISCST2 model predicted the observed hourly concentrations within the desired accuracy only at Bellville (S1) monitoring station. At Goodwood (S3) and Cape Town's CBD (S2), the average under-prediction was by a factor of 2 and 4 respectively.

The reason for the under-prediction at site S2 could lie in the local meteorological effects of Table Mountain and Table Bay. These effects include wind recirculation regimes which trap pollutants, and pollution oscillation carried by land and sea-breezes.

At Goodwood and Bellville, the temporal variation of the predictions revealed higher predicted concentrations before the sunrise (8h00) and after the sunset (18h00). This indicates the necessity of a more accurate characterisation of the point sources, which due to lack of available information, have been lumped into area sources.

One point which has to be noticed, is the fact that the emission variation of the point sources was based on the hours of operation for each factory. If these hours did not comply with the actual emitting time, they could offer a plausible explanation for some of the hourly prediction errors. Thus, the actual emitting hours should also constitute part of the collected information, if the hourly concentrations were to be predicted.

5.4 Performance According to Meteorological Condition

At all three locations the model was found to perform more accurately under unstable and neutral (A, B, C and D) than under stable (E, F) atmospheric conditions. During night-time, the area sources are most responsible for the ground-level concentrations. The Pasquill (P) scheme assigns stable conditions only at night-time. Therefore, its combination with the source characterisation (i.e. area instead of point sources) in the emission inventory can explain the over-prediction during these hours. The Monin-Obukhov method during stable hours was proved to be more accurate than the P scheme. This was based on the fact that the latter method utilises hourly wind speeds and radiation.

When the predictions were grouped according to wind category, the poorest performance was evident at light wind speeds (i.e. $u < 3$ m s^{-1}). Under these conditions, the model tends to over-predict the observed concentrations at site S1, whereas, at sites S2 and S3, due to the overall under-prediction, the model produces the highest concentrations.

In general the ISCST2 model tends to over-predict the observed concentrations during night-time with light wind speeds. However, this could be partially a result of unrepresentative meteorological measurements. Light winds exhibit the great spatial direction variability. Therefore, the wind direction at the sites' location could vary significantly to the one observed at D. F. Malan airport.

5.5 Maximum Concentration Performance

The maximum ground-level concentrations are of greatest importance and should not be under-estimated, since these are the ones that air-quality strategies aim to minimise.

The ISCST2 model revealed best performance when the maximum observed and predicted concentrations were examined. At Bellville (S1) and Goodwood (S3) sites, the predictions were within a factor of two from the observations with a tendency

towards over-predicting. At CBD (S2) site the model showed a consistent bias towards under-predicting.

In conclusion, the application of a Gaussian plume model, such as the Industrial Source Complex 2, is viable at locations with no complicated topography and away from Table Mountain. Further studies should expand the findings of the present thesis towards the following directions:

- Use of local meteorological measurements or a mathematical model to derive the parameters needed at each monitoring site.
- Use of a more detailed emission inventory.
- Use of a model applicable to complex terrain such as the EPA's COMPLEX model for inter-comparison with the ISCST2 at different locations.
- Use of a spatially detailed monitoring network for the model evaluation.

Finally, it is important to stress the necessity of directing the emission related data collection system towards air-pollution modelling studies. Air-pollution dispersion modelling is one of the most reliable and cost-effective tools for the development and testing of air-pollution control strategies, providing the necessary information is available.

APPENDIXES

APPENDIX A
METEOROLOGICAL PARAMETERS

I. Friction Velocity (u.)

The friction velocity can be obtained from the similarity theory using dimensional analysis (Businger, 1973). From this, the wind profile within the surface layer at any height z, is related to the friction velocity as follows (van Ulden and Holtslag, 1985; Venkatram, 1988):

$$u(z) = \frac{u_*}{k}\left[\ln\left(\frac{z}{z_0}\right) - \Psi_m\left(\frac{z}{L}\right) + \Psi_m\left(\frac{z_0}{L}\right)\right] \qquad \textbf{(A1.1)}$$

where $\Psi_m(z/L)$ is a scaling factor, i.e.

unstable conditions $L>0$ (or sensible heat flux H>0)

$$\Psi_m(z/L) = \ln\left[\left(\frac{1+X^2}{2}\right)\left(\frac{1+X}{2}\right)^2\right] - 2\,arctg(X) + \frac{\pi}{2} \quad , \qquad \textbf{(A1.2)}$$

$$X = \left(1+16\frac{z}{L}\right)$$

Stable conditions $L<0$ (or sensible heat flux H<0) (Sutherland et al., 1986)

$$\Psi_m(z/L) = -\frac{1}{2}\left[1-\left(1+60\frac{z}{L}\right)^{1/2}\right] \qquad \textbf{(A1.3)}$$

where z_0 is the roughness length, z the height of wind measurements and L the Monin-Obukhov length.

II. Modified Kazanski-Monin Parameter (μ')

The modified Kazanski-Monin Parameter (μ') can be written as (Sutherland et al.,1986):

$$\mu' = a(z_0)\ \mu\ \sin\phi \qquad \textbf{(A1.4)}$$

where z_0 is the surface roughness length, ϕ the latitude and μ the Kazanski-Monin parameter.

The multiplicative term $\mu\sin\phi$ is given by:

$$\mu\sin\phi = \frac{ku_*}{2\Omega L} \qquad \textbf{(A1.5)}$$

where k is the von Karman constant, u_* the friction velocity, L the Monin-Obukhov length and $\Omega=2\pi$ radians/24h (the earth's angular velocity). The friction velocity (u_*) could be estimated from the similarity theory (see above).

The empirical function $a(z_0)$ can be obtained by:

$$a(z_0) = \left(a \ln\frac{b}{z_0}\right)^{-1} \qquad \textbf{(A1.6)}$$

where a and b are empirical constants and have the values of 10 cm and 750 cm respectively.

In order to calculate the modified Kazanski-Monin (μ') values of the boundaries between the stability classes, it is necessary to know the boundary values of the Monin-Obukhov length (L). The L boundaries can be obtained from a Golder nomogram of the Pasquill stability classes, for a specific roughness length (z_0), on an inverted L versus z_0 scale (Golder, 1972). Knowing L, the friction velocity can be estimated. Table A1.1 shows the calculated boundary values of the multiplicative term $\mu\sin\phi$ of the modified Kazanski-Monin parameter. The values in the Table were obtained using a roughness length (z_0) of 0.5m, a latitude (ϕ) of 34.5 degrees and typical wind speeds at a 10 m reference height. The latitude used is representative of the Cape Peninsula location and the roughness length of the Greater Cape Town landscape.

Using Equation (A1.4) and the $\mu\sin\phi$ values in Table A1.1, the boundary values of (μ') between the Pasquill stability classes can be evaluated. In addition from hourly meteorological measurements the modified Kazanski-Monin parameter may be calculated and compared to its boundary values to yield the atmospheric stability category.

Table A1.1 Boundary values for the Kazanski-Monin parameter. Calculations performed with typical wind speeds (u) at 10m height and a surface roughness height of 50 cm.

Stabil.	u(m/s)	L(m)	$\Psi(z/L)$	$\Psi(z_0/L)$	u.	$\mu\sin\phi$
A-B	1	-13.87	0.88	0.12	0.183	-37.3
B-C	2.5	-55.86	0.40	0.03	0.390	-19.7
C-D	7	-277.29	0.12	0.01	0.996	-10.1
D-E	4	333.33	-0.15	-0.01	0.523	4.4
E-F	1.5	60.97	-0.79	-0.04	0.164	7.6

III. Potential Temperature (θ_*)

Van Ulden and Holtslag (1985) introduced an empirical method to determine the potential temperature θ_*. This method is based on the energy exchange between the atmosphere and the earth's surface. According to the isothermal radiation (Q_*), the day is divided into two periods. When Q_* is positive it is regarded as a diurnal case; when Q_* is negative, as nocturnal. The net radiation is given by:

$$Q^* = K^* + L^* \qquad \textbf{(A1.7)}$$

where K^* and L^* is the shortwave and longwave radiation respectively.

According to the energy balance the shortwave and longwave radiations could be quantified by (van Ulden and Holtslag, 1985):

$$K^* = (a_1 \sin\phi - a_2)(1 - b_1 C^{b_2})(1 - r) \quad ,$$
$$L^* = -\sigma T_r^4 (1 - c_1 T_r^2) + c_2 C \qquad \textbf{(A1.8)}$$

where a_1 = 990 W m^{-2}, a_2 = 30 W m^{-2}, b_1 = 0.75, b_2 = 3.4 are empirical coefficients, ϕ is the solar elevation, r = 0.23 the reflection factor, C the total cloud cover in eighths, T_r the ambient temperature at reference height z_r, $\sigma = 5.67\times10^{-8}$ the Stefan-Boltzmann constant, $c_1 = 9.35\times10^{-6}$ K^{-2} and c_2 = 60 W m^{-2}.

For day-time the potential temperature θ_* is given by:

$$\theta_* = -\frac{[(1-\alpha)S+1](1-C_G)Q^*}{(S+1)(S-C_H)\rho C_p u_*} + \alpha\theta_d \qquad \textbf{(A1.9)}$$

where α=1 for normal wet grass, θ_d=0.033 is a typical value of this empirical temperature scale and

$$C_H = 0.38\left[\frac{(1-\alpha)S+1}{S+1}\right] \qquad \textbf{(A1.10)}$$

$$C_G = \left(\frac{A_G}{4\sigma T_r^3}\right)C_H \qquad \textbf{(A1.11)}$$

$$S = \exp[0.055(T_r - 279)] \qquad (270K < T_r < 310K) \qquad \textbf{(A1.12)}$$

A_G = 5 W m^{-2} K^{-1} is an empirical coefficient for the soil heat transfer.

During night-time (Q^*<0), θ_* is given by:

$$\theta_* = T_r\left\{[(d_1 v_*^2 + d_2 v_*^3)^2 + d_3 v_*^2 + d_4 v_*^3]^{1/2} - d_1 v_*^2 - d_2 v_*^3\right\} \qquad \textbf{(A1.13)}$$

where

$$v_* = \frac{u_*}{(5gz_r)^{1/2}} \qquad \textbf{(A1.14)}$$

$$d_1 = 15$$

$$d_2 = \frac{(1+S)\rho C_p (5gz_r)^{1/2}}{2(4\sigma T_r^3 + A_G)} \qquad \textbf{(A1.15)}$$

$$d_3 = -\frac{Q^*}{4\sigma T_r^A + A_G T_r} + \frac{\Gamma z_r}{T_r} \qquad \textbf{(A1.16)}$$

$$d_4 = \frac{(1+S)\rho C_p (5gz_r)^{1/2}\theta_d}{4\sigma T_r^A + A_G T_r} \qquad \textbf{(A1.17)}$$

where Γ is the dry adiabatic lapse rate and T_r the measured temperature at height z_r.

Utilizing Equations (A1.9) and (A1.13) the potential temperature θ_* can be calculated during the day-time ($Q^*>0$) and night-time ($Q^*<0$) respectively.

IV. Interpolation Procedure for the Mixing Height

D. F. Malan weather station performs daily sounding measurements early in the morning and in the afternoon. The mixing height for these hours can be estimated from the sounding measurements utilising the pressure equation or the Holzworth procedure. Figure A1.1 depicts a schematic presentation of the schemes used to interpolate hourly mixing heights on the basis of twice calculated height values, where:

n = the Julian day

H_{min}^{n-1} = minimum mixing height on the previous day

H_{max}^{n-1} = maximum mixing height of the previous day

H_{min}^{n} = minimum mixing height on the present day

H_{max}^{n} = maximum mixing height of the present day, etc.

The mixing heights are assumed to remain stationary during the hours after midnight until sunrise (8h00), and after noon (12h00) until sunset (18h00). The in between hours are interpolated with the use of a sine function. A maximum value of H_m= 2000 m is assigned to the mixing height when there is no elevated temperature inversion or when the calculated value exceeds H_m.

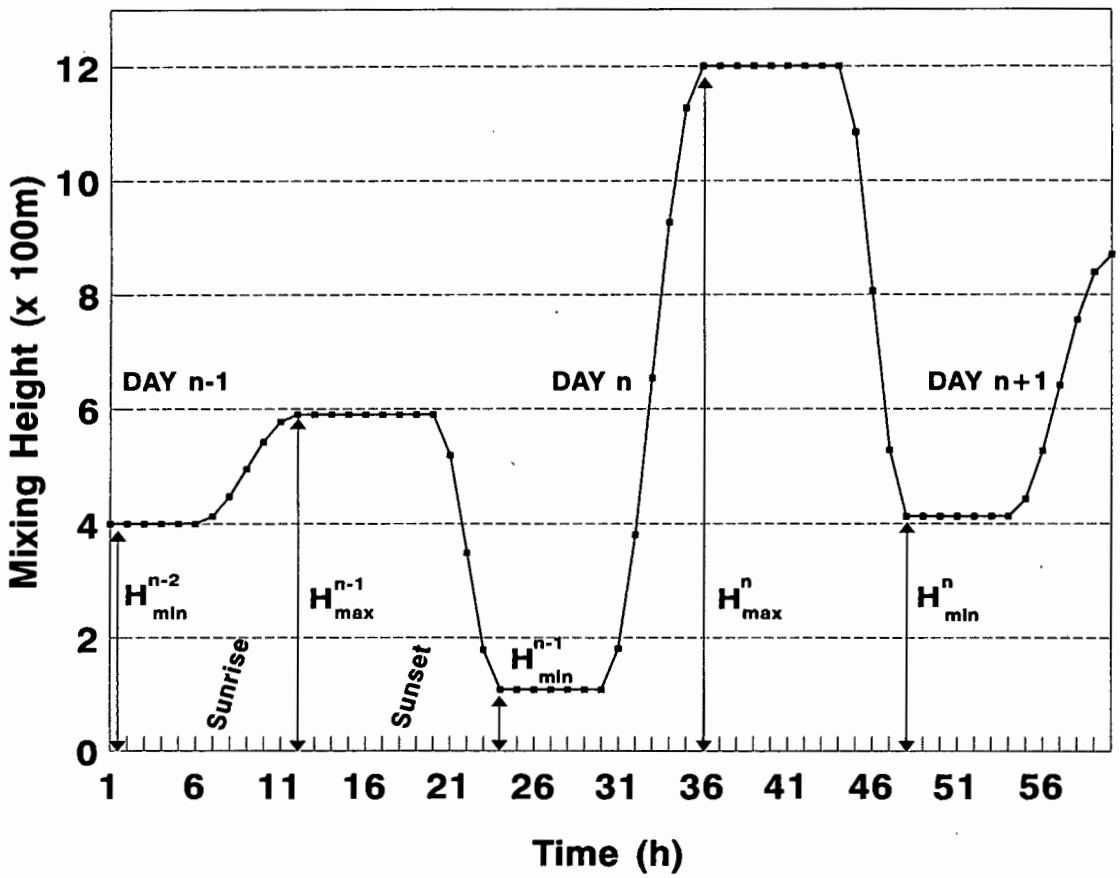

Figure A1.1 Schematic diagram of the interpolation procedures used to assign hourly mixing heights on the basis of the early morning (H_{min}) and afternoon heights (H_{max}) values of each day (n).

V. Temporal Variation of Stability Class and Mixing Height

Figures A1.2 and A1.3 illustrate the temporal variation of the Pasquill (P), Monin-Obukhov (1/L) and Kazanski-Monin ($\mu \sin\phi$) stability classes for the 37 winter and 16 summer days respectively.

The temporal variation of the three mixing height methods for the winter and summer days are depicted in Figures A1.4 and A1.5 respectively.

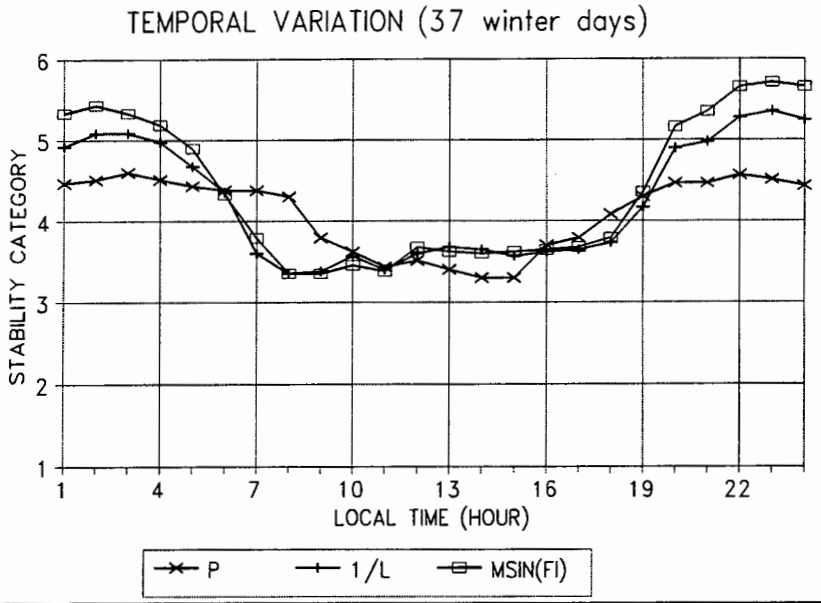

Figure A1.2 Temporal variation of stabilities produced by the Pasquill (P), Monin-Obukhov (1/L) and Kazanski-Monin ($\mu\sin\phi$) methods for the 37 winter days.

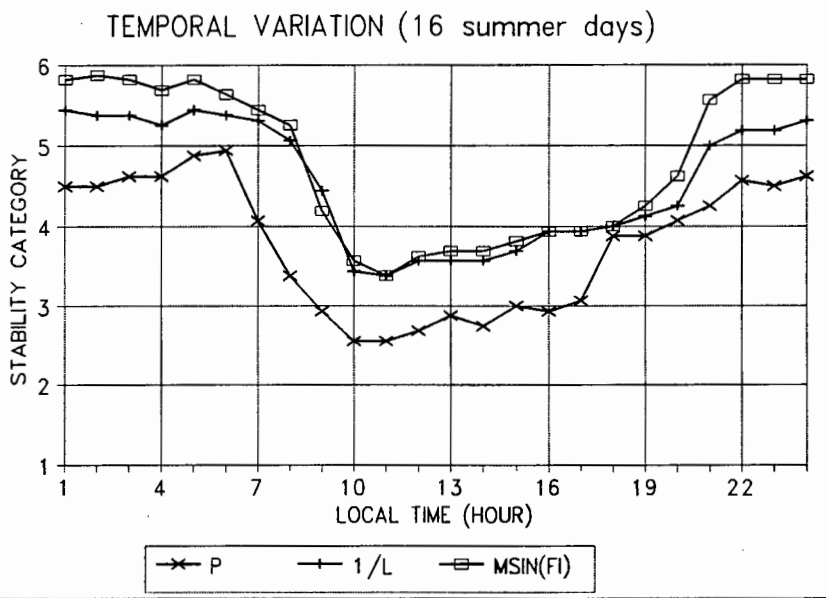

Figure A1.3 Temporal variation of stabilities produced by the Pasquill (P), Monin-Obukhov (1/L) and Kazanski-Monin ($\mu\sin\phi$) methods for the 16 summer days.

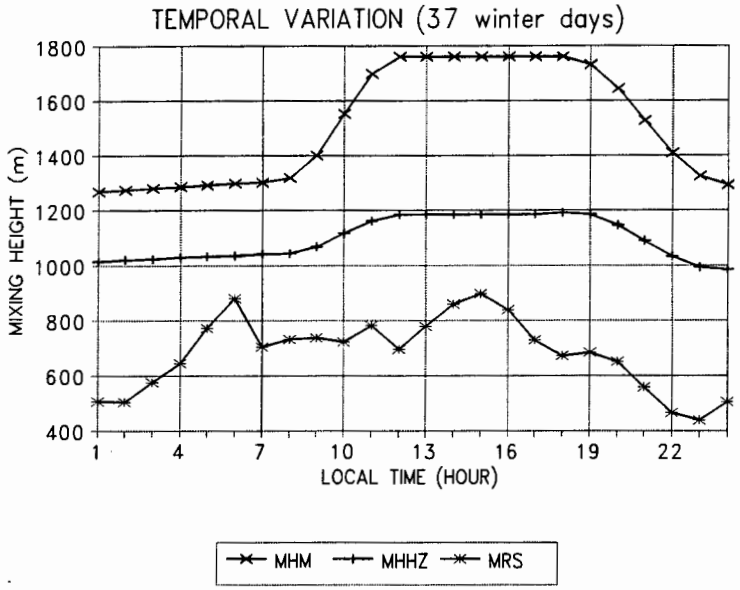

Figure A1.4 Temporal variation of mixing heights produced by the significant pressure level (MHM), the Holzworth (MHHM) and the heat exchange (MRS) methods for the 37 winter days.

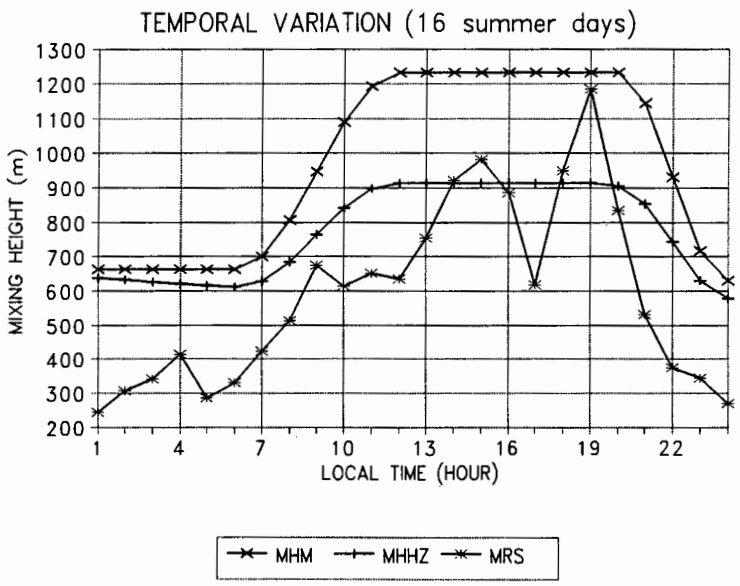

Figure A1.5 Temporal variation of mixing heights produced by the significant pressure level (MHM), the Holzworth (MHHM) and the heat exchange (MRS) methods for the 16 summer days.

APPENDIX B
EMISSION FACTORS

I. Fuel Emission Factors According to Consuming Sectors

The emission factors used in the present study to calculate emissions from different types of fuels, are shown in Table B1.1. The sulphur (S) and ash (A) content of each fuel are also included in this Table.

Since most of the aviation fuel is consumed during the flight, the pollutant emissions of the aviation sector were calculated in terms of take-offs and landings (t-l). These emission factors are shown in Table B1.1 according to two aircraft categories: the first consists of aircraft smaller than or equal to a Boeing 707 and the second from a Boeing 707 up to a Boeing 747.

Table B1.1 Emission factors for SO_2, NO_x and particulate matter according to emitting sectors: industrial, domestic, vehicular and aviation.

FUEL	Emis. Units	SO_2 Emission Factor	NO_x Emission Factor	Part. Matter Emission Factor
Coal (ind)	kg/t	19 S[a] } ⇒19 S=1%[c] }	7.5[b]	6.5 A[b] } ⇒130 A=20%[c] }
Coal (dom)	kg/t	19 S[b] } ⇒19 S=1%[c] }	1.5[a]	10[b]
HFO (ind)	kg/kl	19.6 S[d] } ⇒62.72 S=3.2%[c] }	5.72[d]	2.75[e]
Diesel (ind)	kg/kl	17.6 S[d] } ⇒9.33 S=0.53%[c] }	8.47[d]	13.2[d]
Diesel (veh)	kg/kl	17.6 S[d] } ⇒9.33 S=0.53%[c] }	37[f]	33[f]
Petrol (veh)	kg/kl	1.7[g]	19[f]	14[f]
Gas (dom)	kg/kl	0.0059[d]	1.446[d]	0.22[d]
Paraffin(dom)	kg/kl	17.6 S[e] } ⇒8.5 S=0.5%[b] }	1.5[e]	1.2[e]
Wood (dom)	kg/t	0.75[e]	5[e]	15[e]
Coke (dom)	kg/t	17 S[d] } ⇒25.5 S=1.5%[k] }	9[d]	6.5 A[b] } ⇒55.25 A=8.5%[k] }

FUEL	Emis. Units	SO_2 Emission Factor	NO_x Emission Factor	Part. Matter Emission Factor
Anthracite(dom)	kg/t	19 S^b (S=0.9%[c]) ⇒17.1	9^b	8.5 A^b (A=20%[c]) ⇒170
Waste (ind)	kg/t	1.25[e]	1.5[e]	15[e]
Aircraft (small)[m]	kg/t-l	1.94	11.64	2.05
Aircraft (large)	kg/t-l	3.61	48.76	2.36

[a] Emission factor for industrial coal combustion EPA (1985).
[b] Adopted from Gerson (1992).
[c] South Africa's sulphur content per weight for different fuels (Winter, 1993).
[d] After Kato and Akimoto (1992).
[e] Factors taken from Sitting (1975).
[f] Emissions for South African vehicles after Dutkiewicz (1991).
[g] From De Villiers (1993).
[k] After Williams (1969).
[m] Emissions for every take-off and landing (t-l), EPA (1985).

APPENDIX C
FUEL DATA COLLECTION AND EMISSIONS

I. Point Sources

A Dbase IV computer program was compiled, in order to register information of fuel burning appliances and to calculate the SO_2, NO_x and particulate matter emissions in the Greater Cape Town region. This database was delivered to Cape Town City Council's Air Pollution Control and is currently used by the City's Air Pollution Control Officers.
The collection of data is accomplished with an entry form in a questionnaire format (see Figure C1.1). The entry form also depicts the input fields used by the database.

From this form the source description information is ready to be entered into the database. Look-up tables and multiple choice entries are also used by the program, in order to make the data input less elaborate. Emissions from each appliance and premise are calculated automatically with the application of the emission factors in Appendix B. These factors are entered into the database separately, thus allowing for update and possible changes.

The program's output consists of the following reports:
- Detailed report of registered appliances ordered by premise
- Detailed report of registered appliances sorted by regions
- Lists of all appliances according to different regions
- Emissions by a particular premise and its appliance(s)
- SO_2, NO_x and particulate matter emissions from different districts
- Total SO_2, NO_x and particulate matter emissions

II. Area Sources

All the low strength industrial sources, as well as the residential, vehicular and those of the townships were grouped as area sources. The emission from these sources was calculated according to the fuel consumption of each emitting sector. Table C1.1 depicts the total fuel consumed in the Greater Cape Town region for the year 1991.

The fuel consumption was extrapolated from available figures wherever necessary. This extrapolation was based on the country's percentage change in fuel consumption of the years concerned.

COMPUTER FORM

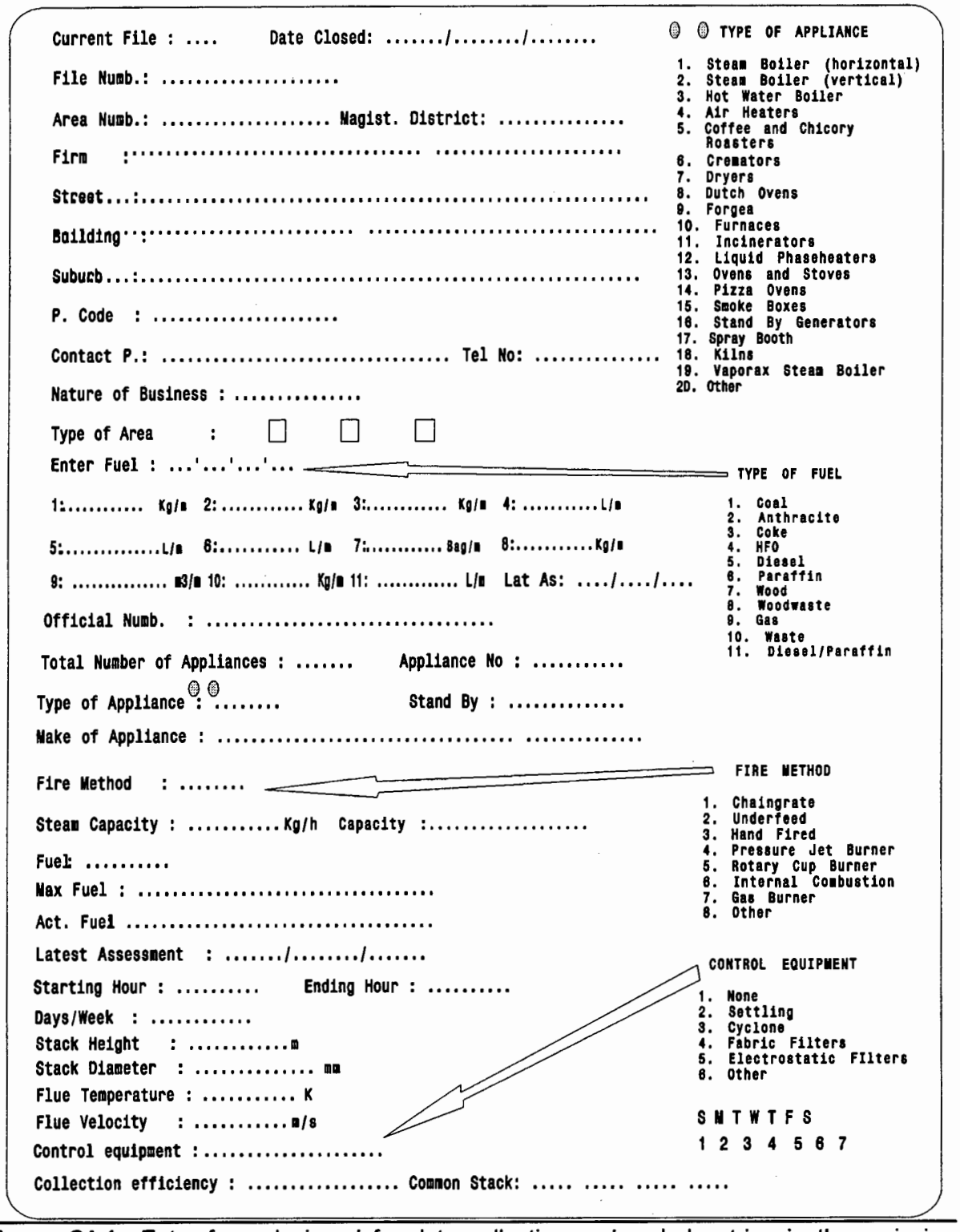

Figure C1.1 Entry form designed for data collection and coded entries in the emission inventory database, currently used by the Cape Town City Council's Air Pollution Control. The form also depicts the input fields of the database.

Table C1.1 Monthly consumption of coal, diesel, HFO, petrol, LPG and wood in the sectors: industrial, residential and vehicular.

	Total Industrial (% from points)[a]	Residential[b]	Vehicular	TOTAL
Coal (kt/m)	46 (39)%	0	—	46
Diesel (kl/m)	15875 (3)%	—	7623	23499
HFO (kl/m)	15688 (71)%	—	—	15688
Petrol (kl/m)	—	—	65910	65910
Gas (kl/m)	13734 (100)%	4229	—	17963
Paraffin (kl/m)	—	2723	—	2723
Wood (kt/m)	—	1	—	1

[a] Values in brackets represent point source consumption from the inventory database program as a percentage of the total industrial consumption.
[b] Residential fuel sales include also the township consumption.

For dispersion modelling the spatial variation of the emissions needs to be allocated as accurately as possible. Consequently, the total fuel consumption was distributed amongst the five magisterial districts of the Greater Cape Town region. This apportionment of the total fuel consumed in the whole area was performed according to the consuming sectors and type of fuel as follows:

a) Industrial sector:

Coal: The coal consumed by the industrial sector (Dutkiewicz, 1993) is apportioned to the five magisterial districts by using the 1988 Gross Domestic Product percentages of the manufacturing sector in each district. (see Table C1.2).

HFO: The heavy furnace oil consumption distribution for the year 1991 is

shown in Table C1.2. This information was obtained from sales figures of liquid fuels in the districts concerned (Mossh, 1993).

Diesel: Diesel consumed by heavy vehicles and busses (De Villiers, 1993) was subtracted from the total figures for each district (Mossh, 1993). The remaining diesel forms the total industrial consumption (Table C1.2) which, in turn, is divided into fuel consumed by point and area sources.

The actual fuel consumed by small industries (grouped as area sources), was calculated by subtracting the fuel consumed by point sources from the total fuel consumption of each magisterial district (see Table C1.2).

Table C1.2 Industrial fuel consumption per magisterial district. The fuel allocated to industrial area sources is the total consumption minus the point sources summated in each magisterial district.

		Magisterial Districts					
		Cape Town	Goodwood	Wynberg	Bellville	Kuilsriver	TOTAL
	GDP%[a] :	38.9%	16.2%	14.2%	24.3%	6.4%	100%
Coal (tons)	Total Ind.[b]	17816	7426	6495	11129	2925	45791
	(Points)[c]	(6997)	(1747)	(4156)	(5024)	0	(17924)
	Areas[d]	10819	5680	2338	6105	2925	27867
HFO (Ml)	Total Ind.	10433	653	761	3329	512	15688
	(Points)	9060	(653)	(761)	(431)	(240)	6975
	Areas	19493	0	0	2899	272	22663
Diesel (Ml)	Total Ind.	6662	1422	1807	4713	1272	15875
	(Points)	(303)	(99)	(92)	0	(16)	(510)
	Areas	6359	1323	1715	4713	1256	15366

[a] Gross Domestic Product by Kind of Economic Activity (1988): Manufacturing Sector.
[b] Coal distribution to magisterial districts was based on the GDP percentage.
[c] Values in brackets were extracted from the emission inventory database program.
[d] The remaining fuel (total-point) is allocated to industrial area sources.

Table C1.3 Coal, LPG, paraffin and wood consumed monthly in Khayelitsha, Langa, Gugulethu, Nyanga and Crossroads. Fuel estimated on the basis of total population in each township, consumption per family and average number of members per family[a].

	Coal (t/m)	LPG (kl/m)	Paraffin (kl/m)	Wood (t/m)
Khayelitsha	102	450	1228	233
Langa	1	4	74	12
Gugulethu	3	11	204	32
Nyanga	6	25	476	74
Crossroads	3	11	219	34
TOTAL	115	500	2201	385

[a] Fuel consumption and number of members per family was adopted from Theron (1992).

Table C1.4 The remaining domestic coal, LPG and paraffin after the total township consumption was subtracted from the total residential figures.

	Coal (t/m)	LPG (kl/m)	Paraffin (kl/m)
Total Residential	179[a]	4229	2723[b]
Total Townships	115	500	2201
Remaining for Urban Areas	64	3729	521

[a] Total residential coal consumption for 1991 was extrapolated from the 1989 consumption adopted from Borchers and Eberhard (1991).
[b] Sales figures (Mossh, 1993)

Table C1.5 Urban domestic coal, LPG, paraffin and wood consumption per magisterial district. The fuel allocated to the urban domestic area sources is the total residential consumption minus the total township fuel consumption.

	Cape Town	Goodwood	Wynberg	Bellville	Kuilsriver	TOTAL
Coal(t/m) [a]	8	11	31	11	3	64
LPG(kl/m)[b]	444	651	1825	636	173	3729
Paraf.(kl/m)[b]	62	91	255	89	24	521

	Cape Town	Goodwood	Wynberg	Bellville	Kuilsriver	TOTAL
Wood(t/m)[c]	37	96	269	94	27	524

[a] Apportionment based on percentage population of each district.
[b] Fuel sales per magisterial district (Mossh, 1993)
[c] Total wood consumption adopted from the Brown Haze study (De Villiers, 1993). The fuel distribution between the districts was based on their population.

C) Vehicular sector:

Petrol: The total petrol consumption per magisterial district (Mossh, 1993) is shown in Table C1.6. During vehicle refilling an amount of petrol is lost (i.e. not burned by the vehicle) due to evaporation and liquid spillage. This amount of petrol loss has been subtracted from the depicted values in the Table.

Table C1.6 Petrol (Gl/m) consumption per magisterial district for 1991.

	Cape Town	Goodwood	Wynberg	Bellville	Kuilsriver	TOTAL
Petrol	195.4	84.8	305.3	158.3	47.0	790.9

D) Aviation sector:

Since most of the aviation fuel is consumed during the flight, sales figures in an area do not depict the actual consumption which effects the ambient pollutant concentrations. Therefore, emission factors which take into consideration the fuel burnt during the take-off and landing of aircraft are adopted in this study. The average number of air planes utilising D. F. Malan airport were grouped according to two categories: small aircraft (up to Boeing 707) and large aircraft (from Boeing 707 to Boeing 747). On a monthly average for 1991, approximately 430 large and 870 small aircraft made use of the airport (Williams, 1993).

III. Total Emissions from Point and Area Sources

By employing the appropriate emission factors, the emissions from different sectors and types of fuel were calculated. The total emissions in the Greater Cape Town

region, according to the type of fuel and consuming sector are depicted in Table C1.7.

Table C1.7 SO_2, NO_x and particulate matter (t/m) emissions according to type of fuel consumed in the five sectors: Industrial, domestic, vehicular, townships and aviation.

		Industrial	Domestic	Vehicular	Townships	Aviation	TOTAL
Coal	SO_2	870	1	—	2	—	873
	NO_x	343	0	—	0	—	344
	Part.	4240	1	—	1	—	4242
Diesel	SO_2	148	—	71	—	—	219
	NO_x	134	—	282	—	—	417
	Part.	210	—	252	—	—	461
HFO	SO_2	1017	—	—	—	—	1017
	NO_x	120	—	—	—	—	120
	Part.	90	—	—	—	—	90
Petrol	SO_2	—	—	112	—	—	112
	NO_x	—	—	1252	—	—	1252
	Part.	—	—	923	—	—	923
LPG	SO_2	1	0	—	0	—	1
	NO_x	202	5	—	2	—	209
	Part.	31	1	—	0	—	32
Paraffin	SO_2	—	4	—	0	—	5
	NO_x	—	1	—	2	—	3
	Part.	—	1	—	6	—	6
Wood	SO_2	—	0	—	19	—	19
	NO_x	—	3	—	3	—	6
	Part.	—	8	—	3	—	11

		Industrial	Domestic	Vehicular	Townships	Aviation	TOTAL
Av. Gas	SO_2	—	—	—	—	5	5
	NO_x	—	—	—	—	48	48
	Part.	—	—	—	—	3	3
TOTAL	SO_2	2036	6	183	21	5	2251
	NO_x	799	9	1534	8	48	2398
	Part.	4570	10	1174	10	3	5768

The total emissions of SO_2, NO_x and particulate matter for each magisterial district can be calculated by summarising all the fuel consumed as shown in Tables C1.2, C1.5 and C1.6. These emissions, excluding the townships and D. F. Malan airport are depicted in Table C1.8. In the Cape Town magisterial district emissions of SO_2, NO_x and particulate matter are more than double in comparison with emissions from each of the remaining four districts. Emissions from the townships are shown separately in Table C1.9. Khayelitsha has the highest emissions of all the other townships together, and contributes more than 65 percent of the townships' total.

Table C1.8 Total SO2, NOx and particulate matter emissions (t/m) per magisterial district.[a]

	Cape Town	Goodwood	Wynberg	Bellville	Kuilsriver	TOTAL
SO_2	1156	217	245	499	110	2225
NO_x	943	240	597	440	123	2343
Part.	2206	949	871	1265	465	5755

[a] Township and D. F. Malan emissions are not included.

Table C1.9 Total SO2, NOx and particulate matter emissions (t/m) for the townships in the Greater Cape Town region.

	Khayelitsha	Langa	Gugulethu	Nyanga	Crossroads	TOTAL
SO_2	12.6	0.7	1.8	4.2	1.9	21.2
NO_x	5.3	0.2	0.5	1.2	0.6	7.8
Part.	6.3	0.3	0.8	1.8	0.8	9.9

The accuracy and detail of the area emissions has a strong influence on the concentrations predicted by a dispersion model. Therefore, the area sources used as input to the ISCST2 model were further distributed within the magisterial districts, according to the objective and subjective inventory techniques.

The objective approach was adopted for the domestic and vehicular sources. Weighting factors from 1 to 3 were introduced on a grid system, according to the population densities of each magisterial district. These population densities are illustrated in Figure C1.2.

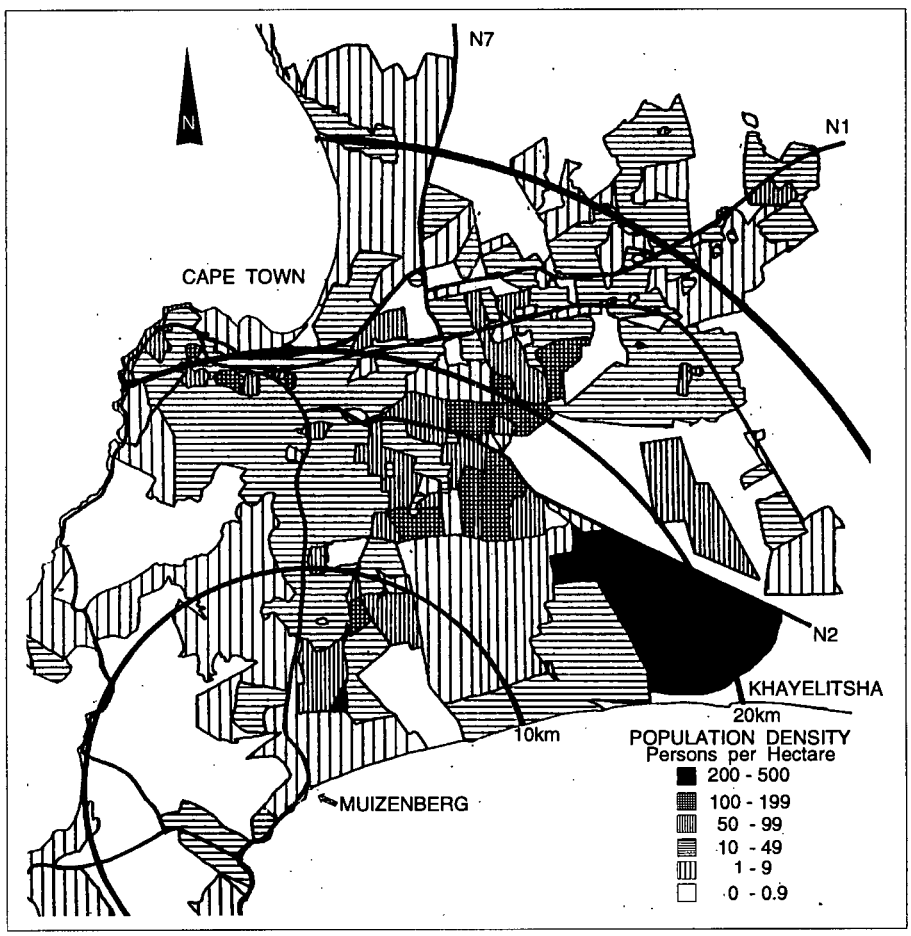

Figure C1.2 Population densities for the Greater Cape Town area based on the 1985 census.

Emissions from the townships and D. F. Malan were assumed to be uniform within their occupied areas. Square grids with sides of 1 and 0.5 km were used to simulate these emissions. For the industrial sources the subjective approach was adopted. An Air Pollution Control officer assisted the industrial grid rating, according to the intensity of industrial activity in each specific area. After the weighting factors had been introduced on the grid system, the industrial, residential and vehicular emissions were calculated from the total magisterial emission and the number of area sources per weight factor. Thereafter, the square grids were incorporated into the ISCST model as square area sources. A total of 263 area sources were allocated to the entire Greater Cape Town region.

The emission and physical characteristics of the point sources, as extracted by the inventory database, formed the point emission input into the ISCST2 model. The total number of the extracted sources was 187.

APPENDIX D
MODEL EVALUATION

I. Bootstrap Resampling for Different Meteorological Inputs

Separate model runs were performed, using combinations of three different calculation methods for the atmospheric stability and three for the mixing height (see Table D1.1).

Table D1.1 The meteorological input data sets calculated from the different stability and mixing height methods. Each code represents a different combination.

Code*	Stability calculation method	Mixing height calculation method
P60	Pasquill classification	Significant levels at D. F. Malan
P61	Inverse Monin-Obukhov	Significant levels at D. F. Malan
P62	Inverse Monin-Obukhov	Holzworth procedure
P63	Pasquill classification	Holzworth procedure
P64	Pasquill classification	Heat exchange
P65	Inverse Monin-Obukhov	Heat exchange
P66	Kazanski-Monin parameter	Heat exchange
P67	Kazanski-Monin parameter	Holzworth procedure
P68	Kazanski-Monin parameter	Significant levels at D. F. Malan

* Code for the combination of meteorological calculations used in the model runs

A source code was developed to perform the blocked bootstrap procedure on the 24 hour averages of the predicted and observed concentrations. The results of this resampling technique for the index of agreement, the fractional bias and the mean difference are depicted in Figures D1.2 - D1.4, for the three monitoring stations. The bounds shown in each Figure are the 95% confidence intervals. In general, the Pasquill stability method and the inverse Monin-Obukhov method produced the best results when combined with the mixing height, as calculated by the Holzworth procedure.

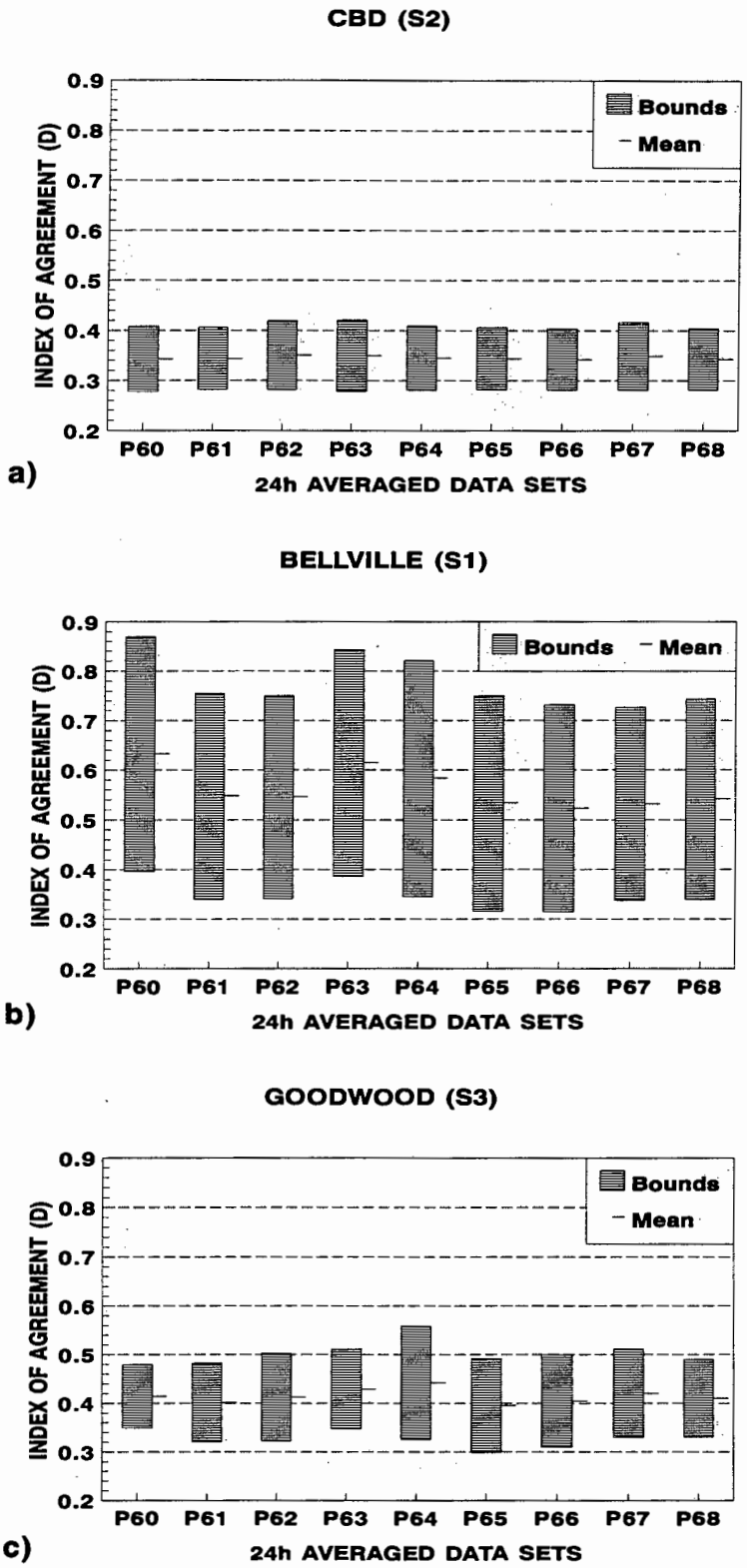

Figure D1.1 The 95% confidence intervals of the index of agreement (D) for the monitoring stations: a) Cape Town's CBD (S2), b) Bellville (S1), and c) Goodwood (S3). The predicted and observed concentrations were averaged for each 24 hours and grouped according to the meteorological calculating methods.

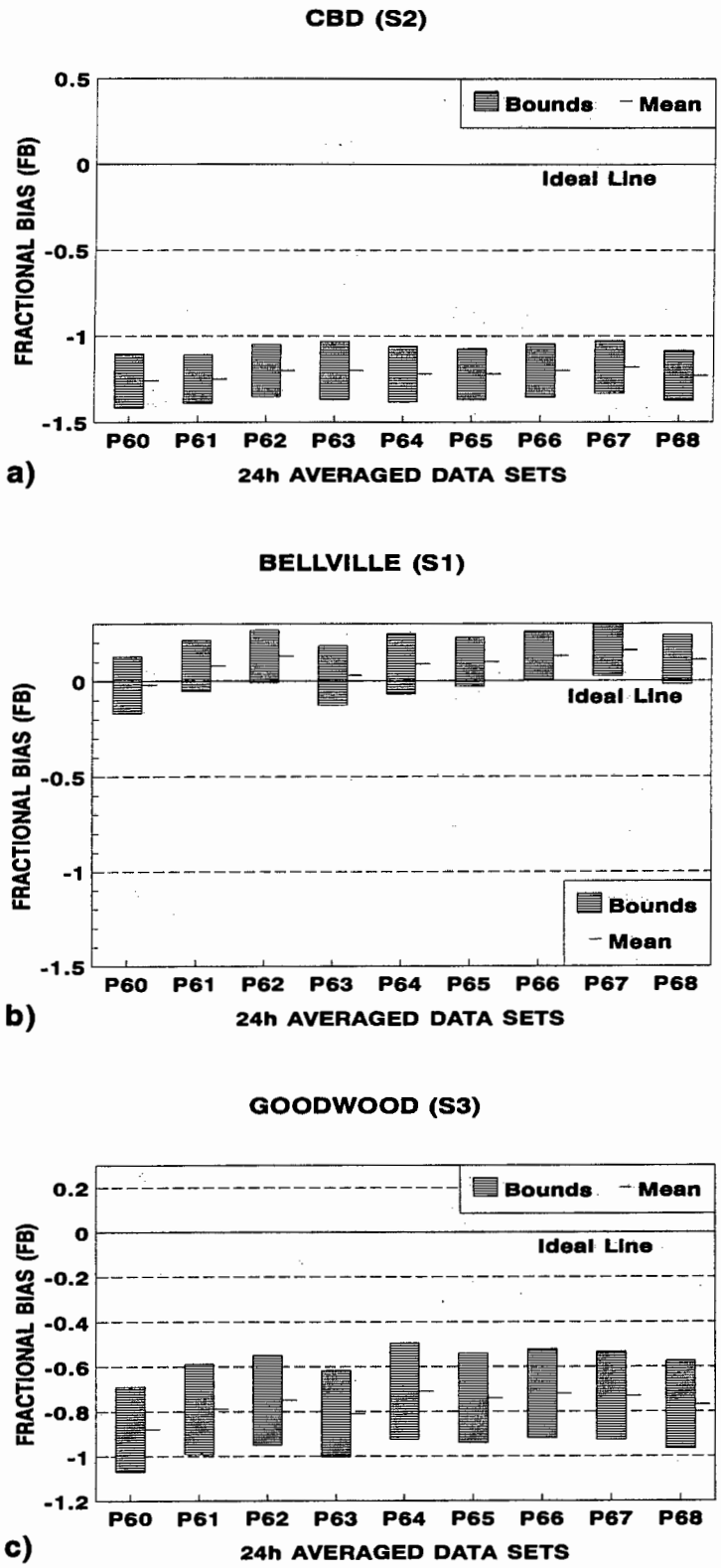

Figure D1.2 The 95% confidence intervals of the fractional bias (FB) for the monitoring stations: a) Cape Town's CBD (S2), b) Bellville (S1), and c) Goodwood (S3). The predicted and observed concentrations were averaged for each 24 hours and grouped according to the meteorological calculating methods.

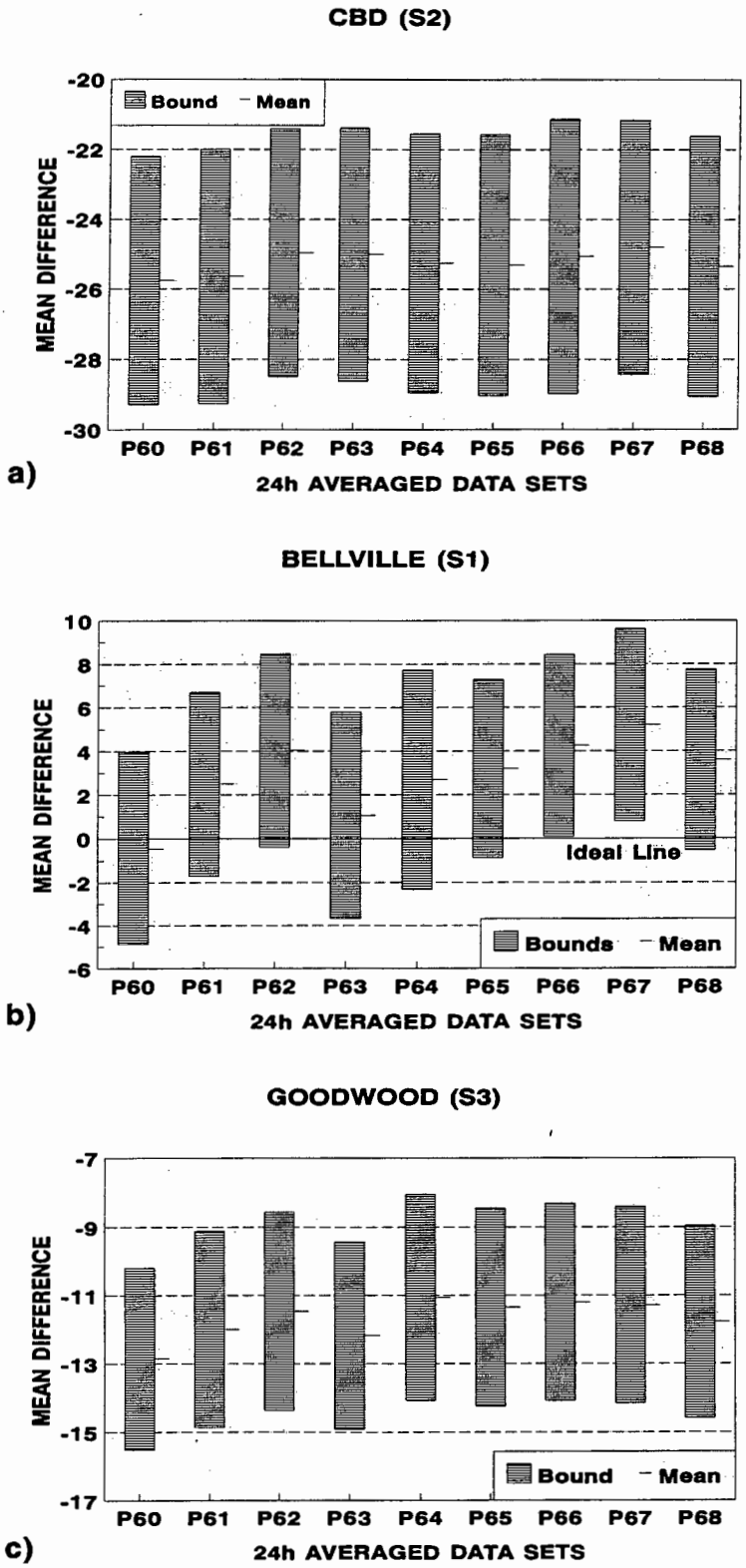

Figure D1.3 The 95% confidence intervals of the mean difference for the monitoring stations: a) Cape Town's CBD (S2), b) Bellville (S1), and c) Goodwood (S3). The predicted and observed concentrations were averaged for each 24 hours and grouped according to the meteorological calculating methods.

II. Model Performance According to Stability Category and Wind Velocity

The selected data set P63 was divided into several subsets, according to the stability category and wind velocity, in order to assess the model performance under different atmospheric conditions. Tables D1.2 and D1.3 contain the statistical measures according to atmospheric stability for the monitoring stations at Cape Town's CBD and Goodwood respectively. The same information shorted according to wind velocity is showed in Tables D1.4 and D1.5.

Table D1.2 Summary of paired statistics according to atmospheric stability for the monitoring station at Cape Town's CBD (S2) (unstable 1-3, neutral 4, and stable 5-6).

	1-3 (Unstable)		4 (Neutral)		5-6 (Stable)	
	Obs.	Pred.	Obs.	Pred.	Obs.	Pred.
Sample size	107	107	438	438	76	76
Range[a]	9-75	0-66	5-79	0-52	5-76	0-74
Mean[a]	40.8	12.7	31.8	6.4	32.9	20.1
Standard deviation (STD)[a]	13.4	12.8	13.1	6.8	13.8	18.4
Average P/O	0.34		0.22		0.81	
Mean difference[a]	-28.2		-25.5		-12.8	
Intercept	6.2		1.74		19.4	
Slope	0.16		0.15		0.02	
Fractional bias (FB)	-1.05		-1.33		-0.48	
Index of agreement (D)	0.387		0.411		0.393	
NMSE	2.09		4.02		1.03	
RMSE[a]	32.9		28.6		26.2	
$RMSE_u$	12.6		6.6		18.4	
$RMSE_s$	30.3		27.8		18.6	
MSE_u/MSE	15%		5%		50%	
MSE_s/MSE	85%		95%		50%	

[a] The units of range, mean, STD, mean difference and RMSE are $\mu g/m^3$

Table D1.3 Summary of paired statistics according to atmospheric stability for the monitoring station at Goodwood (S3) (unstable 1-3, neutral 4, and stable 5-6).

	1-3 (Unstable)		4 (Neutral)		5-6 (Stable)	
	Obs.	Pred.	Obs.	Pred.	Obs.	Pred.
Sample size	200	200	394	394	175	175
Range[a]	1-67	0-100	1-72	0-99	1-71	0-162
Mean[a]	19.9	7.8	22.1	8.9	21.5	10.8
Standard deviation (STD)[a]	11.5	12.3	12.9	14.8	12.8	21.9
Average P/O	0.74		0.55		1.0	
Mean difference[a]	-12.1		-13.3		-10.7	
Intercept	5.8		6.3		12.6	
Slope	0.1		0.11		-0.08	
Fractional bias (FB)	-0.88		-0.86		-0.66	
Index of agreement (D)	0.423		0.444		0.332	
NMSE	2.62		2.68		3.39	
RMSE[a]	20.1		22.9		28.1	
$RMSE_u$	12.3		14.7		21.9	
$RMSE_s$	15.9		17.5		17.5	
MSE_u/MSE	37%		41%		61%	
MSE_s/MSE	63%		59%		39%	

[a] The units of range, mean, STD, mean difference and RMSE are $\mu g/m^3$

Table D1.4 Summary of paired statistics according to wind velocity (u) for the monitoring station at Cape Town's CBD (S2) ($\leq 3m\ s^{-1}$, 3-6m s^{-1}, and $\geq 6m\ s^{-1}$).

	$u \leq 3m\ s^{-1}$		$3m\ s^{-1} < u < 6m\ s^{-1}$		$u \geq 6m\ s^{-1}$	
	Obs.	Pred.	Obs.	Pred.	Obs.	Pred.
Sample size	102	102	216	216	303	303
Range[a]	5-76	0-74	5-78	0-66	9-79	0-36
Mean[a]	36.1	19.4	34.2	8.8	32.1	5.9
Standard deviation (STD)[a]	14.1	17.9	14.6	10.0	12.6	5.5
Average P/O	0.66		0.3		0.2	
Mean difference[a]	-16.7		-25.4		-26.2	
Intercept	17.2		1.8		3.3	
Slope	0.06		0.21		0.08	
Fractional bias (FB)	-0.6		-1.18		-1.38	
Index of agreement (D)	0.415		0.438		0.392	
NMSE	1.11		2.88		4.48	
RMSE[a]	27.9		29.5		29.2	
$RMSE_u$	17.9		9.6		5.4	
$RMSE_s$	21.4		27.2		28.7	
MSE_u/MSE	41%		11%		3%	
MSE_s/MSE	59%		89%		97%	

[a] The units of range, mean, STD, mean difference and RMSE are $\mu g/m^3$

Table D1.5 Summary of paired statistics according to wind velocity (u) for the monitoring station at Goodwood (S3) (≤3m s^{-1} , 3-6m s^{-1}, and ≥6m s^{-1}).

	$u \leq 3m\ s^{-1}$		$3m\ s^{-1} < u < 6m\ s^{-1}$		$u \geq 6m\ s^{-1}$	
	Obs.	Pred.	Obs.	Pred.	Obs.	Pred.
Sample size	156	156	285	285	328	328
Range[a]	1-70	0-162	1-72	0-80	1-51	0-56
Mean[a]	22.5	18.5	20.4	8.3	21.7	5.1
Standard deviation (STD)[a]	13.2	27.9	12.5	12.7	12.3	6.7
Average P/O	1.58		0.59		0.38	
Mean difference[a]	-4.0		-12.1		-16.6	
Intercept	13.9		8.7		4.2	
Slope	0.2		-0.02		0.04	
Fractional bias (FB)	-0.19		-0.85		-1.24	
Index of agreement (D)	0.375		0.383		0.442	
NMSE	2.15		2.78		4.18	
RMSE[a]	29.9		21.7		21.4	
$RMSE_u$	27.8		12.7		6.7	
$RMSE_s$	11.2		17.6		20.4	
MSE_u/MSE	86%		34%		10%	
MSE_s/MSE	14%		66%		90%	

[a] The units of range, mean, STD, mean difference and RMSE are $\mu g/m^3$

REFERENCES

References

Alexopoulos, A. and D. Assimacopoulos (1993). Model for Traffic Emissions Estimation. Atmospheric Environment, Vol 27, pp 435-446.

Aron, R. (1983). Mixing Height - An Inconsistent Indicator of Potential Air Pollution Concentrations. Atmospheric Environment, Vol 17, pp 2193-2197.

Barclay, J. J. (1993). Meteorological Aspects of Brown Haze in Cape Town. Department of Oceanography, University of Cape Town.

Benarie, M. M. (1987). The Limits of Air Pollution Modelling. Editorial. Atmospheric Environment, Vol 21, pp 1-5.

Borchers, M. L. and A. A. Eberhard (1991). Household Energy Supply and Price Trends. Final Project Report NE 14/6/12, Energy for Development Research Centre, University of Cape Town.

Briggs, G. A. (1985). Analytical Parameterization of Diffusion: The Convective Boundary Layer. Journal of Climate and Applied Met., Vol 24, pp 1167-1186.

Briggs, G. A. (1973). Diffusion Estimation for Small Emissions. ATDL Contribution. File No 79, Atmospheric Turbulence and Diffusion Laboratory.

Businger, J. A. (1973). Turbulent Transfer in the Atmospheric Surface Layer. Workshop on Micrometeorology, American Meteorological Society, Boston, Mass., pp 67-100.

Businger, J. A. and S. P. S. Arya (1974). Height of the mixed Layer in the Stably Stratified Planetary Boundary Layer. Advances in Geophysics, Vol 18, pp 73-92.

Cox, W. M. and J. A. Tikvart (1985). Assessing the Performance Level of Air Quality Models. Paper Presented at the 15th International Technical Meeting on Air Pollution and Its Applications, NATO/CCMS Conference, St. Louis, MO.

Cox, W. M. and J. A. Tikvar (1990). A Statistical Procedure for Determining the Best Performing Air Quality Simulation Model. Atmospheric Environment, Vol 24, pp 2387-2395.

De Villiers, M. G. (1993). The Cape Town Brown Haze Study. Final Report. Report No GEN 157. Energy Research Institute, University of Cape Town.

Dracoulides, D. A. (1994). A Statistical Evaluation and Comparison of ISCST2 Model with Measurements of SO_2 Concentrations in the Greater Cape Town Region. In Proceedings of a Responsible Approach to Clean Air Conference 1994.

Dracoulides, D. A. and R. K. Dutkiewicz (1993). Air Pollution Modelling in the Greater Cape Town Region. In Proceedings of Clean Air Challenges in a Changing South Africa Conference 1993. Paper 10.

Draxler, R. (1980). An Improved Gaussian Model for Long-Term Average Air Concentration Estimates. Atmospheric Environment, Vol 14, pp 597-601.

Draxler, R. R. (1987). Accuracy of Various Diffusion and Stability Schemes Over Washington, D. C. Atmospheric Environment, Vol 21, pp 491-499.

Dutkiewicz, R. K. (1993). An Estimate of Emissions from Vehicles in South Africa. Report No INT 183. Energy Research Institute, University of Cape Town.

Dutkiewicz, R. K., R. F. Fuggle and C. S. Keen (1980). Air Pollution Survey of Greater Cape Town. Vol 5: Conclusions and Recommendations.

Dutkiewicz, R. K and R. F. Fuggle (1977). Air Pollution Survey of Greater Cape Town. Vol 1: Interim Report.

Efron, B. and G. Gong (1982). A Leisurely Look at the Bootstrap, the Jackknife and Cross-Validation. Technical Report No 75. Division of Biostatistics, Stanford University, California.

Efron, B. (1982). The Jackknife, the Bootstrap and Other Resampling Plans. CBMMS-NSF-38. Soc. Ind. and Appl. Math., Philadelphia.

EPA (1985). Compilation of Air Pollutant Emission Factors. Volume I: Stationary Point and Area Sources. Volume II: Mobile Sources. U. S. Environmental Protection Agency.

EPA (1992). User's Guide for the Industrial Source Complex (ISC2) Dispersion Model. Volume II — Description of Model Algorithms.

Fontelle, J-P. (1990). CORINAIR: European Emission Inventory of Pollutants Into the Atmosphere, in: Computer Techniques in Environmental Studies III, ed. Zannetti, P. Computational Mechanics Publications, Shouthampton, Boston. pp 241-253.

Fox, D. G. (1981). Judging Air Quality Model Performance. Bull. Amer. Met. Soc., Vol 62, pp 599-609.

Fox, D. G. (1984). Uncertainty in Air Quality Modeling. Bull. Amer. Met. Soc., Vol 65, pp 27-47.

Fuggle, R. F. (1977). Air Pollution Survey of Greater Cape Town. Vol 2: Surface Winds.

Garratt, J. R. (1982). Observations in the Nocturnal Boundary Layer. Boundary Layer Meteorology, Vol 22, pp 21-48.

Gerson, R. (1992). The Environmental Effect of Air Pollution From the Energy Sector in South Africa. M.Sc. Thesis, Energy Research Institute, University of Cape Town.

Golder, D. (1972). Relations Among Stability Parameters in the Surface Layer. Boundary Layer Meteorology, Vol 3, pp 47-58.

Hanna, S. R. (1980). Measured Sigma(y) and Sigma(theta) in Complex Terrain Near The TVA Widows Creek, Alabama, Atmospheric Environment, Vol 14, pp 401-407.

Hanna, S. R. (1989). Confidence Limits for Air Quality Model Evaluations, As Estimated By Bootstrap and Jackknife Atmospheric Environment, Vol 23, pp 1385-1398.

Hanna, S. R. (1988). Air Quality Model Evaluation and Uncertainty. J. Air Poll. Cont. Assoc., Vol 38, pp 406-412.

Hanna, S. R., G. A. Briggs and R. P. Hosker (1982). Handbook on Atmospheric Diffusion. U.S.A. Technical Information Centre.

Holtslag, A. A. M. and A. P. Van Ulden (1983). A Simple Scheme for Daytime Estimates of the Surface Fluxes from Routine Weather Data. American Meteorological Society, Vol 22, No 4, April, pp 517-529.

Holtslag, A. A. M. and F. T. M. Nieuwstadt (1986). Scaling the Atmospheric Boundary Layer. Boundary Layer Meteorology, Vol 36, pp 201-209.

Holzworth, G. C. (1972). Mixing heights, Wind Speeds and Potential for Urban Air Pollution Throughout the Contiguous United States. Publication No. AP-101. U.S. Environmental Protection Agency, Research Triangle Park, North Carolina 27711.

Huber, A. H. and W. H. Snyder (1976). Building Wake Effects on Short Stack Effluent. Preprint Volume for the Third Symposium on Atmospheric Diffusion and Air Quality, American Meteorological Society, Boston, Massachusetts.

Irwin, J. S. (1979). Theoretical Variation of the Wind Profile Power-law Exponent as a Function of Surface Roughness. Atmosspheric Environment, Vol 13, pp 191-194.

Irwin, J. S. and F. S. Binkowski (1981). Estimation of the Monin-Obukhov Scaling Length Using On-Site Instrumentation. Atmospheric Environment, Vol 15, pp 1091-1094.

Jose, R. S. (1991). A simple Approach to Evaluate Mixed Layer Depth. Environmental Software, Vol 6, pp 161-167.

Jury, M., A. Tegen, E. Ngeleza and M. Dutoit (1990). Winter Air Pollution Episodes Over Cape Town. Boundary Layer Meteorology, Vol 53, pp 1-20.

Jury, M. R. and J. Barcley (1992). Air Pollution Meteorology: An Episode in Cape Town 12 May 1992. NACA One Day Seminar: Photochemical Smog/Brown Haze in Cape Town.

Jury, M. R. and J. M. Wilzak (1992). Mesoscale Numerical Models: Cost-Effective Input to Dispersion Prediction Schemes. The Clean Air Journal, Vol 8, pp 12-14.

Kato, N. and H. Akimoto (1992). Anthropogenic Emissions of SO2 and NOx in Asia: Emission Inventories. Atmospheric Environment, Vol 26, pp 2997-3017.

Keen, C. S. (1979). Air Pollution Survey of Greater Cape Town. Vol 4: Meteorological Aspects.

Ku, J. Y., S. T. Rao and K. S. Rao (1987a). Numerical Simulation of Air Pollution in Urban Areas: Model Development. Atmospheric Environment, Vol 21, pp 201-212.

Ku, J. Y., S. T. Rao and K. S. Rao (1987b). Numerical Simulation of Air Pollution in Urban Areas: Model Evaluation. Atmospheric Environment, Vol 21, pp 213-232.

Lamb, R. G. and D. R. Durran (1978). Eddy Diffusivities Derived from a Numerical Model of the Boundary Layer. Il Nuovo Cimento 1c, 1-17 (published in Italy).

Loewenheim, L. L. (1988). Photochemical Smog in Greater Cape Town. M.Sc. Thesis, Department of Environmental and Geographical Science, University of Cape Town.

Ludwig, F. L., W. B. Johnson, A. E. Moon and R. L. Mancuso (1970). A Practical Multipurpose Urban Diffusion Model for Carbon Monoxide, Final Report Coordinating Research Council (CRC) Contract CAPA-3-68 and Nat. Air Poll. Control Admin. Contract CPA 22-69-64.

Lyons, T. J. and W. D. Scott (1990). Principles of Air Pollution Meteorology. Belhaven Press, London.

Melas, D. (1990). Sodar Estimates of Surface Heat Flux and Mixed Layer Depth Compared With Direct Measurements. Atmospheric Environment, Vol 24, pp 2847-2853.

Mitchell, A. E. (1982). A comparison of Short-Term Dispersion Estimates Resulting from Various Atmospheric Stability Classification Methods. Atmospheric Environment, Vol 16, pp 765-773.

Mossh, J. (1993). BP South Africa. Personal Communication.

Pasquill, F. (1961). The Estimation of the Dispersion of Windborne Material. Meteorol Mag., Vol 90, pp 33-49.

Pasquill, F. and F. B. Smith (1983). Atmospheric Diffusion. 3rd ed. New York: Ellis Horwood Limited.

Popkiss, M. E. (1992). Atmospheric Pollution in Cape Town. The Clean Air Journal, Vol 8, No 6, November.

Preston-Whyte, R. A. and P. D. Tyson, 1988. The Atmosphere and Weather of Southern Africa. Oxford University Press, Cape Town.

Rao, S. T., G. Sistla, V. Pagnotti, W. B. Petersen, J. S. Irwin and D. B. Turner (1985). Evaluation of the Performance of RAM with the Regioinal Air Pollution Study Data Base. Atmospheric Environment, Vol 19, pp 229-245.

Rayner, K. N. and I. D. Watson (1991). Operational Prediction of Daytime Mixed Layer Heights for Dispersion Modelling. Atmospheric Environment, Vol 25, pp 1427-1436.

Raghavan, N., P. Goyal and S. Basu (1983). A Gaussian Model for Predicting SO_2 Concentration in the City of Agra. Atmospheric Environment, Vol 17, pp 2199-2203.

Rossano, A. T. and T. A. Rolander (1976). The Preparation of an Air Pollution Source Inventory, in: Manual on Urban Air Quality Management, eds. Suess, M J. and S. R. Craxford. WHO Regional Publications, European Series No 1, Copenhagen, pp 127-152.

Ruff, R. E. (1983). Application of Statistical Methods to Diagnose Causes of Poor Air-Quality Model Performance. Atmospheric Environment, Vol 17, pp 291-297.

Scire, J. S. and L. L. Schulman (1980). Modelling Plume Rise from Low-Level Buoyant Line and Point Sources. Proceedings Second Joint Conference on Applications of Air Pollution Meteorology, 24-28 March, New Orleans, LA. pp 133-139.

Sedefian, L. and E. Bennett (1980). A Comparison of Turbulence Classification Schemes. Atmospheric Environment, Vol 14, pp 741-750.

Sheifeld, J. H. (1975). Air Pollution — Physical and Chemical Fundamentals. McGraw-Hill, New York.

Seinfeld, J. H. (1986). Atmospheric Chemistry and Physics of Air Pollution. Willey Interscience Publication, New York.

Singal, S. P., E. W. D. Lewthwaite and D. S. Wratt (1989). Estimating Atmospheric Stability from Monostatic Acoustic Sounder Records. Atmospheric Environment, Vol 23, pp 2079-2084.

Singh, M. P., P. GOYAL, T. S. Panwar, P. Agarwal and S. Nigam (1990). Predicted and Observed Concentrations of SO2 SPM and NO2 Over Delhi. Atmospheric Environment, Vol 24, pp 783-788.

Sitting, M. (1975). Environmental Sources and Emissions Handbook. Noyes Data Corporation, USA.

Slade, D. H. (1968). ed. Meteorology and Atomic Energy — 1968. USAEC, TID-24190, 445 pp.

Smith, M. Y. (1984). A survey of Photochemical (and Other) Air Pollution in South Africa With Special Emphasis on Cape Town. Report No 80. Energy Research Institute, University of Cape Town.

Snyder, W. H., L. H. Khurshudyan, I. V. Nekrasov, R. E. Lawson and S. T. Thompson (1991). Flow and Dispersion of Pollutants Within Two-Dimensional Valleys. Atmospheric Environment, Vol 25, pp 1347-1375.

Stern, A. C. (1973). Fundamentals of Air pollution. Academic Press, New York.

Stunder, M. and S. SethuRaman (1986). A Statistical Evaluation and Comparison of Coastal Point Source Dispersion Models. Atmospheric Environment, Vol 20, pp 301-315.

Sutherland, R. A., F. V. Hansen and W. D. Bach (1986). A Quantitative Method for Estimating Pasquill Stability Classes from Windspeed and Sensible Heat Flux Density. Boundary Layer Meteorology, Vol 37, pp 357-369.

Tagliazucca, M. and T. Nanni (1983). An Atmospheric Diffusion Classification Scheme Based on the Kazanski-Monin Stability Parameter Atmospheric Environment, Vol 17, pp 2205-2211.

Theron, P. (1992). Analysis of the New Electrification Schemes in the Western Cape. Draft Final Project Report NE 14/6/17. Energy for Development Research Centre, University of Cape Town.

Tjemkes, S. A. and P. G. Guynkerke (1989). The Nocturnal Boundary Layer: Model Calculations Compared With Observations. American Meteorological Soc. Vol 28, pp 161-175.

Tukey, J. W. (1987). Kinds of Bootstraps and Kinds of Jackknifes Discussed in Terms of a Year of Weather-Related Data. Technical Report 292, Department of Statistics, Princeton University, 08544.

Turner, C. R. (1993). The Matimba Air Quality Modelling Database. Report No trr/s/93/010/rw. Scientific Services. ESKOM

Turner, B. (1970). Workbook of Atmospheric Dispersion Estimates. PHS Publication No 999-AP-26. U.S. Department of Health, Education and Welfare, National Air Pollution Control Administration, Cincinnati, Ohio.

Turner, D. B. (1979). Atmospheric Dispersion Modeling. A Critical Review. J. Air Poll. Cont. Assoc., Vol 29, pp 502-519.

Van Ulden, A. P. and A. M. Holtslag (1985). Estimation of Atmospheric Boundary Layer Parameters for Diffusion Applications. Bull. Amer. Met. Soc., Vol 24, pp 1196-1207.

Venkatram, A. (1988). Dispersion in the Stable Boundary Layer, in: Lectures on Air Pollution Modeling, eds. Venkatram, A. and J. C. Wyngaard. American Meteorological Society, Boston.

Weil, J. C. and R. P. Brower (1984). An Updated Gaussian Plume Model for Tall Stacs. J. Air Poll. Cont. Assoc., Vol 34, pp 818-827.

Wieringa, J. (1992). Representative Roughness Parameters for Homogeneous Terrain. Boundary Layer Meteorology, Vol 63, pp 323-363.

Williams, D. (1993). D. F. Malan Air Traffic Control. Department of Transport. Personal Communication.

Williams, J. N. (1969). Steam Generation. George Allen and Unwin LTD, London.

Willmot, C. J. (1982). Some Comments on the Evaluation of Model Performance. Bulletin American Meteorological Society, Vol 63, No 11, November, pp 1309-1313.

Winter, B. (1993). BP South Africa. Personal Communication.

Wohlers, H. C., W. E. Jackson and I. Butmania (1969). A Rapid Emission Survey Procedure for Industrial Air Pollutants. J. Air Poll. Cont. Assoc., Vol 19, pp 309-314.

Wratt, D. S. (1987). An Experimental Investigation of Some Methods of Estimating Turbulence Parameters for Use Atmospheric Environment, Vol 21, pp 2599-2608.

Yamartino, R. J. (1977). A New Method for Computing Pollutant Concentrations in the Presence of Limited Vertical Mixing. APCA Note-Book, 27(5):467.

Zoumakis, N. M. and A. G. Kellesis (1991). The Dependence of the Bulk Richardson Number on Stability in the Surface Layer. Boundary Layer Meteorology, Vol 57, pp 407-414.